2009

Design and characterization of a shock and vibration mitigation seat system

George Samaan Ladkany
University of Nevada Las Vegas

DESIGN AND CHARACTERIZATION OF A SHOCK AND VIBRATION MITIGATION SEAT SYSTEM

by

George Samaan Ladkany

Bachelor of Science Engineering
University of Nevada, Las Vegas
2006

A thesis submitted in partial fulfillment
of the requirements for the

Master of Science in Mechanical Engineering
Department of Mechanical Engineering
Howard R. Hughes College of Engineering

Graduate College
University of Nevada, Las Vegas
December 2009

UNLV
UNIVERSITY OF NEVADA LAS VEGAS

THE GRADUATE COLLEGE

We recommend that the thesis prepared under our supervision by

George Samaan Ladkany

entitled

Design and Characterization of a Shock and Vibration Mitigation Seat System

be accepted in partial fulfillment of the requirements for the degree of

Master of Science
Mechanical Engineering

Douglas Reynolds, Committee Chair

Brian Landsberger, Committee Member

William Culbreth, Committee Member

Edward Neumann, Graduate Faculty Representative

Ronald Smith, Ph. D., Vice President for Research and Graduate Studies
and Dean of the Graduate College

December 2009

ABSTRACT

Design and Characterization of a Shock and Vibration Mitigation Seat System

by

George Samaan Ladkany

Dr. Douglas Reynolds, Examination Committee Chair
Professor of Mechanical Engineering
University of Nevada, Las Vegas

Extensive research has been conducted into the development of pneumatic seat-bladder systems for shock and vibration mitigation for use in current U.S military vehicle envelopes. This research expands on the previous work through an elaborate experimental characterization of four prototype air bladder seat cushion systems. The experimental characterization conducted included shock testing, continuous vibration, and internal dynamic pressure measured during the shock event.

The shock testing was conducted both at the Army Research Lab as well at UNLV. The shock testing conducted at UNLV was performed on a drop tower designed and constructed during the time of this research. The scope of the testing was extended beyond the U.S military's requirements to include random continuous vibrations which can cause physical harm to the occupant over extended durations. The primary considerations are to increase the survivability of crewmembers exposed to mine blasts and mitigation of the vibration experienced in rough or combat related ride situations.

Various suggestions from the tested prototypes are provided for field implementation. This study showed that the seat bladder system produced reductions in dynamic response index (DRI) and from baseline values of pelvic accelerations (up to 77% or 790m/s^2), vibration dosage values (VDV up to 60%), and lumbar spinal load (up to 60% or 6000N).

ACKNOWLEDGEMENTS

I would like to thank all of my family, friends, and advisors that have stood by me and supported me, not only through this process, but throughout my life. You have been with me during both the most difficult and the most memorable of times. Without you, I would not be the man I am today.

TABLE OF CONTENTS

LIST OF TABLES

LIST OF FIGURES

CHAPTER 1

INTRODUCTION

1.1 The Problem

Landmines and improvised explosive devices (IED's) are a major threat to the occupants of military vehicles. The variety of these threats has grown significantly during military operations in Iraq and Afganistan. Landmine and IED blasts can completely destroy a vehicle, killing all its occupants. They can also disable a vehicle, leaving its occupants severely injured. Injuries sustained during a landmine or IED blast come from fragmentation that enters the vehicle through a hull breach, hot gases expanding through the vehicle, or severe shock acceleration in the vehicle structure that is created from the extreme pressure of the blast [1]. Mitigating the high shock acceleration experienced by vehicle occupants during survivable mine blasts is the primary focus of the research addressed in this thesis

Armoring and blast deflection techniques applied to military vehicles have been effective in improving the survivability of vehicle occupants when exposed to blasts from landmines and IED's [2]. However, severe shock from these blasts can still be transmitted through a vehicle's structure. This shock can cause severe leg, spine, neck and head injuries. These injuries can sometimes be fatal. While musculoskeletal injuries are more common, severe soft tissue injuries, which include rupture of the bladder, spleen and aortal artery, can also occur.

Even though the primary focus of this thesis is associated with the mitigation of injuries associated with landmines and IEDs, injuries to vehicle occupants can also occur as a result of continued exposure to repeated low-level shocks associated with the travel

of military vehicles over rough terrains. ISO Standards 2631, Parts 1 and 5 give guidance with regard to allowable vehicle occupant vibration exposure amplitudes associated with this type of vibration and shock exposure [3,4]. They provide methodology for analyzing such events with frequency weighting designed to account for the human response in each of the frequency bands.

1.2 Characterization of the Mine Blast Threat

The threat that mine blasts pose to vehicles is not extensive since the blasts can vary widely in their overall magnitude, pulse shape, and pulse duration. The actual shock transmitted to the occupant cabin is a function of many factors [5], which include charge type, amount of explosive used, relative location of the mine or IED to the vehicle, and the vehicle structural properties. While the primary direction of a blast can vary, the vertical direction is considered to be the cause of the most critical injuries and is typically the orientation in which a variety of injury criteria are defined. The U.S. Army Research Laboratory characterized landmine blasts transmission through the vehicle's floor structure as acceleration pulses ranging from 2,000 to over 4,000 m/s^2 in magnitude. The pulse shapes are roughly triangular or half-sine with sustained durations between 5 to 10 ms.

1.3 Vehicle Seat Systems

Mine blast shock energy travels through a vehicle structure to the base or support of the vehicle seat system. The seat system must be designed to attenuate the acceleration and force transmitted to the body of the seated occupant, from the mine blast shock, at an

amplitude where bodily injury will not result. Seat structures can be attached to the floor, side walls or top of a vehicle crew compartment. Also the mounting of the seat system relative to the vehicle's frame can have a significant effect on the form and effect of the shock.

A common seat system used to attenuate mine blast shock energy employs a force limiting structure. The seat structure attenuates mine blast energy directed into its base or support by applying a nearly constant resisting force that acts over a specified distance, referred to as the seat stroke length. These seat structures are referred to as energy absorbing (EA) structures. The seat's limiting force is selected to be a constant value that, when applied to the body of the seat occupant, is less likely to result in a spinal injury. This value is normally less than 1,500 lb_f (6,672 N) [6,7]. The limiting force in an EA seat system can be applied in several ways. These include, but are not limited to, deformable seat support brackets, collapsible seat frames, crushable-honeycomb panels, crushable tubing, and frictional-based systems relying on cables or rods in tension [8,9].

There are two disadvantages associated with EA seat structures. The attenuation of high mine blast energy amplitudes may require longer seat stroke lengths than can be accommodated in a compact vehicle crew compartment. The second is the inability for the majority of EA systems, particularly those that undergo permanent deformation, to deal with multiple or repetitive blasts. There are normally two shock components associated with a mine blast event. The first is the initial shock from the mine blast. When the mine blast is of significant amplitude and the vehicle is light weight, the blast energy will lift the vehicle off the ground. Therefore, a second shock results when the vehicle impacts the ground at "slam down". If the mine blast shock energy attenuation

obtained through the deformation or collapse of the EA structure is “used up,” the vehicle occupant will experience the full shock amplitude associated with the vehicle slam down. This shock can also result in serious spinal or other related injuries to the seat occupant.

Semi-active and active shock and vibration control system have been considered as a possible means of attenuating mine blast shock energy directed into vehicle seat systems. However, mine blast event occur sufficiently fast that the event is over before current day control systems have a chance to respond.

Seat cushions are part of most vehicle seat systems. The effects of typical seat cushions on the attenuation of mine blast shock are described by E. Wolf [9]. He observed that seat ejection systems used in aircraft systems with purely foam-filled cushions performed poorer than when no foam-cushion was used at all [10]. The foam cushions used in these tests were typically high density foams necessary to support the weight of the occupant. In some cases these foam cushions even caused acceleration amplification.

1.4 Air Bladder Seat Cushion Concept

A prototype vehicle air bladder seat cushion has been developed as part of a co-operative research agreement between the University of Nevada, Las Vegas and the U.S. Army Research Laboratory. A description of this seat air bladder will be given in Chapter 3. Drop tower tests were conducted at the U.S. Army Research Laboratory, using a THOR III 50 percentile anthropomorphic test dummy (ATD), to document the effectiveness of the seat air bladder in attenuating high-intensity shock. While the results of the of the drop tower tests provided good information on the air bladder in attenuating

high-intensity shock, they did not provide information that was necessary to clearly identify the physical characteristics of the bladder that contributed to and defined its shock-reducing characteristics. E. Wolf used the results of the drop tower tests to validate a 5-degree-of-freedom, lump-parameter vibration model that he developed as part of his doctoral research and that can be used to predict the shock response of an individual when he is sitting on the seat air bladder and is exposed to a mine blast shock event.

Properties of the air bladder seat cushion including some potential advantages over common energy-absorbing seat systems include but are not limited to:

- The air bladder seat cushion sustains no permanent deformation under most conditions, and therefore will protect against multiple repeated shocks.
- Air bladder seat cushions, have low initial stiffness and high final stiffness under compression, causing acceleration inputs to be gradually decreased.
- Increases in stroke length by additional air bladder seat cushion thickness can increase acceleration reduction.
- The air bladder seat cushion proposed has an interconnected bottom and back sections, providing simultaneous protection in multiple axes.
- The air bladder seat cushion response is inherently rate dependant on the input acceleration due to internal damping caused by the flow of air from one compartment to another.
- The air bladder seat cushion provides superior support with rough-ride/vibration situations over traditional foam cushions and even stiffer EA devices focused more on shock alone.

1.5 Overview of Work

The primary objective of the research reported in this thesis was to focus on the experimental characterization of the seat air bladder for mine blasts and continuous vibration. This information is essential for the design of future shock and vibration isolated seat systems that can have a wide variety of applications.

The work previously conducted on the topic of the air-bladder seat concept would be incomplete without a proper and robust testing phase. This phase is necessary for immediate implementation of specific bladder configuration in the field, as well as for future improvement and validations of numerical models.

The body of this work will discuss the most recent design phase, which initiates a more elaborate design process by creating a series of four-bladder systems that can be used in a product optimization design of experiment (DOE) in the future. The configurations were constructed using three-parameters at two levels, resulting in four prototypes, which will be described in Chapter 3.

The thorough testing of the bladder-system was conducted through shock, continuous random vibrations including real military ride acceleration data, as well as characterization of the dynamic pressure in the system, which until now had not been conducted.

1.6 Project Objectives

1. Develop air bladder seat cushion technology that is effective in reducing the potential for serious or fatal injuries to military vehicle occupants who are exposed to extreme shocks from mine blasts and improvised explosive devices. Also extend the

technology to also be suitable for reducing the transmitted lower-level continuous vibration which has serious injury potential over normal ride durations.

2. Develop an understanding of how the different system components associated with air bladder seat cushions interact with each other in reducing whole body exposure to shock and vibration through a robust and elaborate testing phase consisting of shock, vibration, and dynamic pressure measurements.

3. Quantify through measurements the effectiveness of air bladder seat cushions in reducing the energy associated with shock inputs to seated individuals that is transferred to the pelvis and spine, through the use of a seated THOR III antropodynamic dummy by analyzing: *pelvic accelerations, spinal loads, and dynamic response indexes (DRI).*

4. Based on the measurements and analyses, make suggestions of air bladder seat cushion configurations that could be used in production seat cushions or suggestions, from the available cushions, for immediate field implementation based on a shock or vibration environment.

5. Create a body of work through measurement information with respect to reductions of input shock acceleration and continuous vibration to accurately upgrade or redevelop analytical models used to predict both sir bladder seat cushion performance and seated biomedical human responses to both shock and vibration.

CHAPTER 2

INJURY ASSESSMENT

This chapter will discuss injury assessment criteria including the international and NATO standards on the human exposure to shock and vibration, and the measurement and evaluation requirements for shock, impulsive vibration, and continuous vibration criteria focused on in this work are Peak-Instantaneous Acceleration, Dynamic Response Index, Spinal Loading, Vibration Dosage Method, and Frequency Weighted Response to Whole Body Vibration. The experimental protocols, test methodology, and measurement procedures will be discussed separately in Chapter 4.

2.1 Injury Criteria and Assessment

A major area of emphasis in the study of biomedical or biomechanical engineering is the quantification and classification of potential injury to the various systems of the body. Although modes of injury and failure of both musculoskeletal and organ systems have been tested by various researchers. Musculoskeletal systems are of particular interest because of their catastrophic nature of their failures. Moreover the most likely initial cause of damage to the occupants is to their musculoskeletal systems in the form of major localized trauma and bone fracture. Those injuries can be fatal or cause permanent damage resulting in the loss of limbs, paralysis, or even simply incapacitation. While not immediately obvious, incapacitation can be just as hazardous in a combat situation eliminating the soldier's ability to defend themselves, leading to capture or death.

Damage to the major organ systems are also relevant as NATO [11] has also addressed injury criteria to the thorax and acknowledged the potential of death due to

aortic complications or traumatic brain injury (TBI), even without the presence of major skeletal damage. This study will primarily focus on the aforementioned skeletal threat. Although it should be noted, that given the massive amount of data collected during this study, this information can lend itself to future analyses of a variety of injury-metrics and injury-scales.

The complexity of injury biomechanics, as well as the large degree of variability between individuals makes quantification of a system's injury reduction potential difficult. There is still not a single widely accepted metric by which to judge injury. However for the available metrics currently used in the field, the majority maintain a "threshold limit," a defined cutoff number which defines the maximum allowable exposure. These threshold limits vary between injury metrics.

2.2 Abbreviated Injury Scale

The Abbreviated Injury Scale (AIS) is a common scale that can be found referred to by several other metrics when describing the severity of an potential injury inducing event, when a certain threshold limit is reached. It is useful to describe the injury potential below the threshold value. Risk curves are usually generated using medical data, particularly *ex vivo* test information. The vertical motion direction, particularly spinal damage is the primary focus of most mine blast studies [12]. Figure 2.1 gives examples of typical risk curves that can be applied to spinal injury in the AIS. Each corresponding curve corresponds to a specific coding of injury severity, given in Table 2.1. Many injury metrics choose to refer back to the AIS scale when describing injury potential.

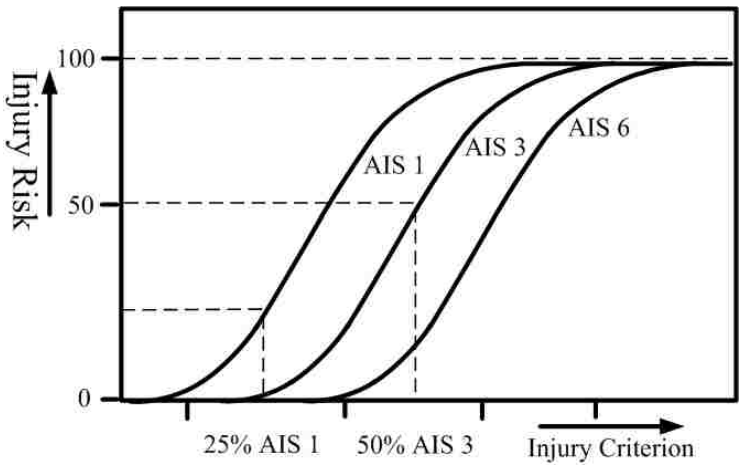

Figure 2.1 Typical Injury Risk Curves

AIS Code	Injury Description
1	Minor
2	Moderate
3	Serious
4	Severe
5	Critical
6	Maximum (currently treatable)
9	Unknown

Table 2.1 Abbreviated Injury Scale Codes

2.3 Evaluation of Human Exposure to Whole Body Vibration

The scope of the ISO Standard 2631 [3,4] encompasses the evaluation of whole body exposure and response to mechanical vibration and shock. ISO 2631-1 specifically deals with the "measurement of periodic, random and transient whole-body vibration." While this does not directly relate to mine-blasts in particular, it does allow for the additional classification of a particular seat-system, specifically air-bladder configuration's response to a random vibration input. In addition the standard provides a weighting system for the frequency range of 0.1-80Hz. Specifying 0.1-0.5Hz for motion sickness and 0.5-80Hz for health, comfort, and perception. Since only the effects of health are considered, the

accelerometers used were all of the piezoelectric nature and thus their loss of accuracy below 1Hz is not an issue.. Whole body-vibration assumes a dose-effect which takes into account not only the overall magnitude of the vibration, but also the time period of exposure.

With respect to vibration exposure to health relevant literature indicates that there are effects to the long-term health of the individual, more specifically risk to the lumbar spine and the connected nervous system when exposed to long-term high-intensity vibration. This particular similarity, the concern and evaluation of the lumbar spine, with mine and shock blasts makes this vibration study on health is interesting. The health risks are due to the excessive mechanical stress and/or disturbances of nutrition distribution to the disc tissue. This may contribute to the degenerative processes in the lumbar segments including spondylosis deformans, osteochondrosis intervertebralis, and arthrosis deformans. Moreover whole-body vibration exposure may also worsen certain endogenous pathologic disturbances of the spine.

2.4 Health Risks

The EU Physical Agents Directive on Vibration or PAD(V) [13] sets the following limiting values for exposure to vibration in the workplace. However it is reasonable to use a similar approach cannot be applied as a simple means of characterizing how much exposure a given type of combat ride scenario transmits to its occupants.

	Daily Exposure Limit		Daily Exposure Action Value	
	A(8) [m/s^2]	VDV [$m/s^{1.75}$]	A(8) [m/s^2]	VDV [$m/s^{1.75}$]
Hand-arm vibration	5	91	1.15	21
Whole-body vibration	2.5	45.5	0.5	9.1

Table 2.2 EU Vibration Exposure Limit and Action Value in the Workplace.

The EU Physical Agents Directive on vibration evaluates non-impulsive vibration in terms of A(8), which is the rms vibration over an 8hr period required to give the worker the same vibration dose actually experienced in a given day. It can also be expressed using the fourth power vibration dosage value (VDV), discussed in Section 2.9.

2.5 Pelvic and Spinal Injury Criteria

For shock pulses similar to the one shown in Figure 2.2 that have a duration of less than 20 ms [14,15] the tolerance limit for the potential onset of pelvis/spine injuries for a man sitting in an upright position is a peak velocity change (V_{max} in Figure 2.2) of 20 ft/s (4.5 m/s) for the seat structure supporting the pelvis. However, that level increases to a peak velocity change of 60ft/s (18.3 m/s) when the shock pulse duration is greater than 20 ms. This typically corresponds to an average acceleration (Figure 2.3) of 15 g's (147 m/s^2). Figure 2.3 indicates that spinal injuries can occur when the pelvis/spine tolerance limit is exceeded.

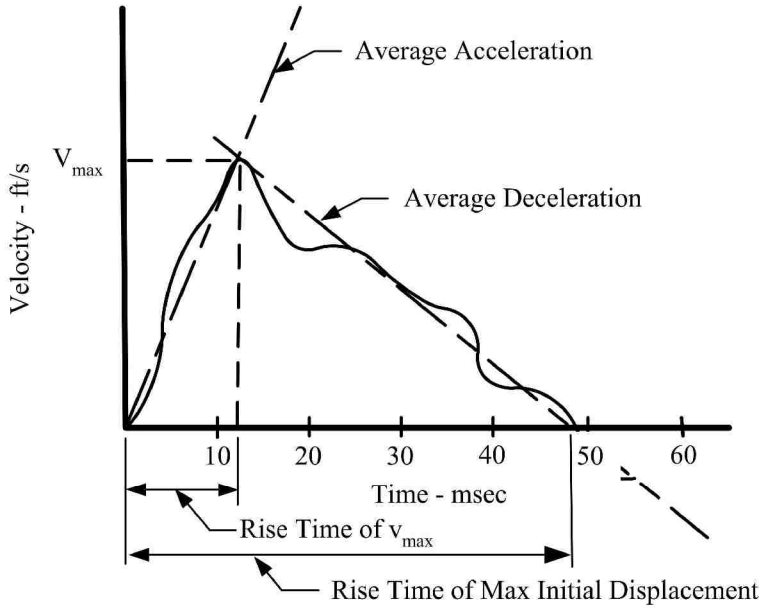

Figure 2.2 Shock Motion Terminology

The Dynamic Response Index (DRI) was developed to predict the probability of thoracolumbar-spine fracture, using a one-dimensional displacement model, during an flight ejection event [14,15,16].

Federal Aviation Regulation 29 sets the maximum allowable lumbar spine load to be 1,500 lb (6,672 N) measured between the pelvis and lumbar spine to be considered safe [17]. Table 2.3 lists the lumbar spine tolerance levels recommended by the US Army.

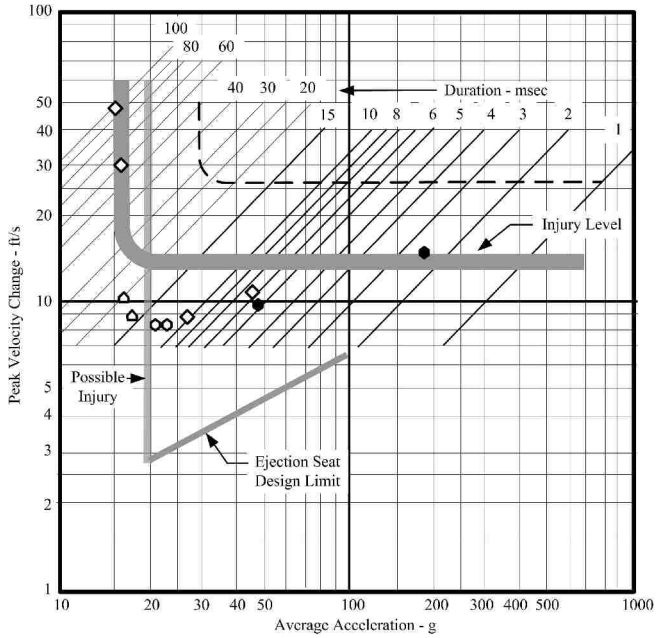

Figure 2.3 Shock Input Tolerance Levels for a Seated Man [14]

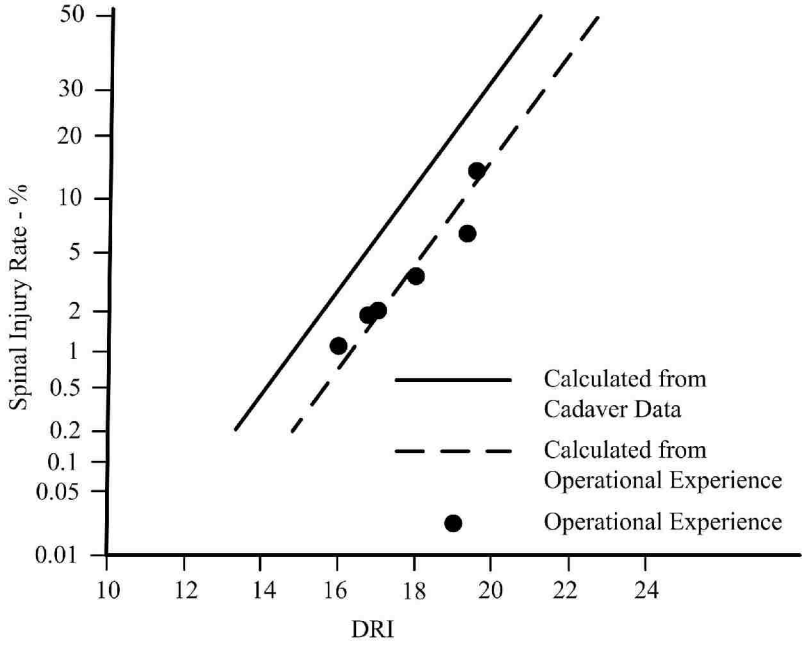

Figure 2.4 Spinal Injury Rate as a Function of DRI for Aircraft Seat Ejection Events [17]

Vehicle Occupant Size (Percentile)	Lumbar Load Tolerance (lb_f)
5th Female	1,281
50th Female	1,610
50th Male	2,065
95th Male	2,534

Table 2.3 Lumbar Spine Tolerance Levels Recommended by the U.S. Army

For whole body injuries related to exposure to whole body shock events the Eiband criterion is used to predict the potential risk [15,16,17]. Vertical peak acceleration for short-term shock inputs to the pelvis should not exceed 15 g's [Figure 2.5].

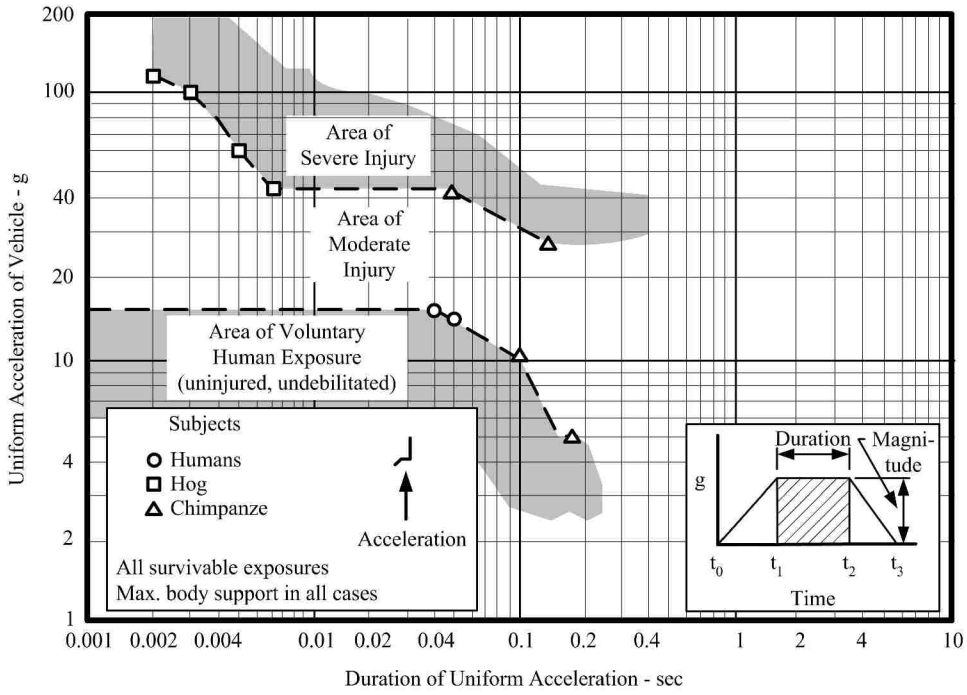

Figure 2.5 Duration and Magnitude of Vertical Acceleration (Eiband) [18]

When considering a soldier's ability to continue on with their duties, and not necessarily immediate death, another report prepared by the US Army [18] suggests that

complete incapacitation at levels where longitudinal pelvic acceleration exceeding 40 g's (392 m/s^2) for more than 7 ms or vertical pelvic accelerations exceeding 23 g's (225 m/s^2) for more than 7 ms. Also levels that would render a soldier unable to complete military tasks occurs with lumber spine bending moments in excess of 10,932 in.-lb_f (1235 N-m) in forward flexion, 3,276 in-lb_f (370 N-m) in rearward extension, and 5,976 in-lb_f (675 N-m) in lateral bending, regardless of their duration period.

As previously mentioned, such an event can be considered nearly as severe as a fatal accident because it can expose the soldier to capture, or even the death of the fellow crew members whom rely on effective performance of said tasks for survival.

2.6 Mine Blast Injury Criteria

In addition to the usage of DRI for evaluation of a mine blast event, Table 2.4 summarizes landmine injury criteria proposed by Axelsson [15]. Table 2.5 summarizes landmine injury criteria proposed by Alem et. al. [19]. Figure 2.6 summarizes the recommended injury criteria for vehicles exposed to landmines that is presented in the U.S. Army's Occupant Crash Protection Handbook for Tactical Ground Vehicles [17].

Body Part	Type of Load	Tolerance Value
Brain	$HIC = (t_2 - t_1)\left[\frac{1}{t_2 - t_1}\int_{t_1}^{t_2} a(t)dt\right]^{2.5}$	1,000
Neck	Compression	250-900 lb_f
Neck	Tension	250-750 lb_f
Neck	For-Aft Shear	250-700 lb_f
Chest	Serious Thoratic Injury	60 g's
Lumbar Spine	Vertical Direction	1,500-1,800 lb_f
Seat Design Limit	Vertical Direction	< 14.5 g's

Table 2.4 Landmine Injury Criteria Proposed by Axelsson.

Foot/Ankle Shock Acceleration	Average Acceleration < 10 g's or Maximum Velocity Change < 3 m/s
Pelvis/Spine Shock Acceleration	Average Acceleration < 15 g's or Maximum Velocity Change < 4.5 m/s
	DRI $\leq$ 16

Table 2.5 Landmine Injury Criteria Proposed by Alem et. al.

2.7 NATO Testing and Evaluation Injury Criteria

The North Atlantic Treaty Organization published a report in April 2007 [11] summarizes injury criteria for the purpose of the experimental testing and design of vehicle occupant protection systems. Vehicle and occupant interaction was studied taking into consideration human biomechanics, vehicle structural behavior during blast occurrences, and experimental measurements. It is this report that recommends the usage of the Dynamic Response Index (DRI) for shocks and mine-blast occurrences. They even suggest that the DRI be the sole evaluation standard for protection against thoraco-lumbar spine injury. The decision to do so was because only the DRI model accounts for the duration of the pelvic-acceleration and has been validated with medical data. The NATO committee recommends using an anthropomorphic test device (ATD) and calculating the resulting DRI with only the vertical z-axis acceleration from the pelvis, measurement variability is at a minimum in this location. With this technique a threshold level of 17.7 DRI will correspond to a 10% risk (AIS 2+) spinal vertebrae injuries. The committee also adds that this is only valid for spine inclinations of less then or equal to 5 degrees.

Hybrid III Simulant Response Parameter	Symbol (units)[a]	SAE Filter	Assessment Reference Values[b]
Head resultant acceleration Head injury criterion	A (G) HIC	CFC 1000 (1650 HZ)	150 G @ 2 msec. 750, ~ 5 % risk of brain injury for $t_2 - t_1$ < / = 15 ms *
Chest resultant acceleration	A (G)	CFC 180 (300 HZ)	60 G @ 3 ms, 40 G @ 7 ms
Pelvis forward acceleration Pelvis lateral acceleration Pelvis vertical acceleration	Ax (G) Ay (G) Az (G)	CFC 180 (300 HZ)	40 G @ 7 ms 23 G @ 7 ms 23 G @ 7 ms
Seat (Pelvis) forward DRI Seat (Pelvis) lateral DRI Seat (Pelvis) vertical DRI	DRI – x (G) DRI – y (G) DRI – z (G)	CFC 180 (300 HZ)	35, 40, 46 Gx (low, med, high risks) 14, 17, 22 Gy (low, med, high risks) 15, 18, 23 Gz (low, med, high risks)
Neck shear force Neck axial compressive force Neck axial tensile force	Fx or Fy (N) - Fz (N) + Fz (N)	CFC 1000 (1650 HZ)	1100 N (45 ms), 1500 N (25-35 ms), 3100N (0 ms) 1100 N (30 ms), 4000 N (0 ms) * 1100 N (45 ms), 2900 N (35 ms), 3300 N (0 ms)
Neck lateral moment Neck forward flexion moment Neck rearward extension moment	Mx (N-m) + My (N-m) - My (N-m)	CFC 600 (1000 HZ)	105 N-m 190 N-m 57 N-m
Lumbar spine shear force Lumbar spine axial compression force Lumbar spine axial tension force	Fx or Fy (N) - Fz (N) + Fz (N)	CFC 1000 (1650 HZ)	[c] 3800 N (45 ms), 5200 N (25-35 ms), 10700 N (0 ms) 3800 N (30 ms), 6673 N (0 ms) [c] 3800 N (45 ms), 10200 N(35 ms), 12700 N (0 ms)
Lumbar spine lateral moment Lumbar spine flexion moment Lumbar spine extension moment	Mx (N-m) + My (N-m) - My (N-m)	CFC 1000 (1650 HZ)	675 N-m 1235 N-m 370 N-m
Femur or Tibia axial compression force	Fz (N)	CFC 600 (1000 HZ)	7562 N (10 ms), 9074 N (0 ms)
Tibia axial compressive force combined with Tibia bending moment	F (N) M (N-m)	CFC 600 (1000 HZ)	F / Fc – M / Mc < 1 Where: Fc = 35,584 N and Mc = 225 N-m

[a] x = Longitudinal, y = Lateral, z = Vertical
[b] Exceeding values indicates a moderate to high risk of major injury
[c] Approximately 3.4 times neck force values
* Recommended deviations to referenced values.
DRI = Dynamic Response Index. CFC = Channel Frequency Class

Reference: Chapter 6, "Physical Testing and Data Analysis", of Final Report entitled, "Protection of Wheeled Vehicle Occupants from Landmine Effects", Land Systems Div, U.S. Army Aberdeen Test Center

Figure 2.6 Recommended Injury Criteria for Landmine Testing by the U.S. Army [18], 2000

2.8 ISO Weighting of 1/3-Octave Band Data for Continuous and Impulsive Vibration

As in the consideration of shock information, although there is some belief that the horizontal seated axes (x and y axes) could possibly provide some useful information, only the vertical axis and the concern for the lumbar spine will be analyzed. ISO 2631, referenced in section *2.3 Evaluation of Human Exposure to Whole Body Vibration* provides a weighting scale shown here. The weighting factors applied in the vertical direction to a seated-subject (Wk) represented for the relevant 1/3-octave band. For the purposes of this study, the frequency range is extended to 100Hz:

Hz	**Wk**		**Hz**	**Wk**
1	0.482		12.5	0.902
1.25	0.484		16	0.768
1.6	0.494		20	0.636
2	0.531		25	0.513
2.5	0.631		31.5	0.405
3.15	0.804		40	0.314
4	0.967		50	0.246
5	1.039		63	0.186
6.3	1.054		80	0.132
8	1.036		100	0.0887
10	0.988			

Table 2.6 Third-Octave Band Weighting Factors for the Vertical Direction for Whole Body Vibration

2.8.1 Whole-Body Weighted Acceleration

The weighted r.m.s acceleration is expressed in m/s^2 for translational vibration and $radians/s^2$ for rotational vibration. Where T is the measurement duration is seconds, the weighted r.m.s acceleration should be calculated by:

$$a_w = \left[\frac{1}{T} \int_0^T a_w(t)^2 dt \right]^{\frac{1}{2}}$$ **Equation 2.1**

Or the frequency domain equivalent where i represent the frequency band number, in this case, more specifically the 1/3 octave-band frequencies:

$$a_w = \left[\sum_{i=1}^{N} \left(W_i a_i^{\,2} \right) \right]^{\frac{1}{2}}$$ **Equation 2.2**

where:

a_w is the frequency weighted acceleration as a function of time (m/s^2 or rad/s^2).

Wi is the weighting factor for the i-th one-third octave band given in Table 2.6.

a_i is the r.m.s acceleration for the i-th one-third octave band.

If it is determined that there is more than one significant acceleration direction, than the overall weighted acceleration can be calculated by:

$$a_v = \left[k_x^{\,2} a_{wx}^{\,2} + k_y^{\,2} a_{wy}^{\,2} + k_z^{\,2} a_{wz}^{\,2} \right]^{\frac{1}{2}}$$ **Equation 2.3**

Where:

a_{wi} refers to the r.m.s weighted acceleration in each basicentric axis

k_i are the multiplying factors in each major axis dependent on the body configuration.

Weighting Multiplication Factors		
k_x	k_y	k_z
k=1.4	k=1.4	k=1

Table 2.7 Multiplying Factors for Health in the Seated Position

2.9 Impulsive Vibration and the Vibration Dosage Value (VDV)

There has been some discussion to the benefit of using a "dosage method" as opposed to a purely running r.m.s acceleration method. The vibration dose value (VDV) is more sensitive to peaks than the basic evaluation method. The fourth-power vibration dose method (VDV) is in $\frac{m}{s^{1.75}}$ or $\frac{rad}{s^{1.75}}$ and is defined as:

$$\mathrm{VDV} = \left[\int_0^T a_w(t)^4 dt\right]^{\frac{1}{4}} \qquad \textbf{Equation 2.4}$$

However, since vibration measurements are typically conducted in the frequency domain, it is often more useful to consider a method of evaluating the VDV without the necessity of measuring and weighting the complete time history of an event. The estimated vibration dosage value (eVDV) has been used in some studies and shows good agreement when the crest factor, the ration of the frequency weighted maximum peak to its r.ms. value, is less than 6.

$$\mathrm{eVDV} = 1.4 a_w T^{\frac{1}{4}} \qquad \textbf{Equation 2.5}$$

Where T is again the duration in seconds.

2.10 Dynamic Response Index (DRI) Measurement

The DRI uses a simple mass-spring-damper system (Figure 2.7) with base excitation to predict the response of an aircrew member subjected to abrupt vertical acceleration during seat ejection. The equation of motion is given by [DRI EQUATION]:

$$\frac{d^2\delta(t)}{dt^2} + 2\xi\omega_n \frac{d\delta(t)}{dt} + \omega_n{}^2\delta(t) = \ddot{z}(t) \qquad \textbf{Equation 2.6}$$

where

$\delta(t)$ = defection of the seat system (in, m)

ξ = damping ratio (dimensionless)

ω_n = resonance frequency (rad/s)

$\ddot{z}(t)$ = acceleration of seat supporting the pelvis (in/s^2, m/s^2).

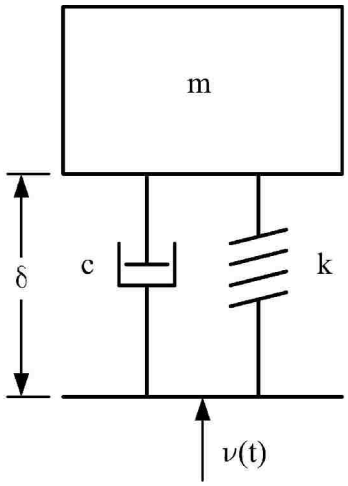

Figure 2.7 DRI Mass-Spring-Damper System

A Equation 2.6, the DRI is representative of the maximum dynamic compression of the vertebral column. The DRI model assesses the response of the human body to transient acceleration-time profiles. The equation for computing the DRI is:

$$DRI = \frac{\omega_n{}^2\delta(t)_{MAX}}{g} \qquad \textbf{Equation 2.7}$$

where:

δ_{max} = maximum defection of the seat system (in, m).

The solution to the DRI Equation 2.6-2.7 is solved by using a known input acceleration signal in the vertical direction of the pelvis, $\ddot{z}(t)$ for the case where ω_n equals 52.9 rad/s (8.4 Hz), ξ equals 0.224 [12], and g is the acceleration of gravity (386 in./s^2, 9.8 m/s^2. The maximum displacement δ_{max} (in, m), is used in Equation 2.7 to determine the DRI value. This pelvis acceleration signal is difficult to obtain unless the researcher has access to an anthropomorphic dummy. Figure 2.4 shows a plot of the spinal injury rate percentage as a function of DRI [14,17]. An injury limit of a DRI of 17.7 was used as a metric during testing at the Army Research Lab as well.

CHAPTER 3

AIR BLADDER SEAT CUSHION DEVELOPMENT

Extensive testing at the University of Nevada, Las Vegas, Center for Mechanical and Environmental Technology laboratory has been performed to determine the physical parameters of the air pneumatic seat cushion and its response to a variety of shock and vibration situations. In addition to the more elaborate shock and vibration testing, the seat cushion development was accomplished in part by creating four prototype cushions, each with varying parameters designed to fulfill a fractional design matrix for a future design of experiment (DOE) setup, not conducted in the main body of this work. This was done with three parameters at two levels each, creating a fully orthogonal Taguchi Test matrix. A summary of this development is given in this chapter.

3.1 Air Bladder Seat Cushion Description

The air bladder seat cushion was constructed by using a low-density, open-cell foam which has been bonded only by its top and bottom surfaces in an impermeable outer covering (Figure 3.1), and allowed to inflate itself to atmospheric pressure, at which time the air vents are closed and the system becomes completely enclosed. The system itself consist of two major components, the seat bottom and the seat back, which are joined by a series of tubes acting as vents to allow the passage of air from the seat bottom to the back as the seat is compressed during any number of vibration or shock events. To facilitate the flow of the air between the two components, the foam has had channels cored through it using a proprietary process, the pattern of which is also proprietary.

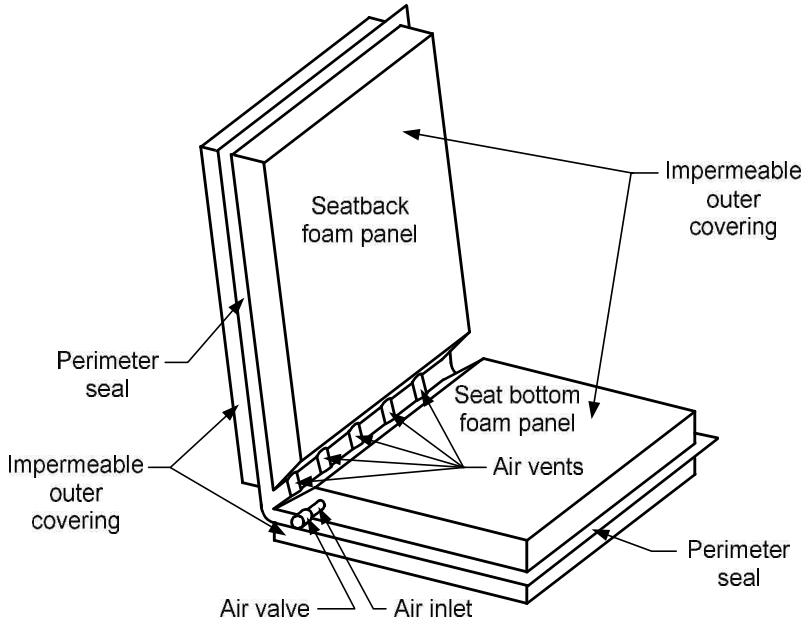

Figure 3.1 Drawing of Pneumatic Seat-Bladder System with Connected Seat-Bottom and Seat-Back

3.2 Prototype Configurations for future Design of Experiment (DOE)

A total of four seat configurations are being tested in hopes of leading towards a more ideal configuration for latter phases of the design project. Three parameters are varied at two levels in order to perform a fully orthogonal Taguchi-test matrix. The parameters are *Foam Density, Foam Hole Diameter, orifice-tube inner-diameter*. The prototypes were redesigned to accommodate simultaneous dynamic pressure testing of both the seat bottom and seat back of the pneumatic air-cushion.

Bladder Configuration Parameters			
Bladder Number	**Foam Density**	**Foam Hole Diameter**	**Internal Tube Diameter**
1	1 lb/ft^3	0.5 in	0.375 in
2	1 lb/ft^3	1 in	0.25 in
3	2 lb/ft^3	0.5 in	0.25 in
4	2 lb/ft^3	1 in	0.375 in

Table 3.1 Parameter Configurations of Seat Prototypes

3.3 Previous Modeling

The previous work developed an intricate numerical model of the body, cushion, and load-limiter interactions. However, a significant portion of the modeling revolved and depended upon the ability to predict the effect of internal pressure, and its effects on stiffness and damping, and thus the transmissibility to the seated occupant. The response of the air was determined using an isentropic compression equation.

A finite differencing, marching solution was chosen to solve the equations in terms of the known input acceleration of the floor. Velocity and displacement were calculated by:

$$\dot{z}_0(i+1) = \dot{z}_0(i) + \ddot{z}_0(i+1)\,\Delta t \qquad \textbf{Equation 3.1}$$

$$z_0(i+1) = z_0(i) + \dot{z}_0(i+1)\,\Delta t \qquad \textbf{Equation 3.2}$$

where:

Δt = the numerical solution time step (s).

The numerical model to determine the performance of seat system components, a multi-dimensional model was written in MATLAB. The model was a five-degree-of-freedom mass-spring-damper (MCK) representation of the seat system's components and a human occupant. Figure 3.2 and Figure 3.3 shows the schematic of Wolf's model and its free-body diagram respectively.

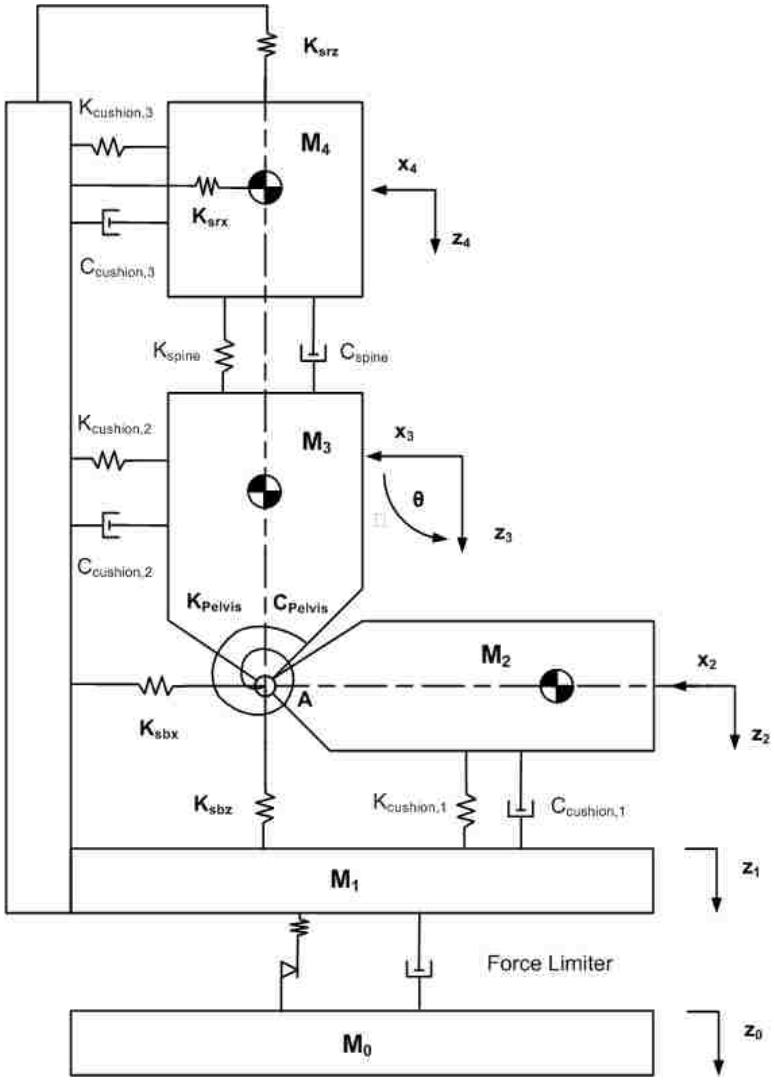

Figure 3.2 Numerical Model Schematic

The MCK parameters for the human body that were used were developed by Cheng [8]. That work developed the human model for use in modeling helicopter seat cushions. Cheng's two-mass model is a semi-definite system with a resonance frequency (52.9 rad/sec) and damping ratio (0.224) equal to that of the DRI model, and found in the NATO standard.

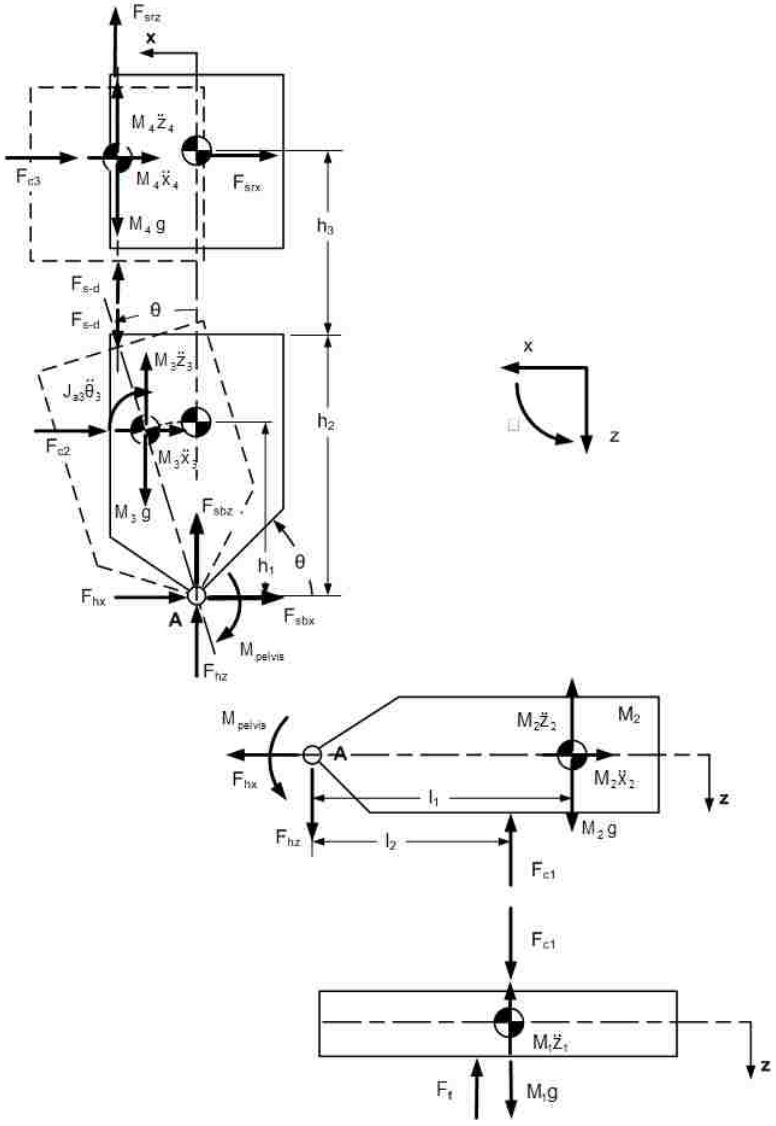

Figure 3.3 Free Body Diagram

Component	Mass	K (N/m)	C (Ns/m)
Legs	12		
Pelvis	8.18	8065.2	513.7
Upper Torso	34.52	96600	818.8
Resonant Frequency	52.0 rad/s		
Damping Ratio	0.224		

Table 3.2 Human Body Model Parameters [12]

3.4 Pressure Consideration

While this model worked reasonably well, it is believed that the model underestimated the dynamic magnitude of the pressure. This is one issue that is addressed in this study as the dynamic pressure in both the seat-bottom and seat-back are now measured.

The numerical portion of the model representing the pressure response to compression, as previously mentioned, is that of isentropic compression.

$$P_{cush} = P_{atm}\left(\frac{V_1}{V_2}\right)^{\gamma} - P_{atm}$$

where:

γ = ratio of specific heats ($^{Cp}/_{Cv}$) **Equation 3.3**

V_1 = the total volume of the seat cushion (m)

V_2 =the reduced vloume of the cushion during compression (m)

P_{atm} = atmospheric pressure $(101325\ \mathrm{Pa})$

The model assumed that the volume of the seat back expands linearly while the seat-bottom is compressed until it the back is fully inflated or stretched, at which point it ceases to expand. The resilient material of the cushion covering is responsible for this. Moreover, during the initial compression of the bottom, the cross-sectional perimeter does not change, stating that this results in a minimal pressure increase at the beginning of the cycle. Wolf accounts for this by modifying the isentropic pressure equation to:

$$P_{cush} = \left(P_{atm}\left(\frac{V_1}{V_1 - EF\{V_0 - [(L_{leg} + \delta_{cush})^2\,\delta_{cush}]\}}\right)^{\gamma} - P_{atm}\right) \quad \textbf{Equation 3.4}$$

where:

P_{cush} = internal cushion pressure (Pa)

EF = the expansion factor, a ratio representing the expansion of the seat cushion back to the compression of the bottom. (0.58)

V_1 = the original air cushion volume (m^3)

V_0 = the original seat cushion bottom volume (m^3)

L_{leg} = the length of the leg contacting the seat cushion (m)

δ_{cush} = the z-axis compression of the cushion bottom (m).

3.5 Force- Compression Testing

This portion of the testing was conducted both at the original conception of the project and during this current characterization phase. All variations of the seat underwent low speed compressions on a Material Test Systems (MTS) hydraulic tensile test machine. In order to separate previous work (with Wolf and Ladkany) with current testing, all of the most recent testing protocols will be located in Chapter 4 while all pressure testing results will be presented in Chapter 6.

The previous round of testing on the MTS machine was done by placing the seat cushion bottom oversized aluminum plate on the bottom and a human seat form made from dense fiberboard. The internal pressure of the cushion at the start of the test was 0 psig. The same procedure was repeated with the bottom of the seat cushion separated entirely from the back to determine the response of the foam alone. The principle behind the testing was to validate the numerical model and was done so by assuming that the foam and the air responses could be calculated using the principle of superposition.

Discussion of the pressure and force-compression measurements will be provided in Chapter 6 along with the dynamic pressure data collected simultaneously from UNLV drop tower shock tests.

3.6 Dynamic Pressure Consideration

While the Wolf's numerical model shows strong agreement with the experimental results at low speeds, and even reasonable agreement with peak responses for both pelvic accelerations as well as DRI the remainder of the response would benefit from improvement. More importantly the four prototype configurations previously described were configured with two ports, one on the seat bottom while the second on the seat back allowing for simultaneous dynamic pressure measurements. This is of great interest because it provides a foundation for future work in developing a more accurate and complete model of coupled air-bladder seat systems. This gives the design potential for modifications to suit a wider variety of applications and shock and vibration profiles. In doing so, such systems could be relatively quickly, individually tailored for any application, whether it be for commercial trucking, landmine occupant protection, or even medium-scale repetitive shocks.

One of the issues in the previous experimental testing addressed in this study was the nonlinearity during shock and impulse events. The numerical modeling was fairly successful in describing the response of the cushion as a whole, and this is in part to the detailed description of the isentropic pressure within the cushion. Preliminary testing showed that the dynamic pressure could reach as high as 12psig in the seat bottom when drop heights were set as high as 50in with a violent non-periodic pulse.

The high internal pressures in the seat cushion during a dynamic compression caused by shock were not discovered until the testing drop/shock towers at UNLV were constructed and dynamic pressure measurements were even possible. A more complete description will be given in Chapter 6 along with a description of the shock profiles

causing the dynamic pressure pulses, while a description of the UNLV shock performance is given in Chapter 8.

CHAPTER 4

TEST PROTOCOLS AND EXPERIMENTAL CHARACTERIZATION

As previously mentioned, the primary focus of this project is the experimental characterization of various configurations of the pneumatic seat cushion. In order to provide a complete representation of the seat system's capability and provide information for future modeling and design iterations the following general experimental test categories were explored: internal pressure (both quasi-static and dynamic), force-deflection, vibration transmissibility, and shock response.

During the previous phase of this project one configuration of the cushion was actually tested at the Army Research Lab in Maryland, and this test was only performed using a drop tower at their facility. Moreover the drop tower used only a single configuration of mitigating material to create the shape of shock pulse. This shock pulse on average, had a pulse width of 5 ms and amplitude dependent on the drop height used for that specific experiment.

The testing performed at UNLV's own facilities was more extensive and also included quasi-static and dynamic pressure as well as random vibration testing.

4.1 Army Research Lab Testing

All though the Army tests were both informative and useful; they only represented one possible configuration for this pneumatic seat cushion. Three separate trips and testing series were conducted in Maryland all of which were of a shock nature and consistently produced of 5 ms sine shock pulse. This was done because of the Army's particular interest in the usage of the Dynamic Response Index (DRI) to characterize

damage to the spinal column, where DRI has been validated through aircraft ejection seat studies, catapult tests, and drop tests [20,21] however a 2007 ARL report by McAndrew [22] states that using DRI to predict injury sustained from blast loading has not yet been validated.

The data collected during the drop tests was done using a THOR III 50% male anthropomorphic dummy weighing 170lbs. This anthropomorphic test device (ATD) is designed to mimic of the human body and is instrumented in many measurement locations. Of particular interest to ARL and our testing are the pelvic acceleration as well as the force measured in the spinal column. In addition to the instrumentation in the ATD, two accelerometers are in the base of the drop platform, one on each side; the shock pulse shown is an average of the two signals. Also an SAE seat-pad accelerometer, the same used in the UNLV drop tests with a nominal sensitivity of 10mV/g, and peak acceleration of 500g was used.

4.2 UNLV Drop Tower Testing

Two drop towers were designed and constructed in-house over the course of the grant. One of the drop tower stands at the total height of 12 feet, with a steel platform weighing in excess of 300 lbs. The first drop tower uses two robust bearing shafts, located on either side, which controlled the dissent of the seat platform. The second of the drop towers was much lighter in its overall construction carrying an lighter aluminum platform which consisted of four bearing shafts one located at each of the corners of the seat platform. The usage or four bearing shafts, as well as a lighter platform and an impacting surface of the smaller area, capable of various mitigating materials, were

implemented in hopes of creating a less noisy input signal and a more controlled descent than that of the larger and heavier drop tower.

For instrumentation the same SAE seat-pad accelerometer was used to measure acceleration at the seat-butt interface, and a 2mV/g dytran shock-accelerometer, capable of a 2500g peak. The shock accelerometer was mounted into the impact plate. This accelerometer was chosen because other more typical accelerometers which are designed with a lower sensitivity and capable of much higher accelerometers have a much higher noise floor, and a more sensitive accelerometer while also limiting the overall noise of the measured acceleration, is more appropriate for the testing done at the UNLV facilities.

Moreover, a 6 x 6" impacting plate on the located the bottom surface of the seat platform was used in order to place different mitigating materials, typically rubbers of different durometers, in order to create different shaped and width shock input pulses. Although many materials were experimented with as the impacting and mitigating contacts material, eventually a combination of a 1in thick rubber plate on the impact plate along with a thin gel-elastomer “impact gel” on the striking plate were used. This is in contrast to ARLs drop tower which uses a large mass for its strinking plate designed to smooth out the pulse and a “pulse programmer,” which helps shape a drop acceleration into a variety of desired profiles.

4.3 Quasi-Static and Dynamic Pressure Testing.

4.3.1 Force- compression testing

While using the MTS machine, the seat cushion bottom was placed between an oversized aluminum plate on the bottom and a human seat form made from MDF fiberboard. The human butt form that was used was created using specifications of the British Military of a 50% soldier's seated-impression, and had a surface area of 0.108 m^2.

The test was run at the maximum speed of the test machine at 2ips, or 0.0508m/s in compression. The acquired data was from both the machine's load cell, and simultaneous pressure measurement mounted on both fill tubes, from the seat bottom and the seat back. The internal pressure of the cushion at the start of the test was 0 psig. The cushion was also tested with both fill tubes completely opened to the atmosphere, so that only the foam-bladder skin response could be measured. It is assumed that at the low compression speed that any internal air movement would be negligible and not contribute to the foam's response, as it would if the fill tubes and the system were closed.

4.3.2 Dynamic Pressure Testing

While Wolf's numerical model shows strong agreement with the experimental results at low speeds, and even reasonable agreement with peak responses for both pelvic accelerations as well as DRI (See Chapter 3), the remainder of the response would benefit from improvement, in this case particularly a direct measurement of the dynamic pressure during a shock scenario.

The four prototype configurations previously described were configured with two ports, one on the seat bottom while the second on the seat back allowing for simultaneous dynamic pressure measurements. This is of great interest because it provides a foundation

for future work in developing a more accurate and complete model of coupled air-bladder seat systems. This gives the design potential for modifications to suit a wider variety of applications and shock and vibration profiles. In doing so, such systems could be relatively quickly, individually tailored for any application, whether it be for commercial trucking, landmine occupant protection, or even medium-scale repetitive shocks.

One of the issues in the previous experimental testing addressed in this study was the nonlinearity during shock and impulse events. The numerical modeling was fairly successful in describing the response of the cushion as a whole, and this is in part to the detailed description of the isentropic pressure within the cushion. Preliminary testing showed that the dynamic pressure could reach as high as 12psig in the seat bottom when drop heights were set as high as 50in with a violent non-periodic pulse. However, this was not discovered until the testing drop/shock towers at UNLV were constructed and dynamic pressure measurements were even possible. All of the pressure measurements were acquired with Omega pressure transducers with a constant applied voltage of 5V with a range of 0-15psig.

A complete discussion of the data will be given in Chapter 6 along with an introduction to the shock profiles associated with it. The complete description of the shock testing conducted at UNLV, during which the dynamic pressure was measured, will be provided in Chapter 8.

4.4 Random Vibration Excitation

Although only one shaker system was actually used; due to the programmability of the shaker controller a variety of vibration input spectra were capable of being tested or

recreated. Of particular interest was a signal provided to the project by the British Military. This signal was of a rough-terrain condition in a Warrior Military Transport Vehicle at the bare seat-pan. Essentially saying that this acceleration signal was taken at the soldier's seated location without any available cushioning. This is of particular interest because although this signal lacks the easily controllable profile of an artificially created signal, it gives us an insight into the actual conditions that a soldier may experience in the field. Moreover it allows us to create other vibration profiles, while acknowledging them as unrealistic field scenarios, which will be of more appropriate vibration magnitudes. This is important to realistically characterize such a device so that no artificial skewing of mitigating performance will take place.

ISO 10819 [23] discusses the methodology for testing anti-vibration gloves in accordance with other standards governing the health of individuals experiencing hand-arm vibrations. The standard is mentioned, because unlike ISO 2631, which discusses the measurement analysis of whole body vibration, potential revisions to ISO 10819 provides a suggested random vibration profile. That specific vibration profile, in regards to hand-arm vibration, is a random vibration profile consisting of a constant r.m.s-velocity of 0.01 m/s in each of the third octave center band frequencies between 25 to 1250 Hz.

For whole body vibration, the frequency range of interest is more practically between 1 and 100 Hz. It was decided to adopt the same principle of a constant r.m.s-velocity random vibration spectrum, to develop a new vibration profile that the cushion system would be subjected to. The warrior signal has more energy in the lower frequencies, so this profile would be developed to instead have higher energy levels at the higher frequencies.

One advantage afforded to the project during any and all of the vibration testing is the usage of a one-dimensional anthropomorphic dummy, which replicates the damping features of the human body and places the natural frequency of the dummy near that of the human body near 5 Hz. This 1-D “HVLab” Passive Anthropodynamic Dummy has been developed by the University of Southhampton [24]. For the vibration-transmissibility measurements, rather than using the same SAE seat-pad accelerometer used in the shock testing, a more sensitive SAE seat-pad accelerometer with a nominal sensitivity of 100mv/g and capable of only peak accelerations of 60gs was used. Again this choice for an increased sensitivity transducer was made based on the lower magnitude of the peak accelerations experienced during the two vibration signals.

4.4.1 Physical Setup

The physical seat-frame is clamped to the input-plate of the shaker in order to prevent any unwanted vertical motion. A pneumatic-seat cushion is placed in a standard seated configuration. The SAE Seat-pad accelerometer is mounted to the center of the seat cushion at the approximate location of the center of mass of a seated individual. A fiberboard butt-form is placed on top of the accelerometer and a 1-D Anthropomorphic Dummy is secured on top of the butt-form and strapped to the seat back to prevent any transverse motion of the Dummy.

Figure 4.1 Experimental Setup for Seat Vibration Transmissibility

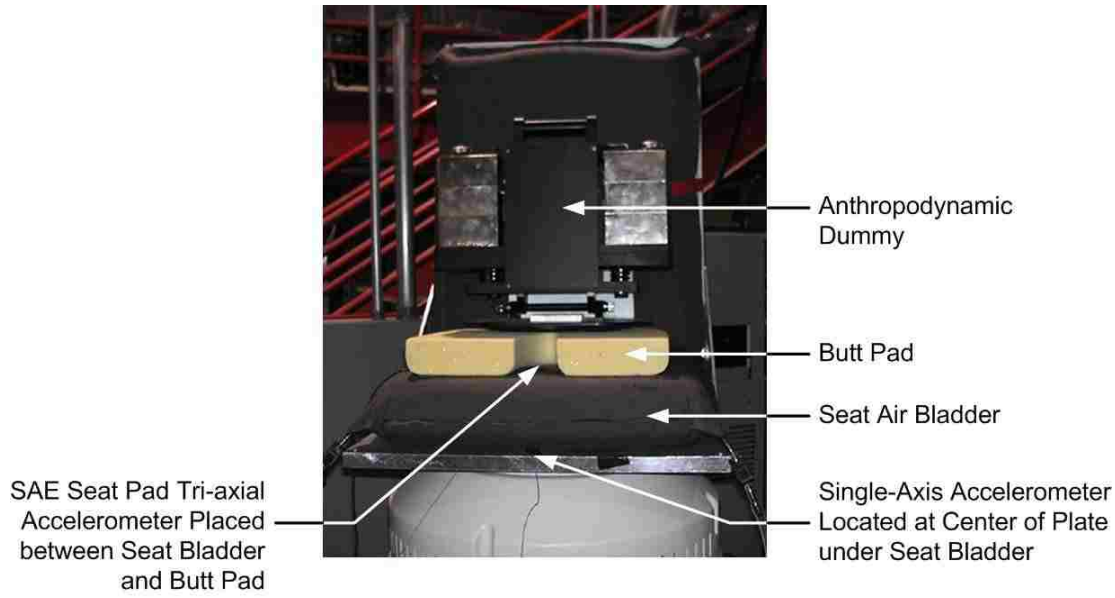

Figure 4.2 Testing and Instrumentation Overview

4.4.2 Warrior Signal Characterization

The warrior signal acquired from the British Military was a 20 second signal which was converted into a random-vibration signal with controlled frequency components from 1-400Hz. The signal was placed on an infinite loop so that the accelerometer

measurements could take place over several cycles to ensure an ergodic signal. The signal had the following dynamic properties:

Warrior Signal – Shaker Input Characteristics	
r.m.s Acceleration	1.866 m/s^2
Peak Acceleration	17.727 m/s^2
Peak Velocity	15.7653 m/s
Peak Displacement	0.1000 m peak-peak

Table 4.1 Warrior Signal Shaker Input Characteristics

These properties were calculated by the shaker and were the global properties of the signal containing all frequency components. However the actual signal properties within the 1-100Hz range, measured at the input plate are presented in the Signal Comparison section.

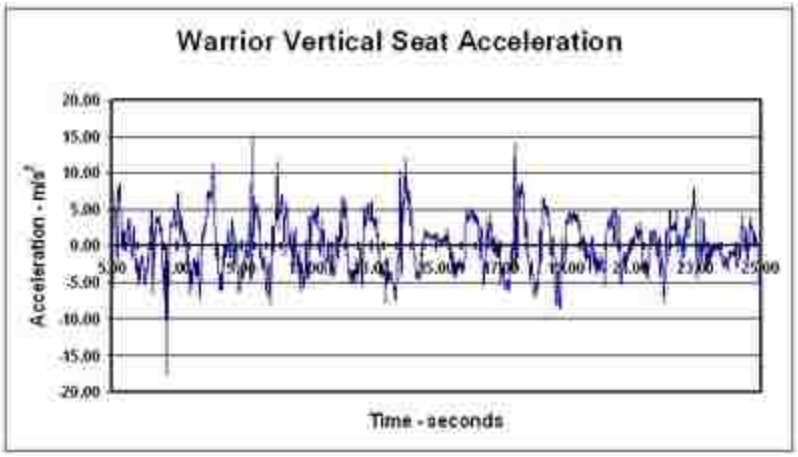

Figure 4.3 Warrior Signal Time History

4.4.3 Constant R.M.S-Velocity Signal Characterization

This signal was designed so that it has an overall ISO weighted r.ms. acceleration

similar to that of the Warrior Signal, while maintaining a constant r.m.s Velocity across each of the third octave bandwidth frequencies. Knowing that the r.m.s acceleration at a given frequency, based on its r.m.s velocity is determined by:

$$a_{r.m.s}(i) = 2\pi f(i) v_{r.m.s}(i) \qquad \textbf{Equation 4.1}$$

where:

$f(i) = i^{th}$ frequency band[Hz]
$v_{r.m.s}(i)$ = r.m.s velocity in the i^{th} frequency band
$a_{r.m.s}(i)$ = r.m.s acceleration in the i^{th} frequency band

The Power-Spectral-Density profile that the shaker system uses for its controller was developed by squaring the resulting R.M.S acceleration in each of the 1/3-Octave bands and dividing it by the appropriate frequency-bandwidth.

$$P.S.D(i) = \frac{\left[a_{r.m.s}(i)\right]^2}{\Delta f_{1/3-Octave}(i)} \quad \left[\frac{(m/s^2)^2}{Hz}\right] \qquad \textbf{Equation 4.2}$$

where:

$a_{r.m.s}(i) =$ r.m.s acceleration in the i^{th} 1/3-octave frequency band
$\Delta f_{1/3-Octave}$ = the frequency range of the i^{th} 1/3-octave frequency band

The resulting signal had the following dynamic properties calculated by the shaker and contain all present frequency components:

Constant Velocity Signal – Shaker Input Characteristics	
r.m.s Acceleration	7.381 m/s^2
Peak Acceleration	N/A
Peak Velocity	N/A
Peak Displacement	0.0055 m peak-peak

Table 4.2 Constant Velocity Signal – Shaker Input Characteristics

Again the signal properties within the 1-100Hz range, measured at the input plate are presented in the Signal Comparison section. Since this signal was not created from an actual time-history, peak instantaneous acceleration and velocity are not calculated nor were they measured separately.

4.4.4 Signal Comparison

The frequency composition of the Warrior signal could not be altered to contain only the frequencies of interest, nor was that deemed beneficial or necessary and therefore, was left unaltered. However to gain a better understanding of the signal properties and how they compare to each other, the actual outputted acceleration to the shaker plate was measured and presented here. These vibration signals and their respective outputs are weighted according to the ISO 2631:1 standard, whose weighting factors can be found in Table 2.6.

CHAPTER 5

SEAT VIBRATION TRANSMISSIBILITY RESULTS

The two aforementioned signals used in these analyses are the Warrior Transport Vehicle signal collected from a real world ride situation, and the developed Constant-RMS Velocity Signal inspired by the revision to ISO 10819. As discussed in Chapter 4, the tests were conducted on an electro-magnetic shaker, using each cushion, an SAE seat-pad accelerometer, and a 1-D anthropomorphic dummy developed by the University of Southhampton.

The signal characteristics, the vibration-transmissibility, frequency-response, and measurement characteristics are presented in this chapter. The complete discussion and analysis of the data presented here can be found in Chapter 9.

5.1 Signal Characteristics

The signals development and their acceleration profiles as entered into the shaker are presented in Chapter4.4.4. The measured plate inputs of each signal with each of the individual bladders are shown in sections 5.1.1 and 5.1.2 which characterize the two signal.

5.1.1 Warrior Signal

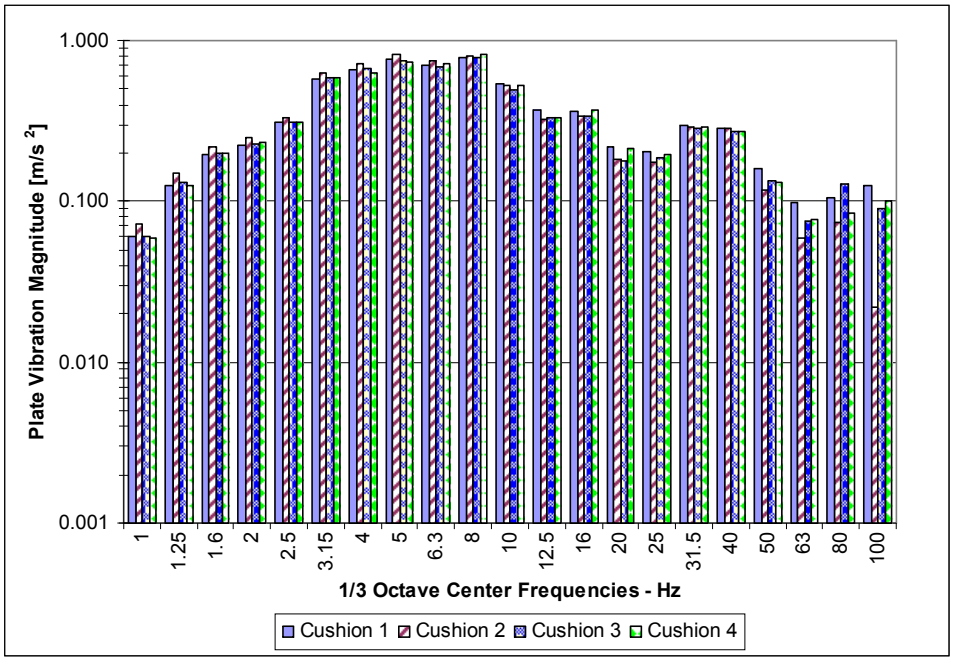

Figure 5.1 Warrior Signal Autospectrum

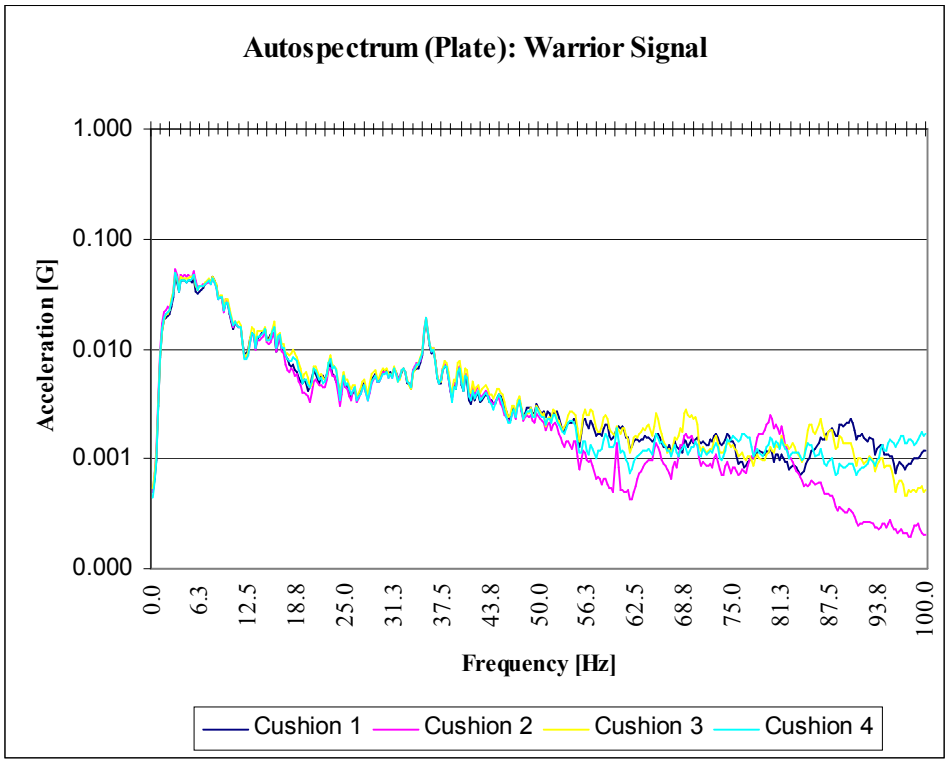

Figure 5.2 Warrior Signal FFT

5.1.2 Constant RMS Velocity Signal

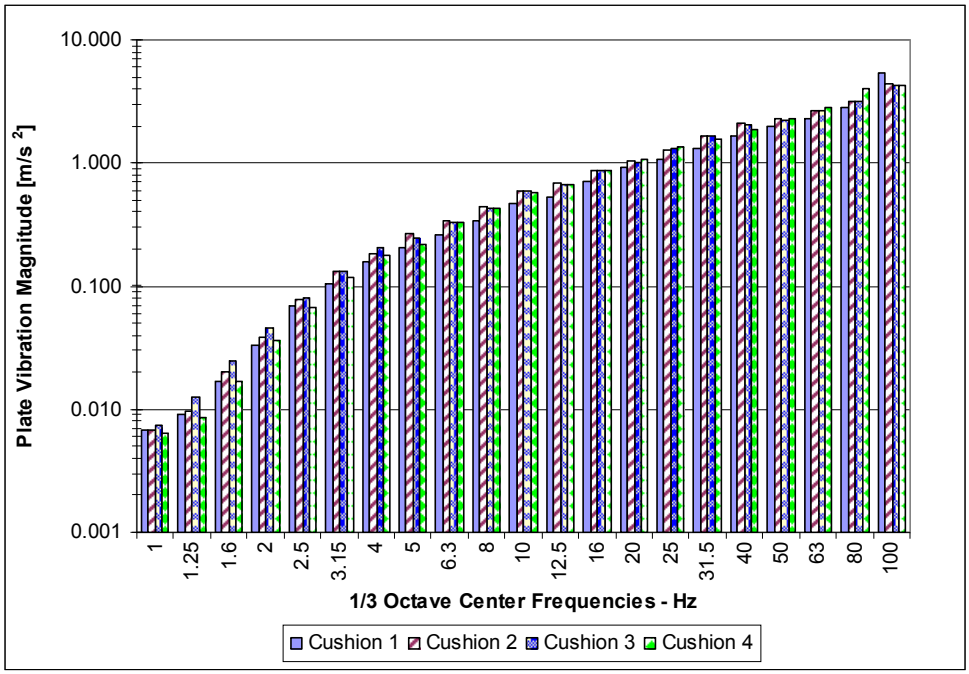

Figure 5.3 Constant R.M.S Velocity Signal Autospectrum

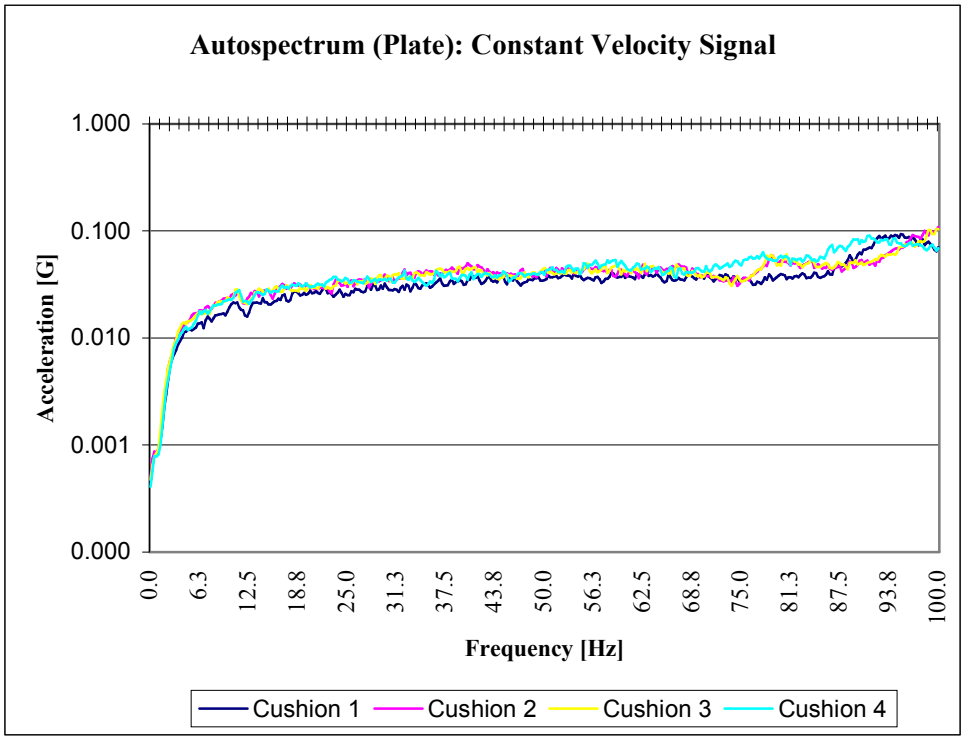

Figure 5.4 Constant R.M.S Velocity FFT

5.1.3 Signal Comparison Analysis

In comparing the structure and frequency-composition of the two signals the warrior signal contains significantly more energy in the lower 1/3 Octave Bands, and is again obtained from a real ride-terrain experiment. However the constant-r.m.s velocity signal is designed to have nearly the opposite property, increasing the energy in the higher bands. The robustness of the two signals in their respective range allows for a complete testing of the cushion, in two different scenarios, across the entire frequency range of interest from 1-100Hz.

However it should be remembered that the coherence will be low in each signal's frequency range where the energy level is low, ultimately affecting the validity of the data in that range for each signal.

5.2 Coherence

The coherence is presented here before presenting the Seat Pad Output in order to give the reader perspective on the validity and reliability of the remainder of the data.

The coherence gives an indication of the validity of a single output caused by a single input. That is to say that if there is a low coherence, a valid conclusion cannot be made that the output at a given frequency is caused by the reference input at that same frequency. See Equation 9.2.

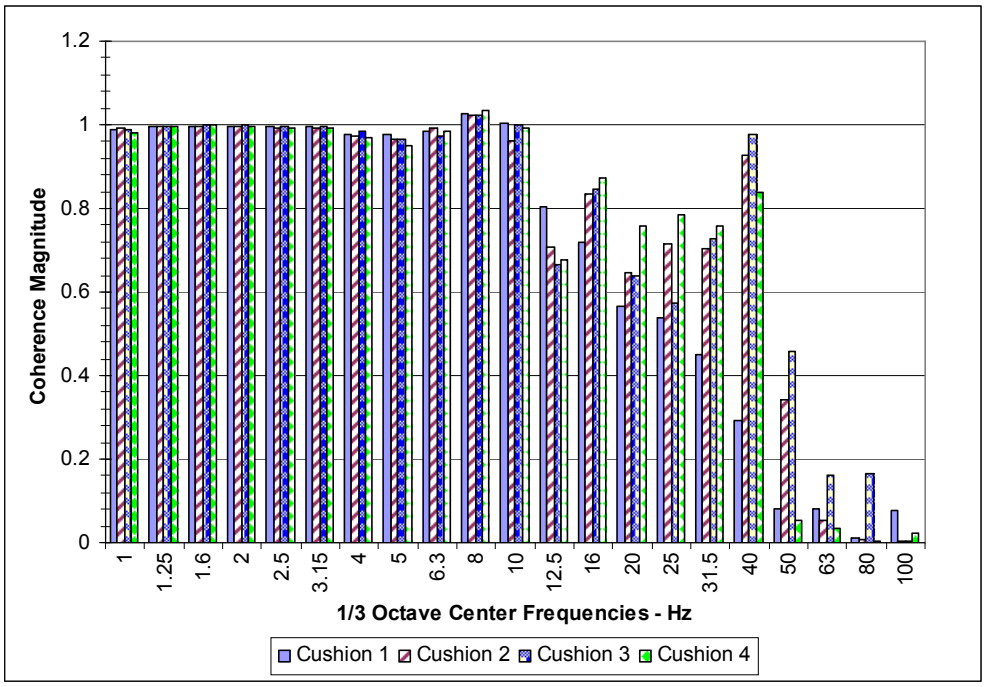

Figure 5.5 Coherence Warrior Signal

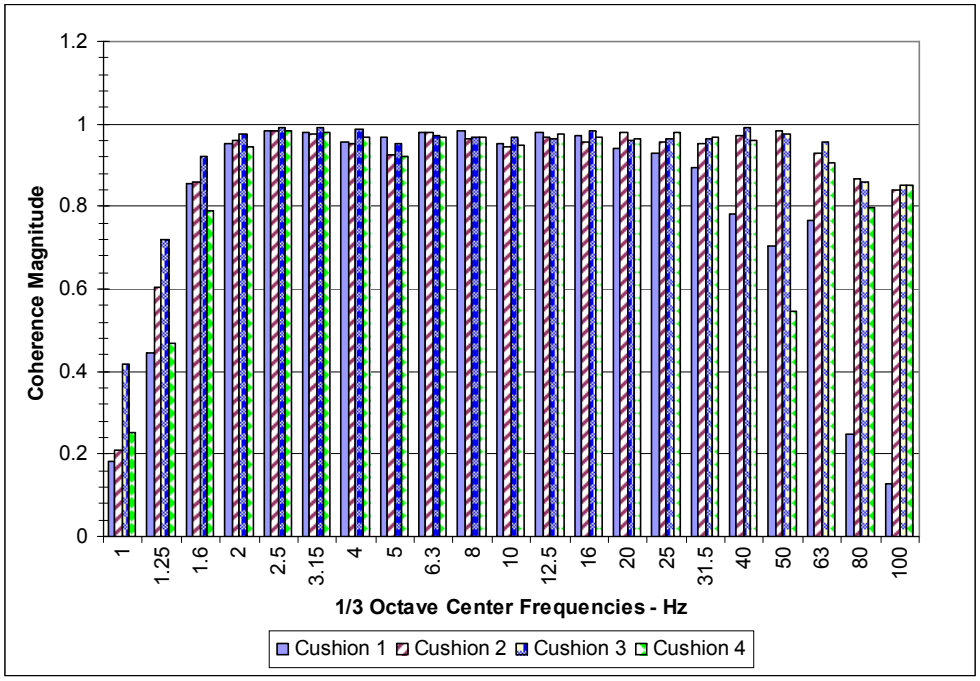

Figure 5.6 Coherence Constant Velocity Signal

5.3 Air Bladder Seat Pad Cushion Autospectrum

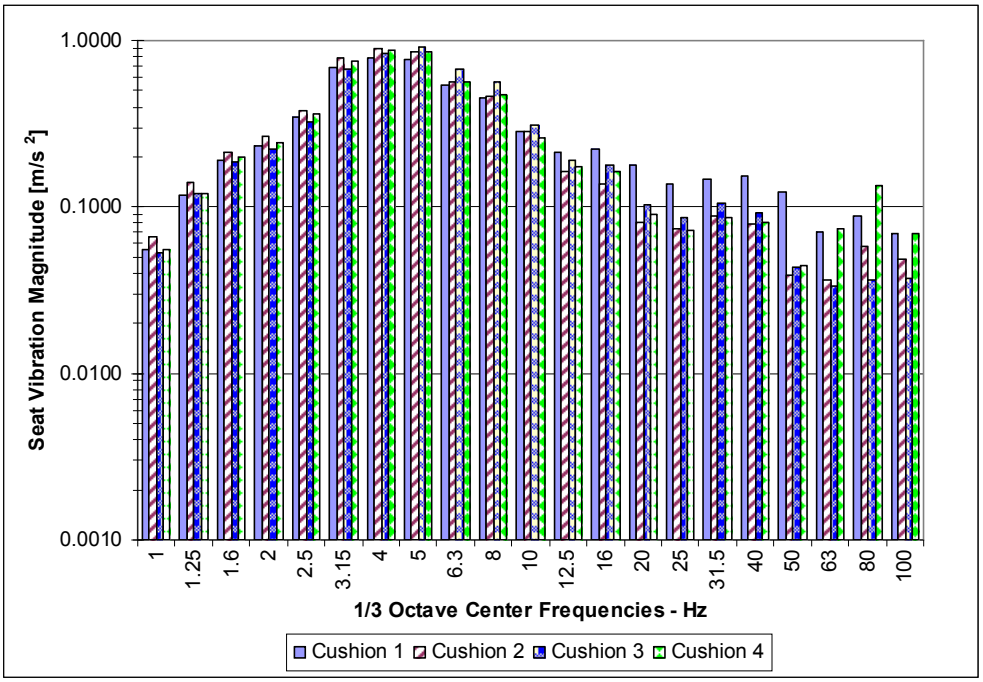

Figure 5.7 Seat Pad Warrior Autospectrum

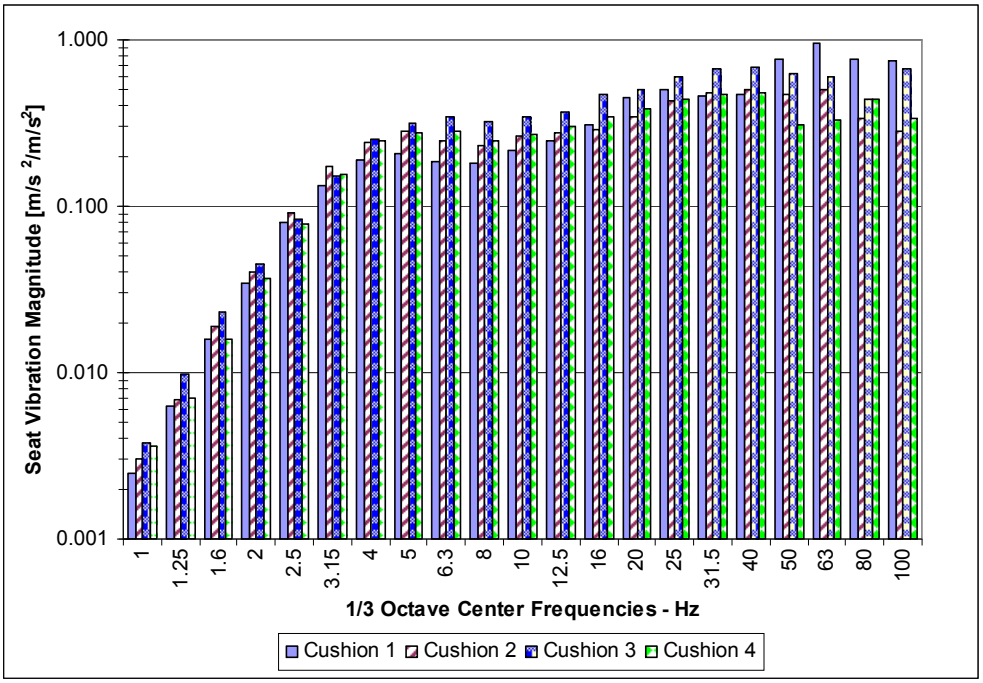

Figure 5.8 Seat Pad Constant Velocity Autospectrum

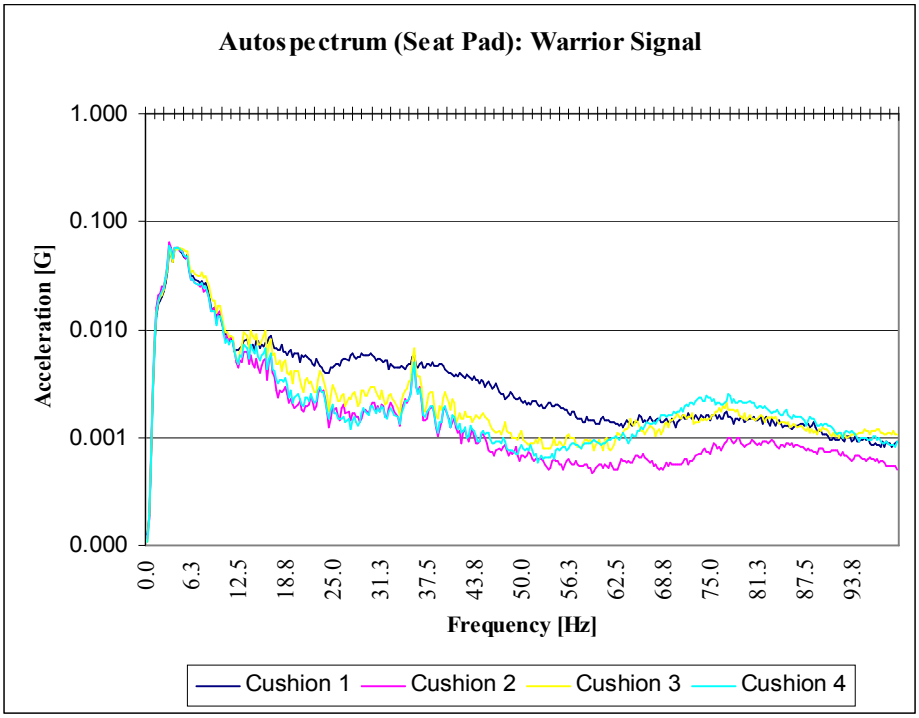

Figure 5.9 Seat Pad Warrior Signal FFT

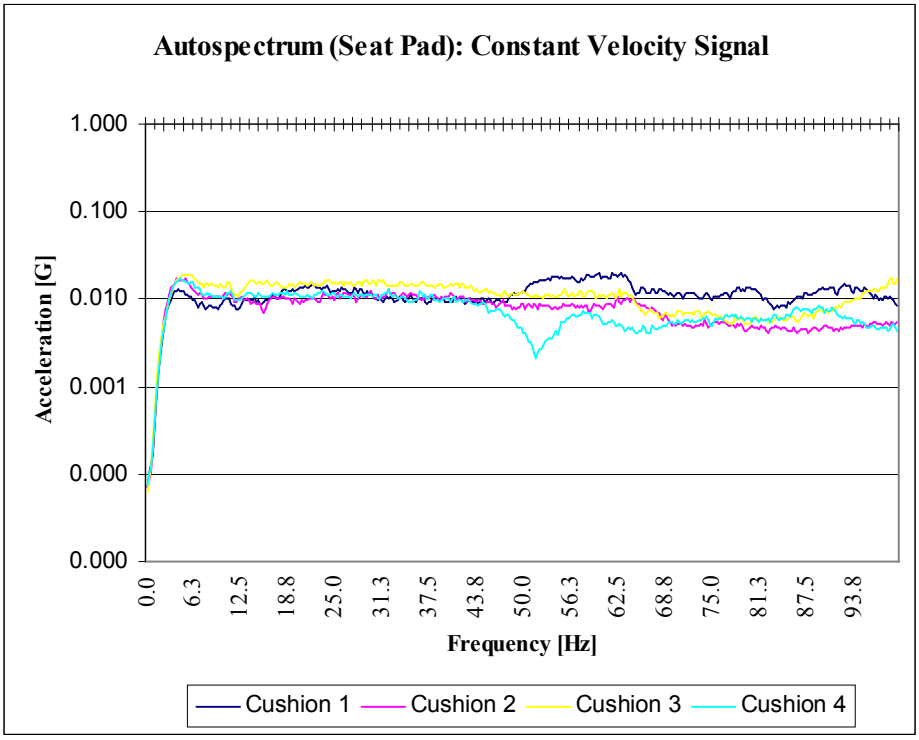

Figure 5.10 Seat Pad Constant Velocity FFT

By looking at the spectrum-response of the seat-pad accelerometer we can see that there is a peak in the response at approximately 5Hz for all the cushions in both signals. This is to be fairly expected since the natural frequency of the 1-D Anthropomorphic Dummy is tuned to that of the human-body, which also lies at approximately 5Hz.

5.4 ISO Weighted Seat Pad Autospectrum

The ISO weighting used is for a human in the seated position for the vertical direction. It is described in ISO 2631 and is relevant between 1-100Hz for issues relating to human health.

5.4.1 ISO 2631 Weighting Factors

The frequency weighting for the 1/3-octave bands in the vertical direction are:

Hz	Wk		Hz	Wk
1	0.482		12.5	0.902
1.25	0.484		16	0.768
1.6	0.494		20	0.636
2	0.531		25	0.513
2.5	0.631		31.5	0.405
3.15	0.804		40	0.314
4	0.967		50	0.246
5	1.039		63	0.186
6.3	1.054		80	0.132
8	1.036		100	0.0887
10	0.988			

Table 5.1 ISO Weighting Factors for the Vertical Direction (ISO 2631)

5.4.2 ISO Weighted Seatpad Autospectrum

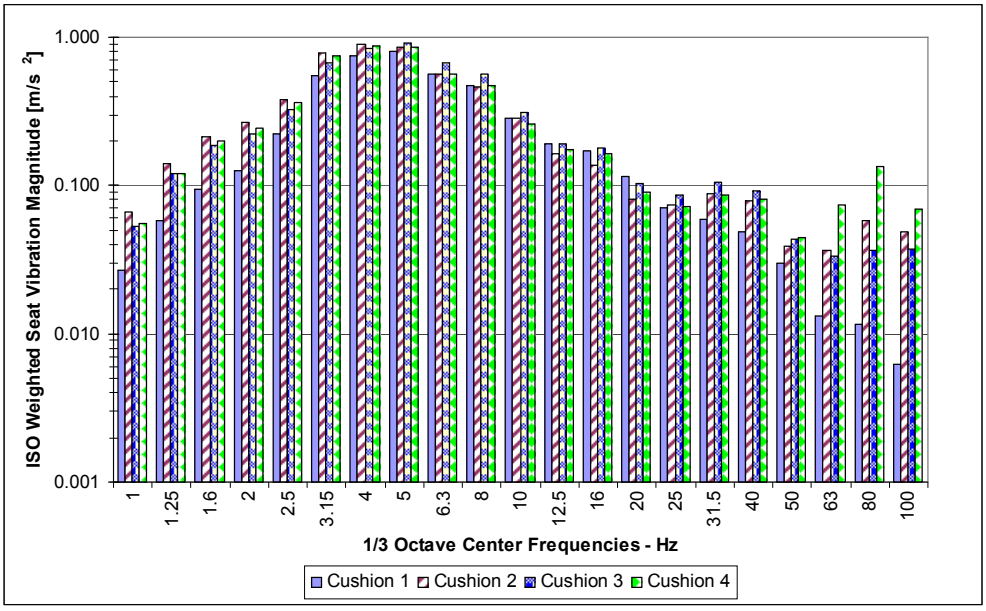

Figure 5.11 ISO Weighted Seat Pad Warrior Autospectrum

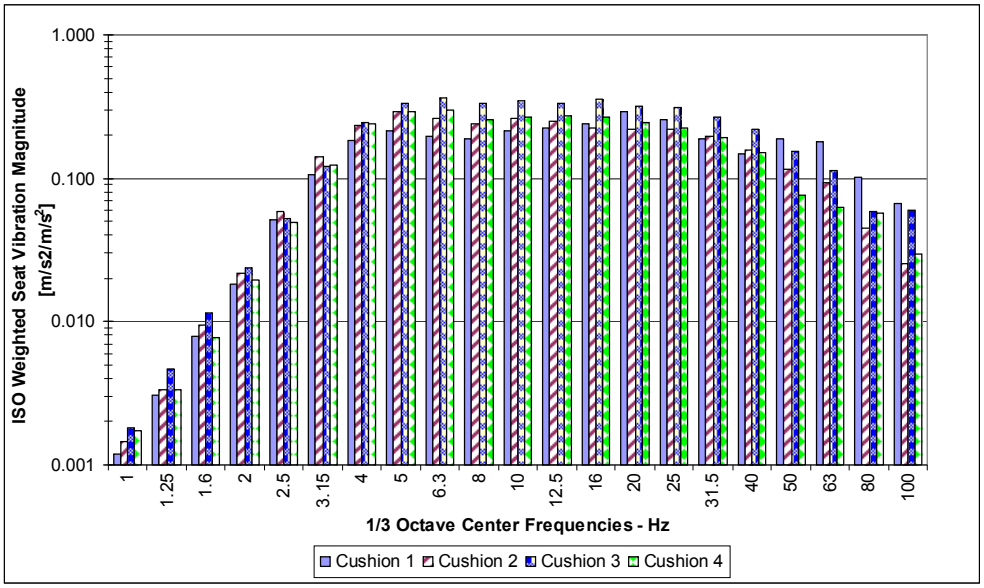

Figure 5.12 ISO Weighted Seat Pad Constant Velocity Autospectrum

5.5 Seat Transmissibility

For the purpose of the Transmissibility ratio of output/input, the figures only show the frequencies that had good coherence. Warrior Signal={1,10}Hz and Constant Velocity Signal={1.6,40}Hz.

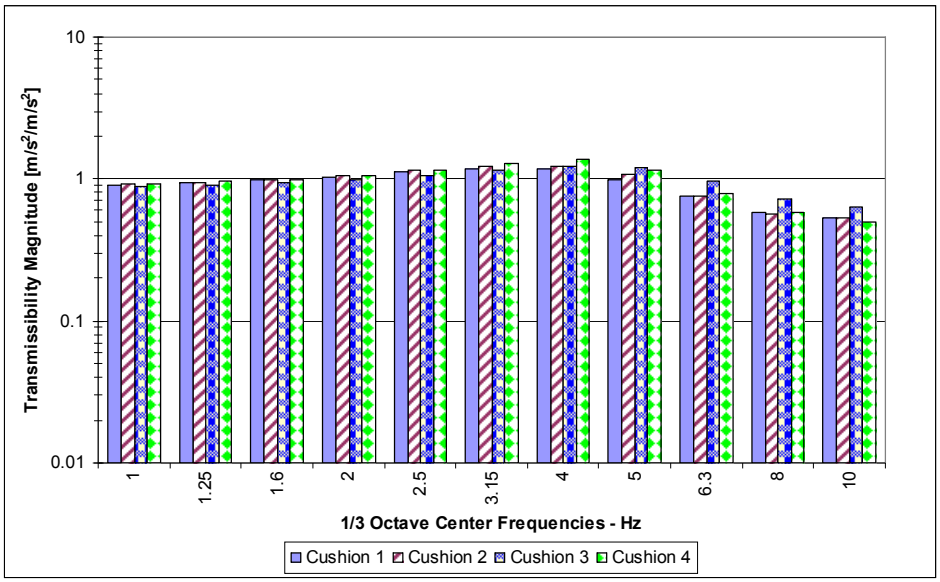

Figure 5.13 Warrior Signal Transmissibility

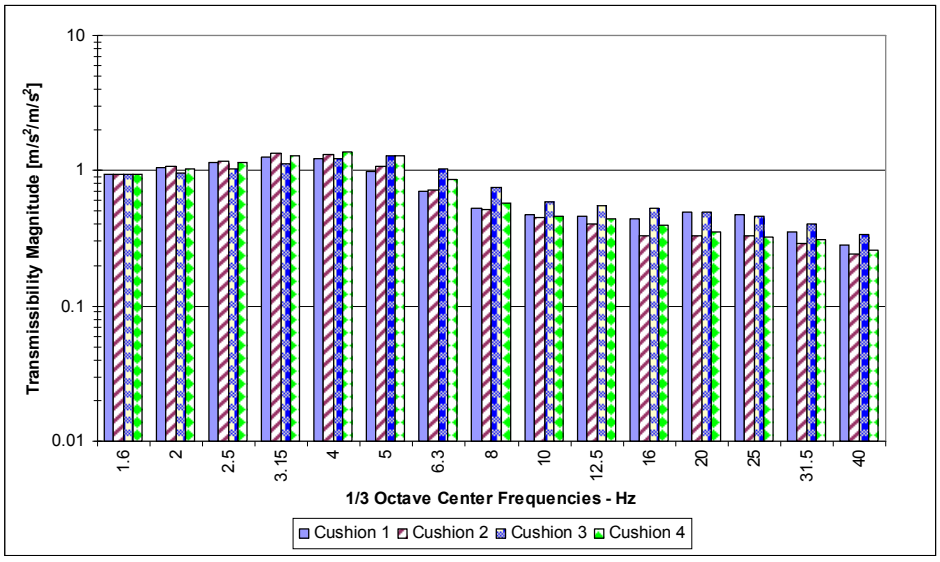

Figure 5.14 Constant Velocity Signal Transmissibility

5.6 Frequency Response

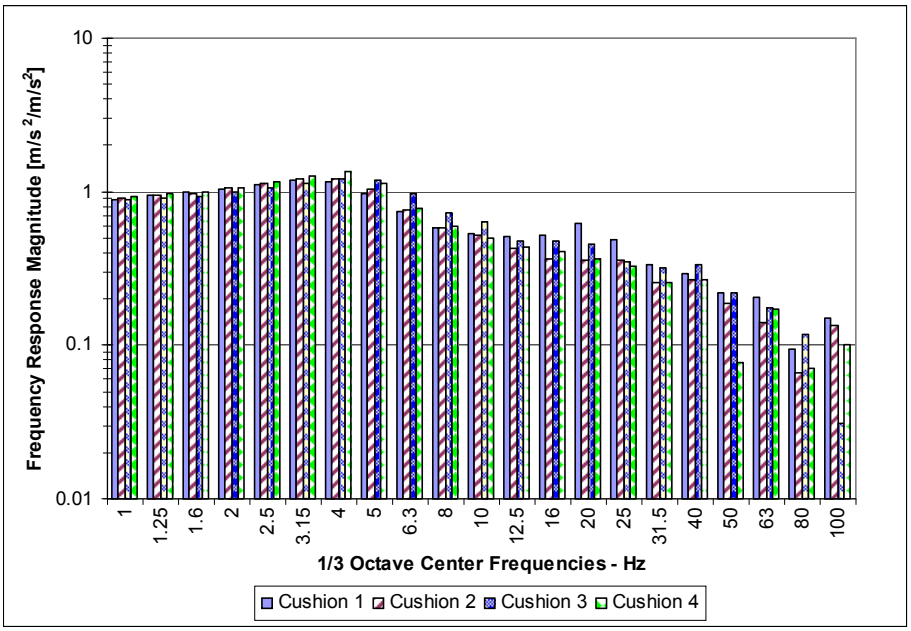

Figure 5.15 Magnitude of Frequency Response Warrior Signal

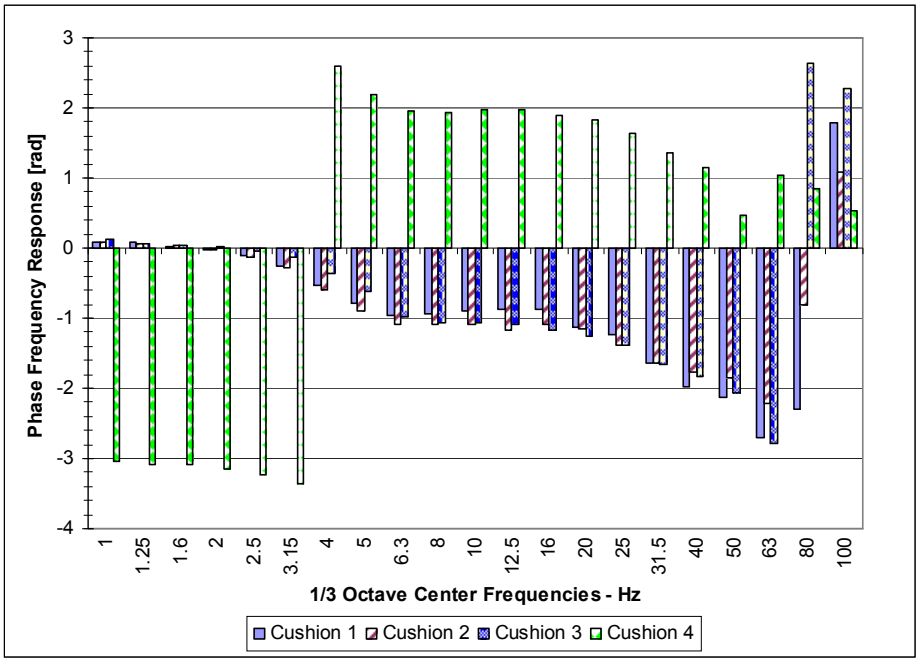

Figure 5.16 Phase of Frequency Response Warrior Signal

Figures 5.17 and 5.18 show the amplitude of the magnitude and phase associated with the air bladder seat cushion configurations excited with the constant velocity signal.

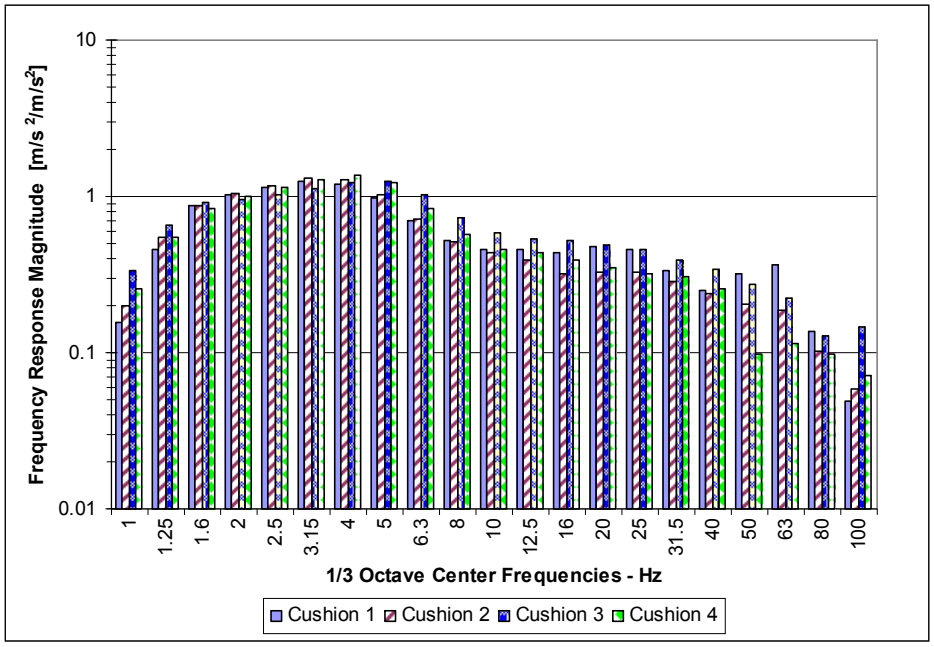

Figure 5.17 Magnitude of Frequency Response Constant Velocity Signal

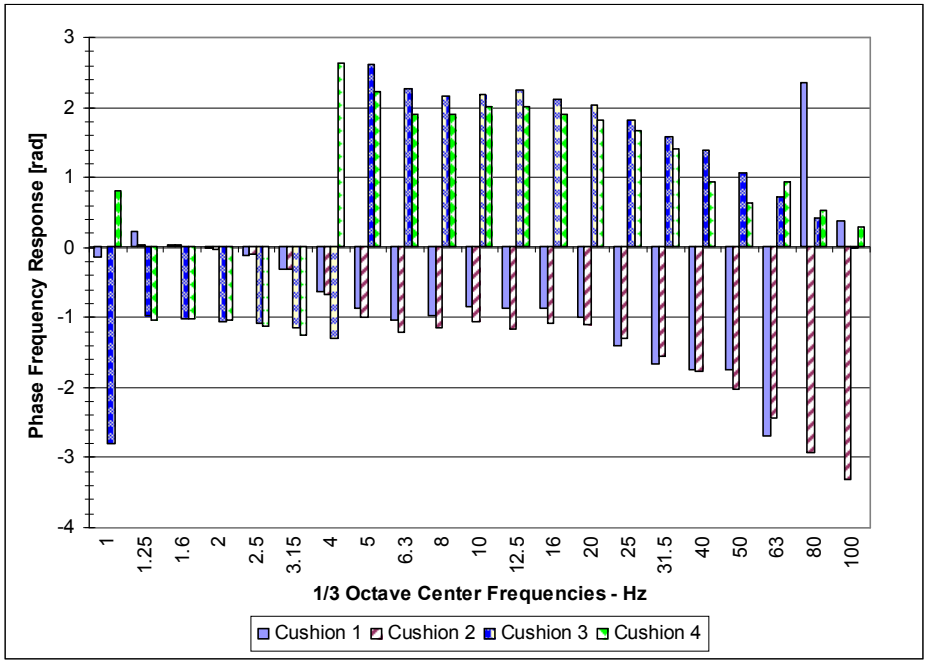

Figure 5.18 Phase of Frequency Response Constant Velocity Signal

CHAPTER 6

QUASI-STATIC AND DYNAMIC PRESSURE RESULTS

The internal pressure of the pneumatic seat system, of both the seat bottom and the seat back were tested under two separate testing conditions: quasi-static using the Material Test Systems (MTS) hydraulic tensile test machine with a fiberboard butt-form; and dynamic pressure measured during the battery of drop-tower shock tests conducted at UNLV. The complete discussion and analysis of the data presented here can be found in Chapter 9.

6.1 Foam and Air Individual Contributions to Force-Compression

The foam's response to experimental, quasi static compression was previously calculated and fit with an empirical function:

$$F_{foam} = \frac{4.448}{(1.005 - \varepsilon)^{2.7}} \qquad \textbf{Equation 6.1}$$

where ε is the cushion compression divided by the original thickness (cushion strain). This equation gives the foam force in units of Newton's.

Figure 6.1 shows the air pressure sensor data plotted against the predicted results of Equation 6.1. The foam and air forces were treated as parallel springs. Figure 6.3 shows the results associated with adding the foam and air pressure results.

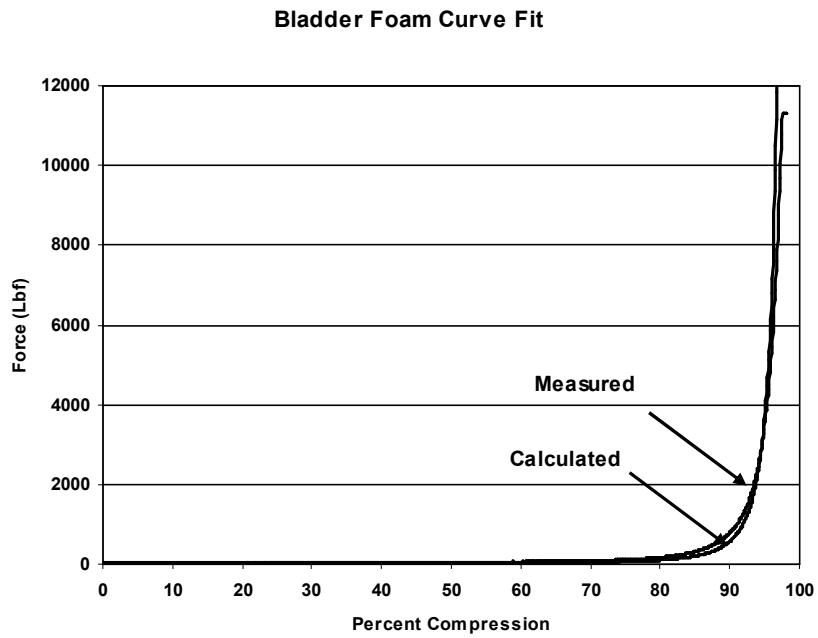

Figure 6.1 Foam Compression Test Results

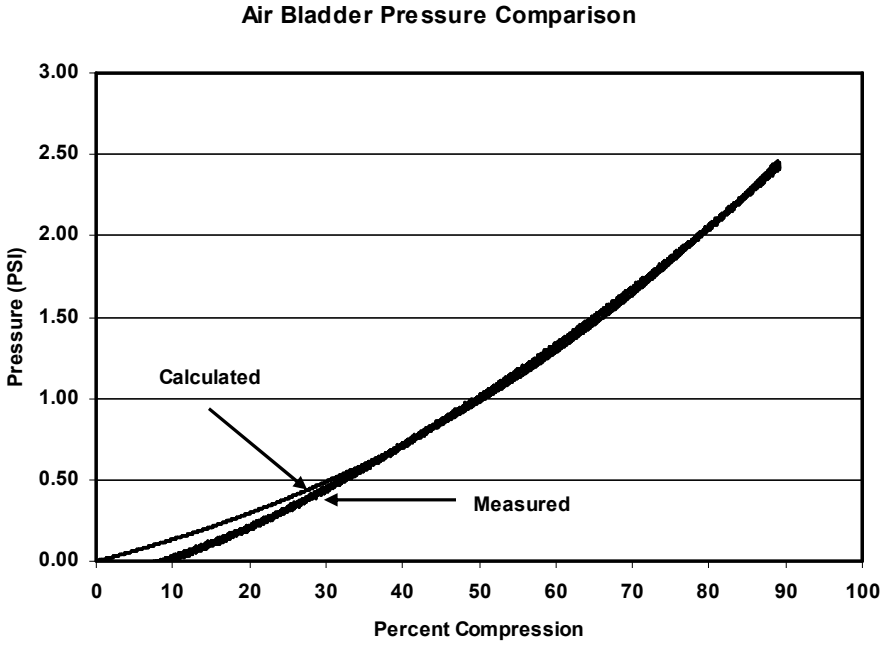

Figure 6.2 Bladder Compression-Pressure Test Results

The Air + Foam curve represents the compressive force measured by the test machine load cell on a closed cushion system. The Air curve is derived from the pressure sensor data from the same test multiplied by 2 times the surface area of the seat form. The Foam curve is a load cell force measurement from a separate test on a cushion opened to the atmosphere. Figure 6.4 shows a comparison between predicted results and measured data for the cushion force.

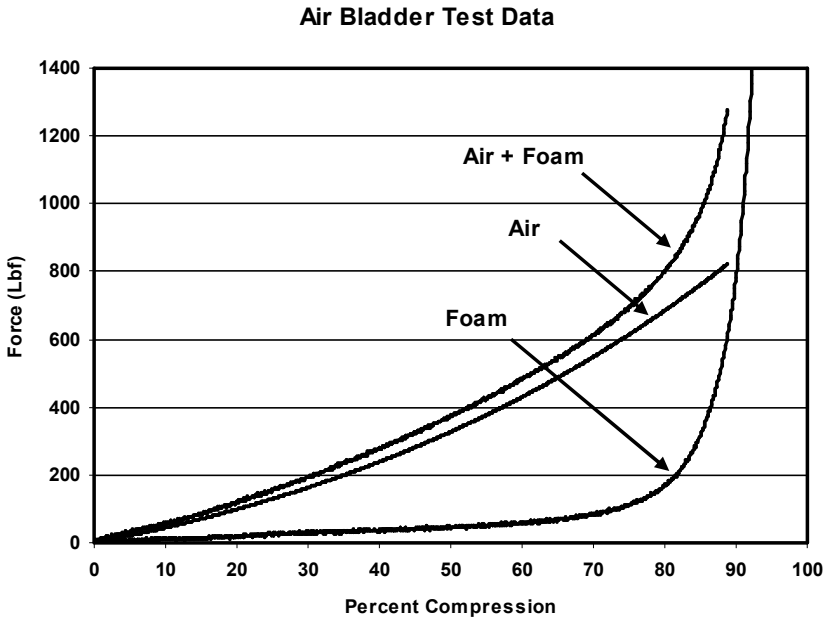

Figure 6.3 Air Bladder Individual Components Performance

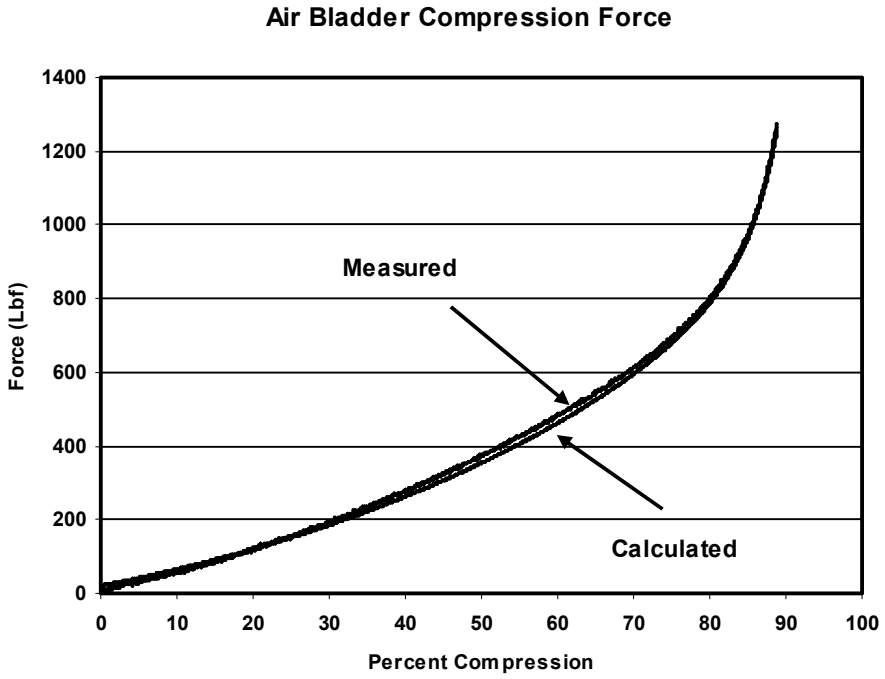

Figure 6.4 Air Bladder Compression –Force Results

6.2 Dynamic Pressure Consideration

The directly measured dynamic pressure from both the seat bottom and the seat back were acquired from drops at 10, 20, and 30in with the 150lb Sandbag Dummy placed directly on-top of the cushion. First an example of the shocks at each of the drop heights are provided as a reference, and then the individual pressure performances are given for each of the bladders.

6.2.1 Characterization of the Input Shock for Pressure Consideration

The shocks produced by the UNLV drop tower consistently have multiple pulses with approximately 2-5 millisecond pulse widths. This is different than the pulse produced by the Army Research Lab which are simple shocks consisting of half-sine pulses of approximately 5 milliseconds.

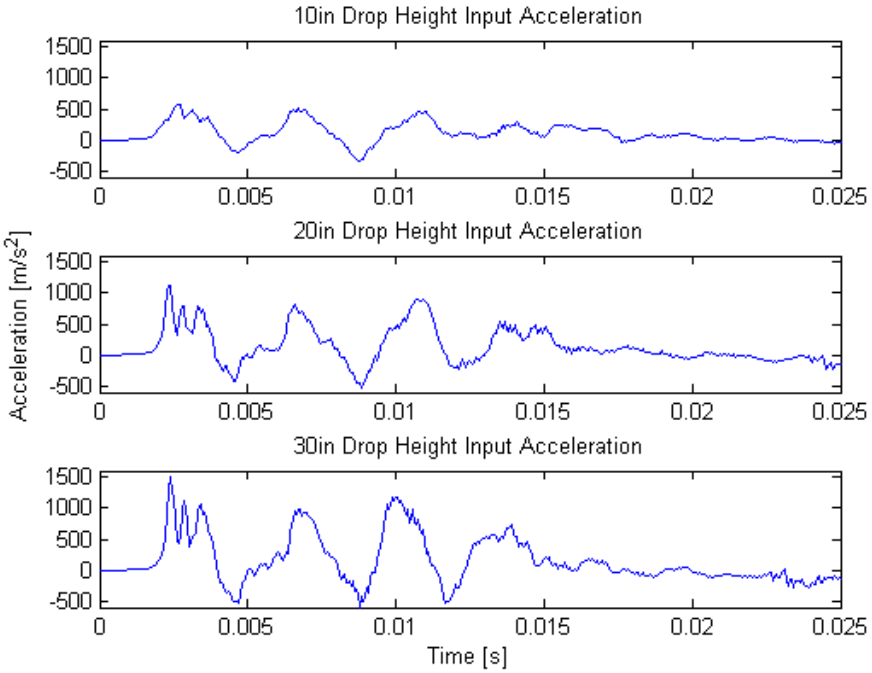

Figure 6.5 UNLV Input Shock Profiles from All Drop Heights

The UNLV shock pulses do not resemble classic shocks such as ARL's half-sine; rather they more resemble a pyrotechnic shock even though peak accelerations were reasonably similar. However the peak-peak values are greater when the positive-to-negative peak values are taken into account.

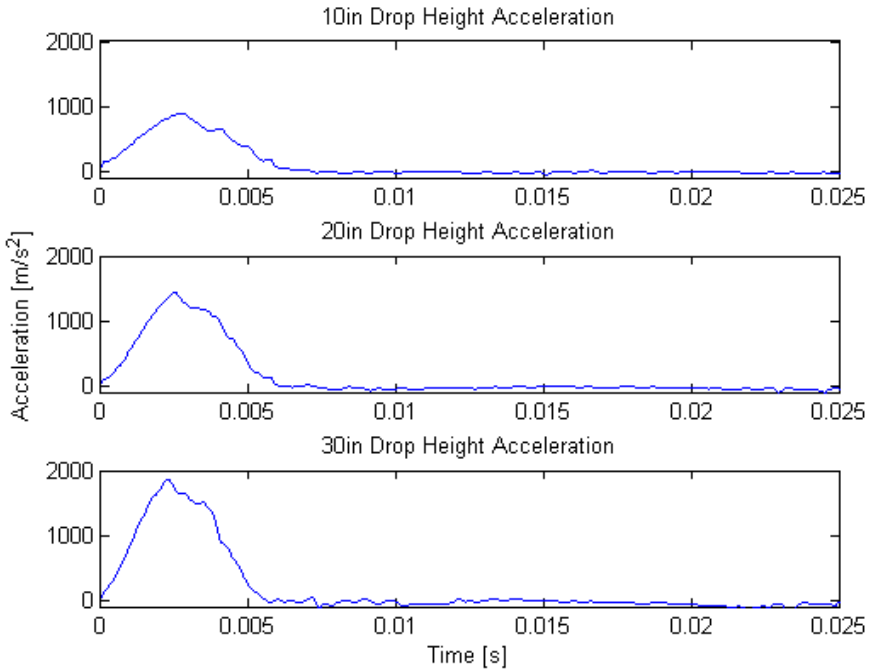

Figure 6.6 ARL Input Shock Profiles from All Drop Heights

The difference in the appearance of the input is a welcomed fact in this case because it subjects the air cushions to a second variety of shock inputs. Moreover it showcases the ability of the cushion to act like a mechanical filter, producing resulting in nearly half-sine pressure histories, regardless of the more dynamic shock acceleration inputs.

6.3 Dynamic Pressure Results

6.3.1 Pressures from 10in Drop Heights

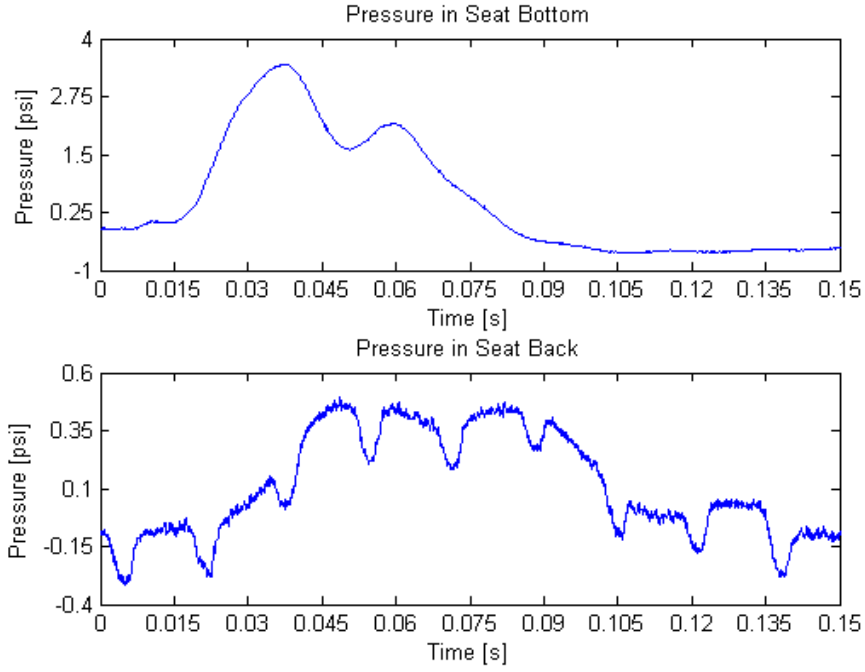

Figure 6.7 Bladder 1 Pressure- 10in Drop Height

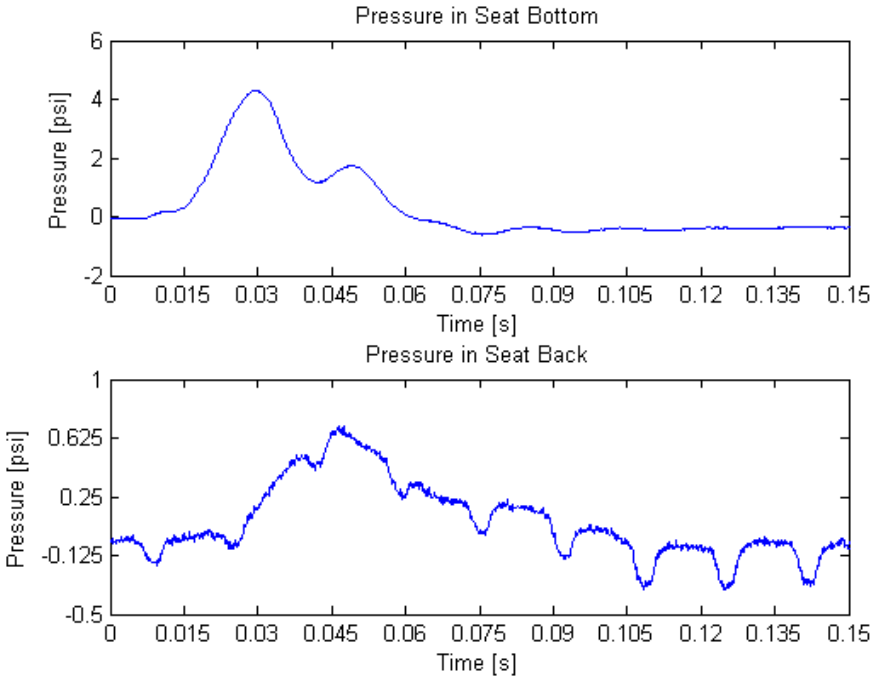

Figure 6. 8 Bladder 2 Pressure- 10in Drop Height

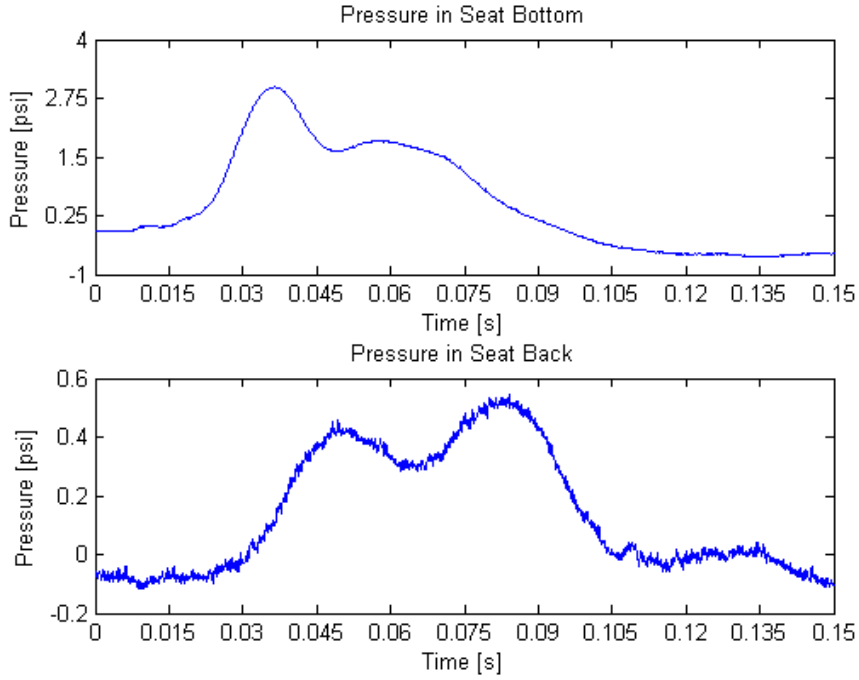

Figure 6.9 Bladder 3 Pressure- 10in Drop Height

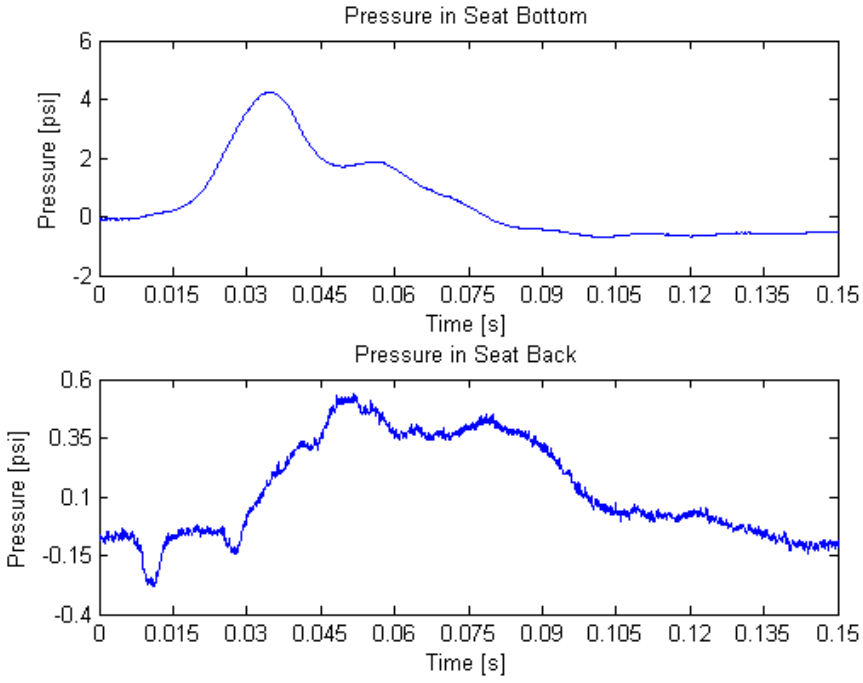

Figure 6.10 Bladder 4 Pressure- 10in Drop Height

6.3.2 Pressures from 20in Drop Heights

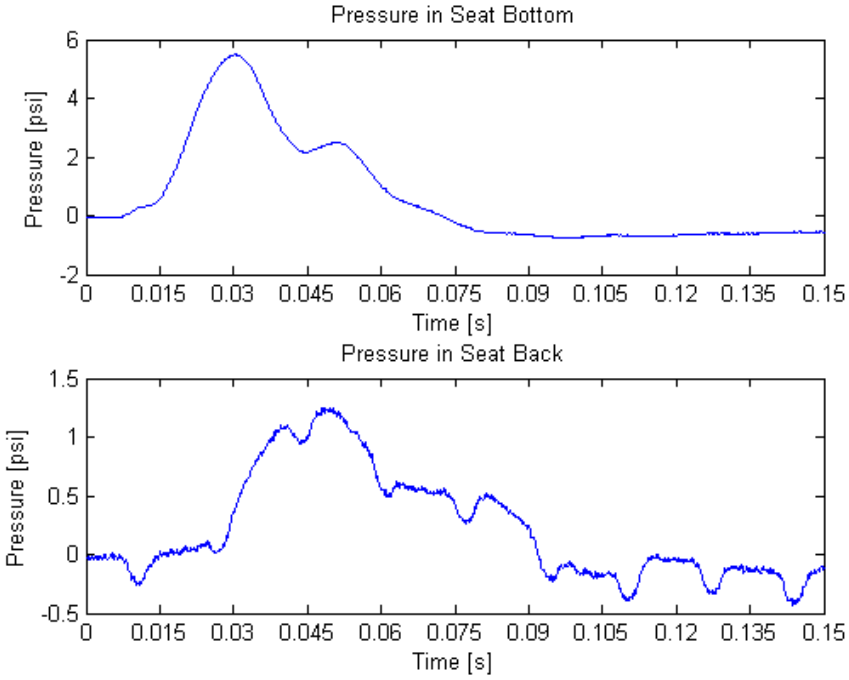

Figure 6.11 Bladder 1 Pressure- 20in Drop Height

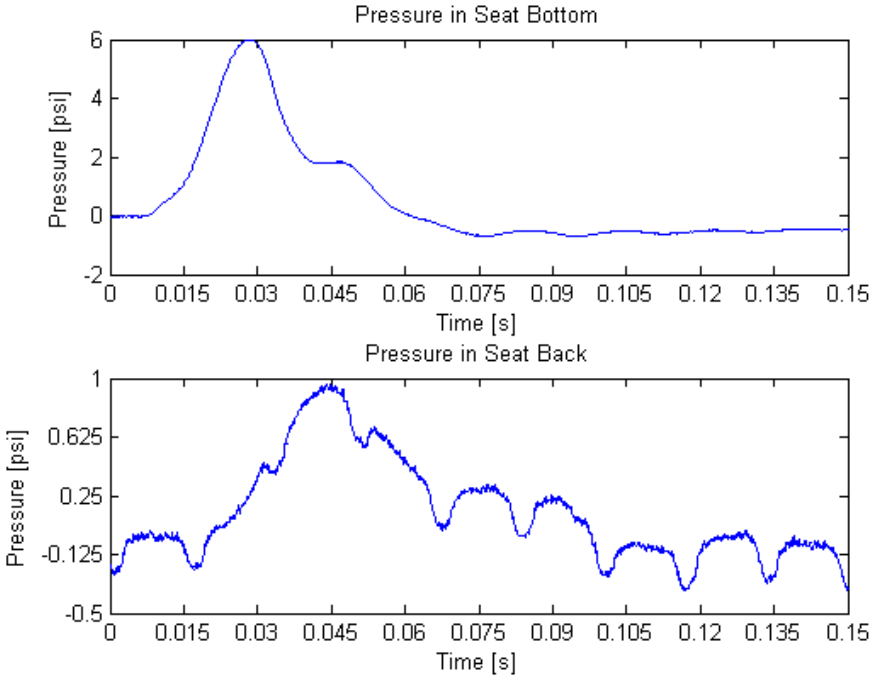

Figure 6.12 Bladder 2 Pressure- 20in Drop Height

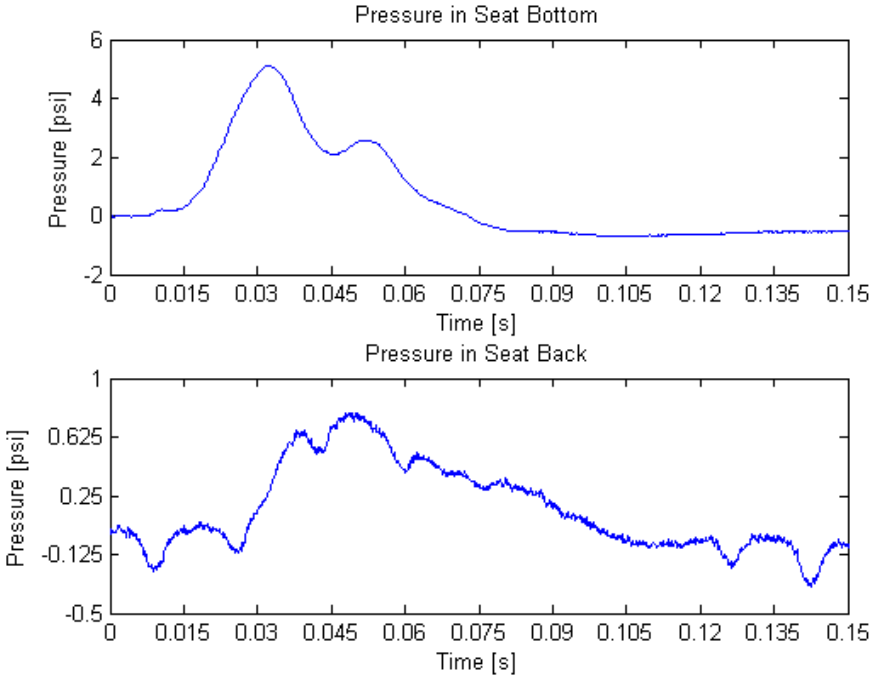

Figure 6.13 Bladder 3 Pressure- 20in Drop Height

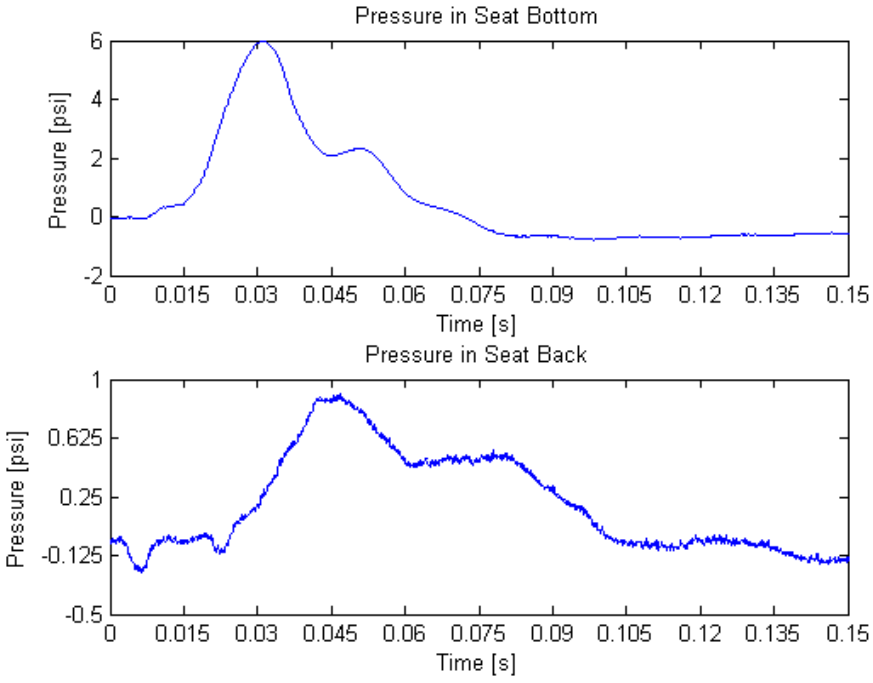

Figure 6.14 Bladder 4 Pressure- 20in Drop Height

6.3.3 Pressures from 30in Drop Heights

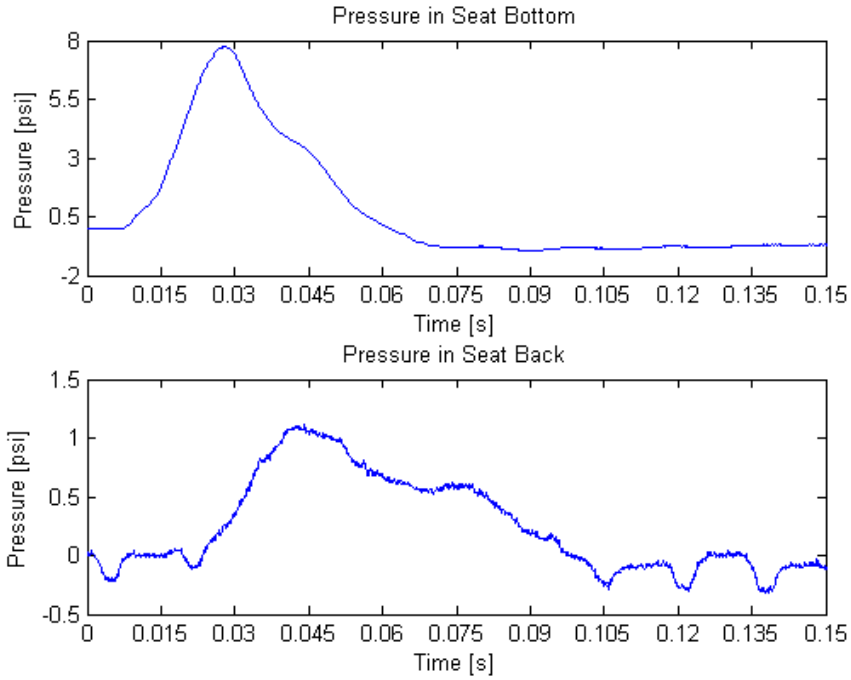

Figure 6.15 Bladder 1 Pressure- 30in Drop Height

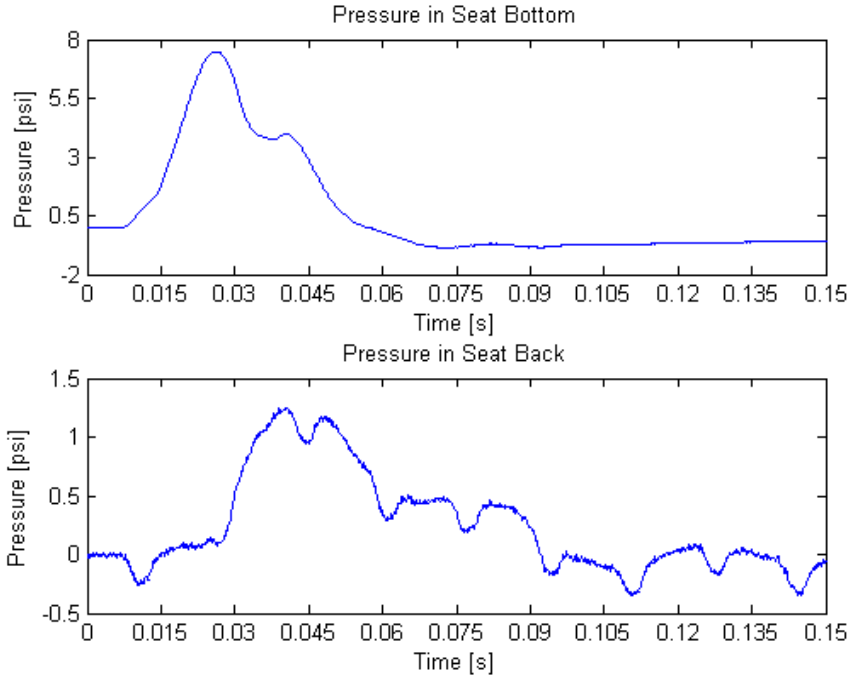

Figure 6.16 Bladder 2 Pressure- 30in Drop Height

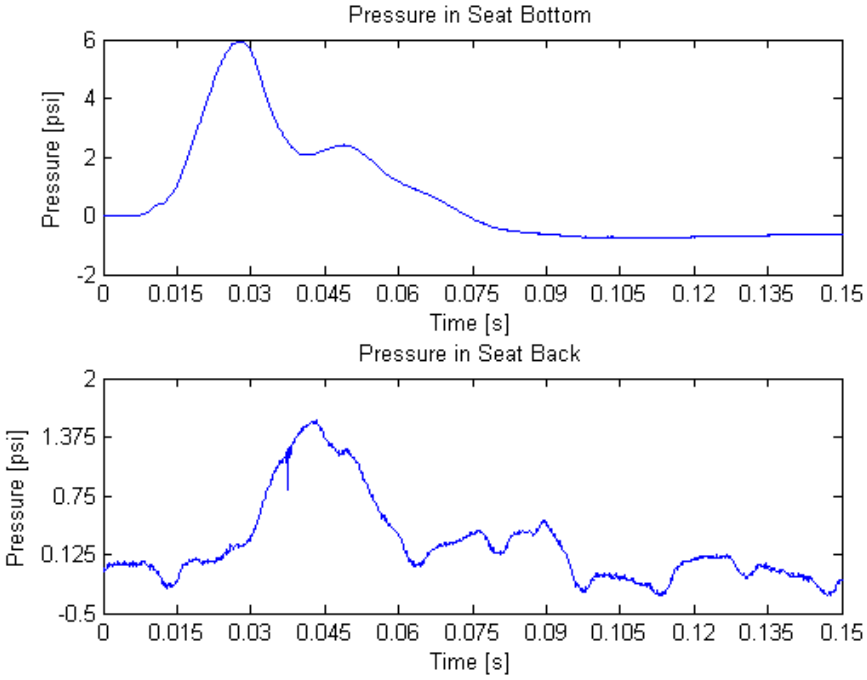

Figure 6.17 Bladder 3 Pressure - 30in Drop Height

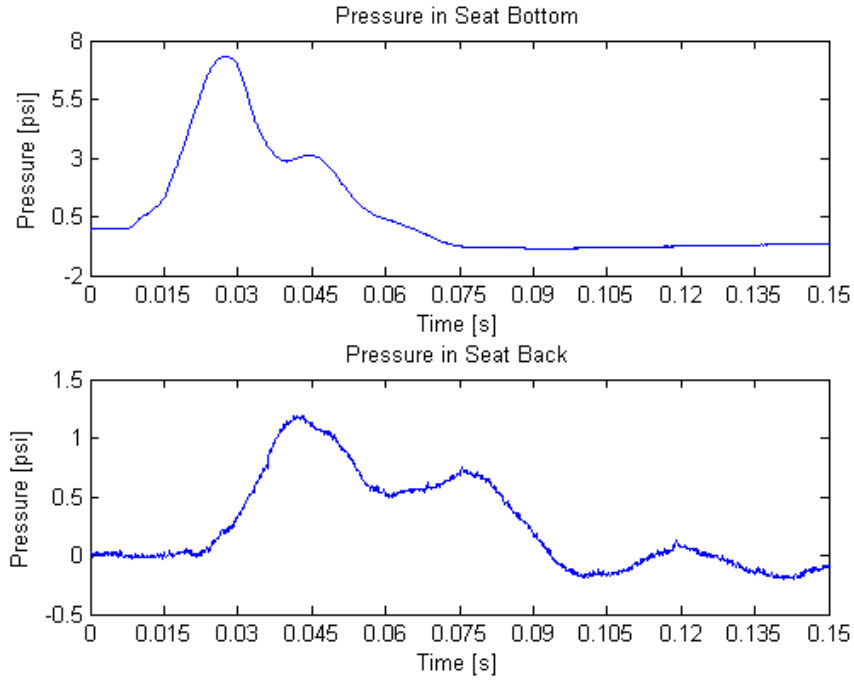

Figure 6.18 Bladder 4 Pressure- 30in Drop Height

CHAPTER 7

ARL SHOCK TESTING AND ANTHROPOMORPHIC RESPONSE RESULTS

7.1 ARL Shock Characterization

The ARL Drop tower configuration uses a pulse programmer to consistently produce a nearly 5ms shock pulse with amplitude depending on the height of the drop occurrence. This shock is a simple-zero-mean shock with no rebound. The UNLV shock profile, its corresponding test results, and a comparison to the ARL Shock Profile will be discussed in Chapter 8. The complete discussion and analysis of the data presented here can be found in Chapter 9.

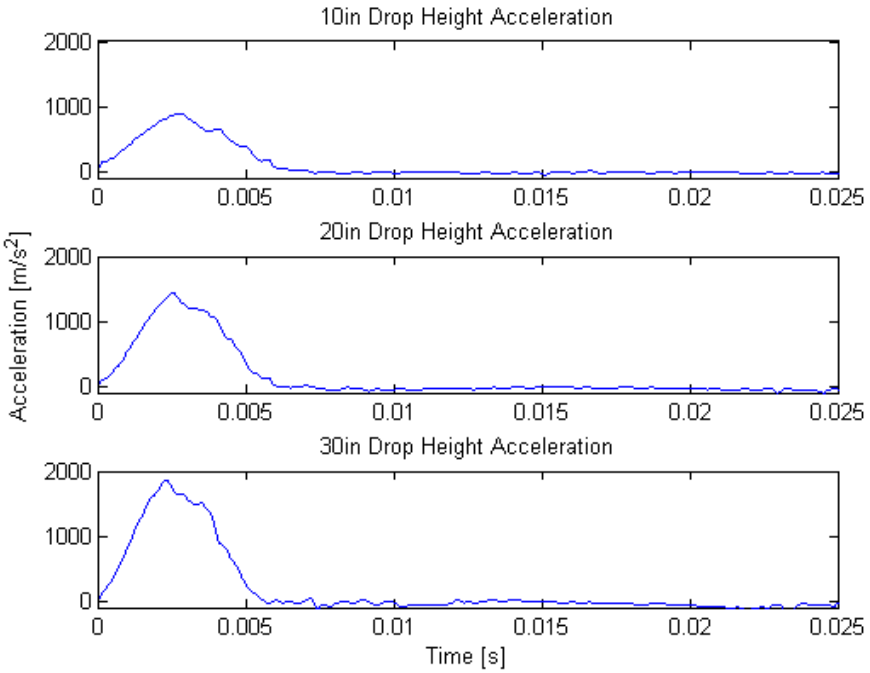

Figure 7.1 ARL Input Shock Profiles from All Drop Heights

7.2 Presentation of Shock Data Results

Because of the large amount of data collected in this series of tests, portions of the data can be found in the Appendix. Therefore this presentation will focus on the most severe of the drops at 30in, for many of the data sets from both the UNLV and ARL battery of tests. The results from all three drop heights will be presented in a few examples for the purpose of giving the reader context to the difference in magnitudes and wherever else is deemed necessary.

7.3 ARL Anthropomorphic Dummy and Bladder Acceleration Performance

A series of tests were performed on the Anthropomorphic Test Dummy (ATD) in order to get a baseline for the remainder of the tests. From hereon out, the ATD performance will be designated as *Baseline.* Figure 6.2 of the Baseline Input Accelerations can be considered the input for the remainder of the ARL Drop Tests.

7.3.1 Baseline/ATD Acceleration Performance – ARL

ARL did not perform drop tests with the ATD at heights above 25 in for fear of damaging the instrumented dummy. The input accelerations associated with the following plots were similar to the acceleration profiles shown in Figure 7.1. The acceleration profiles for both the seat-pad acceleration and the pelvic accelerations can be compared to the input profile in figures that have similar scales for ease of comparison and analysis. To reduce the overall length of this chapter, the combined response plots for 10 and 20 in. drop heights will be provided in the Appendix.

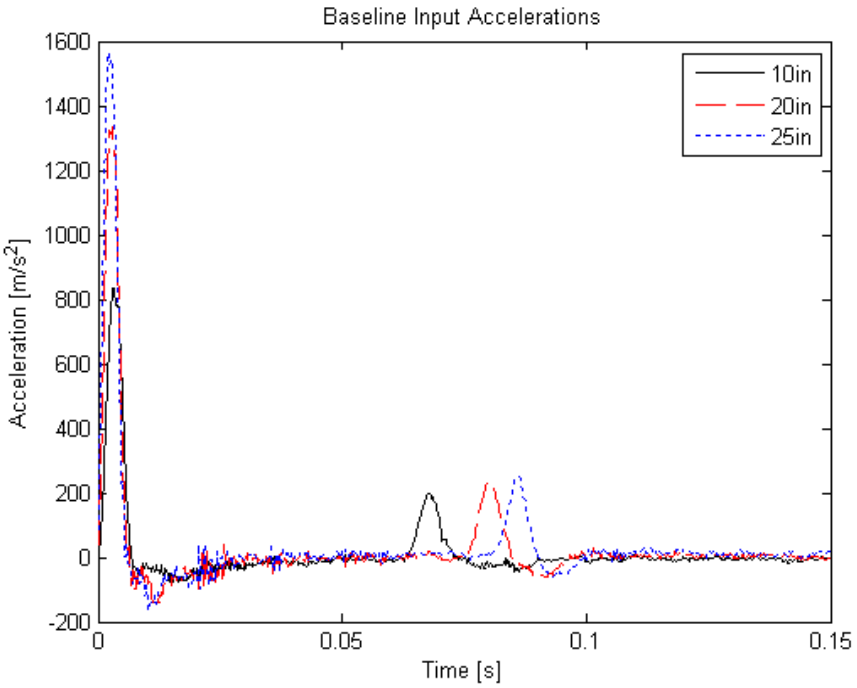

Figure 7.2 Baseline/Dummy Table Input Accelerations – All Drop Heights

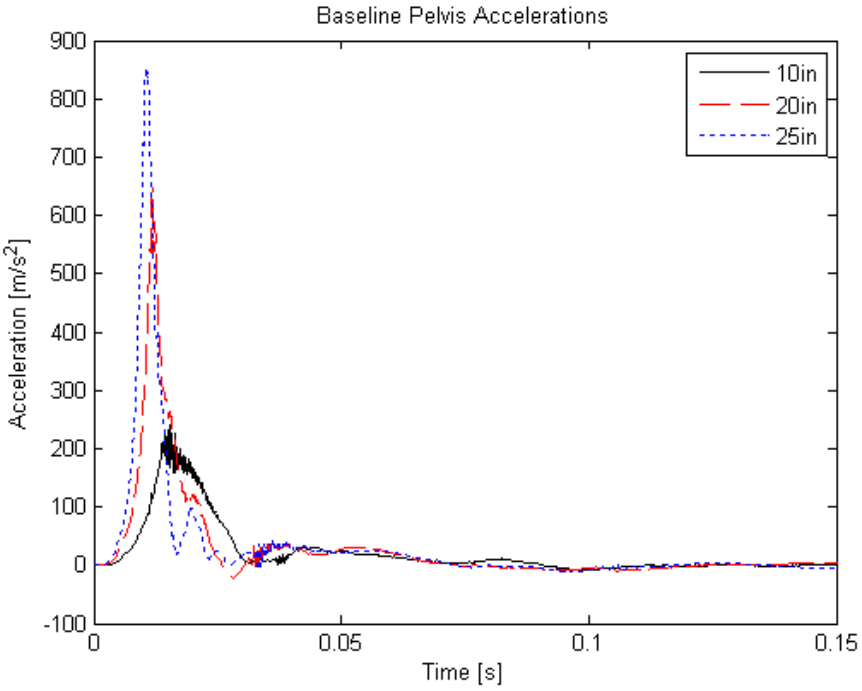

Figure 7.3 Baseline/Dummy Pelvic Accelerations – All Drop Heights

7.3.2 Combined Acceleration Plots for 30 in. Drop Height– ARL

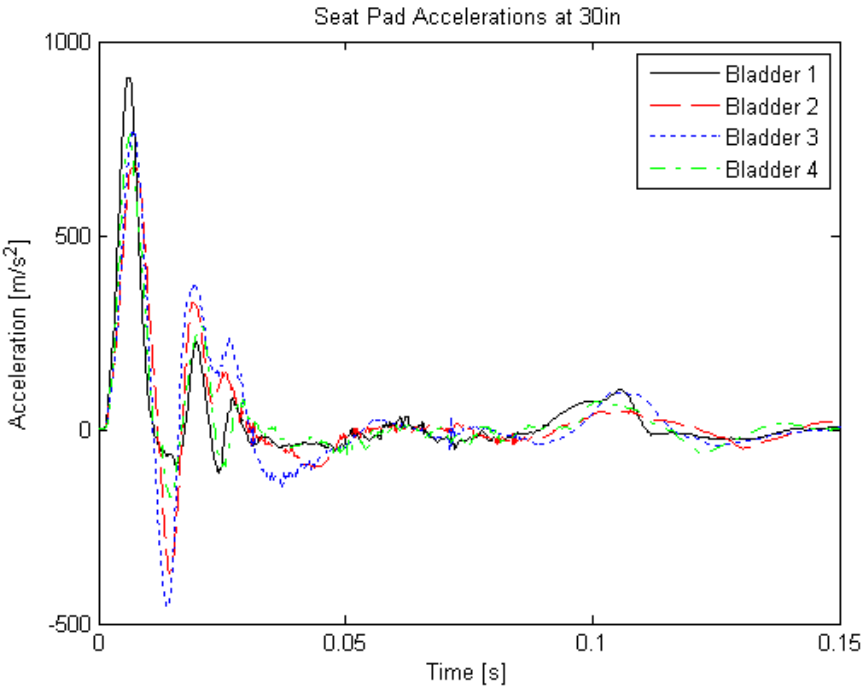

Figure 7.4 Seat Pad Accelerations of all Bladders – 30in Drop Height

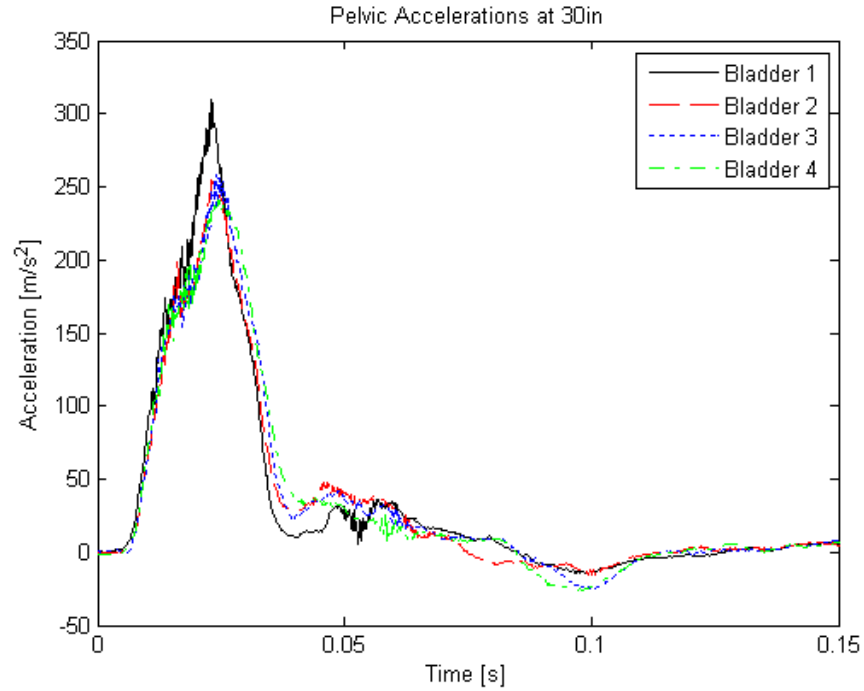

Figure 7.5 Seat Pad Accelerations of all Bladders – 30in Drop Height

7.3.3 Bladder 1 Acceleration Performance – ARL

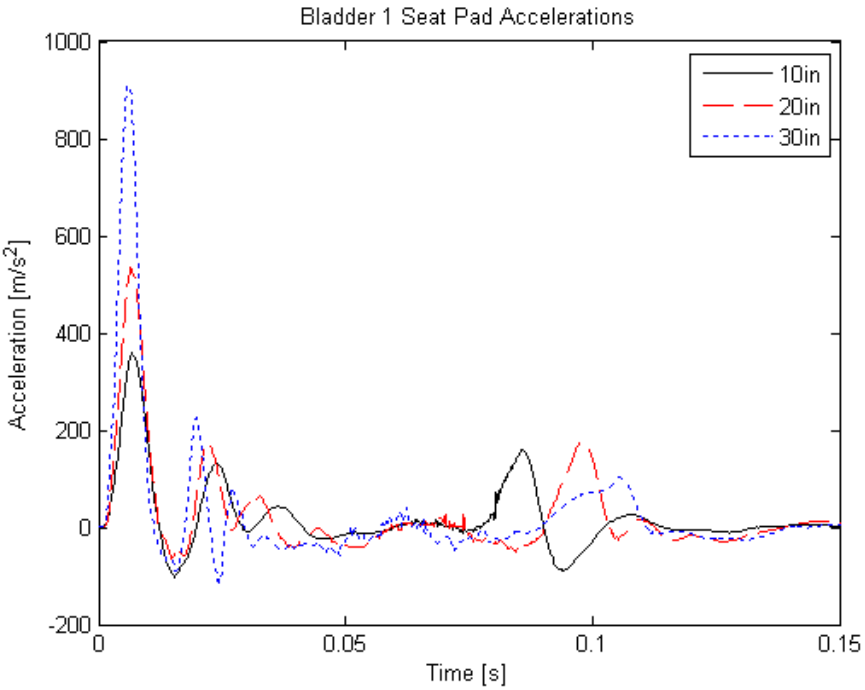

Figure 7.6 Bladder 1 Seat-pad Accelerations – All Drop Heights

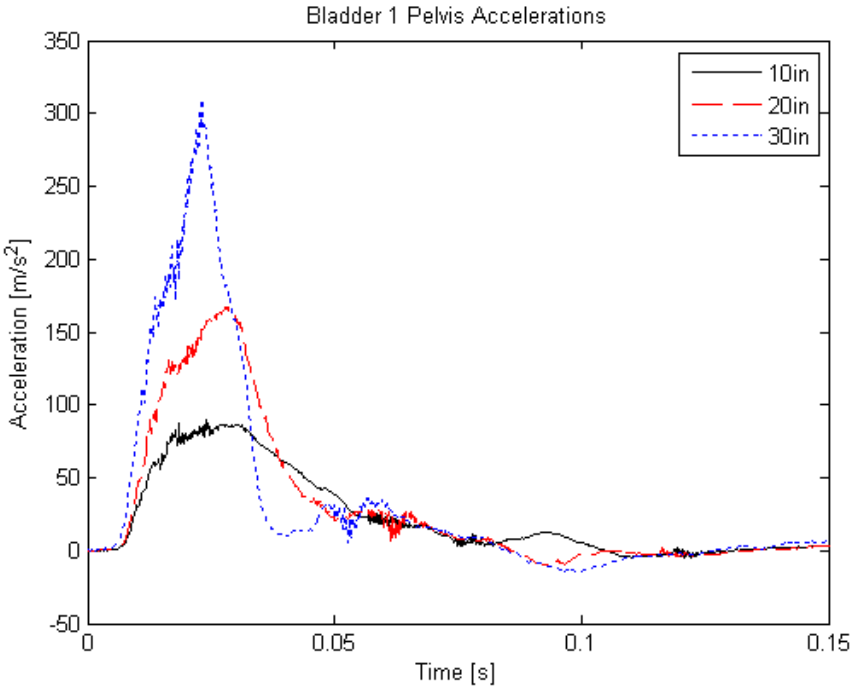

Figure 7.7 Bladder 1 Pelvic Accelerations – All Drop Heights

7.3.4 Bladder 2 Acceleration Performance – ARL

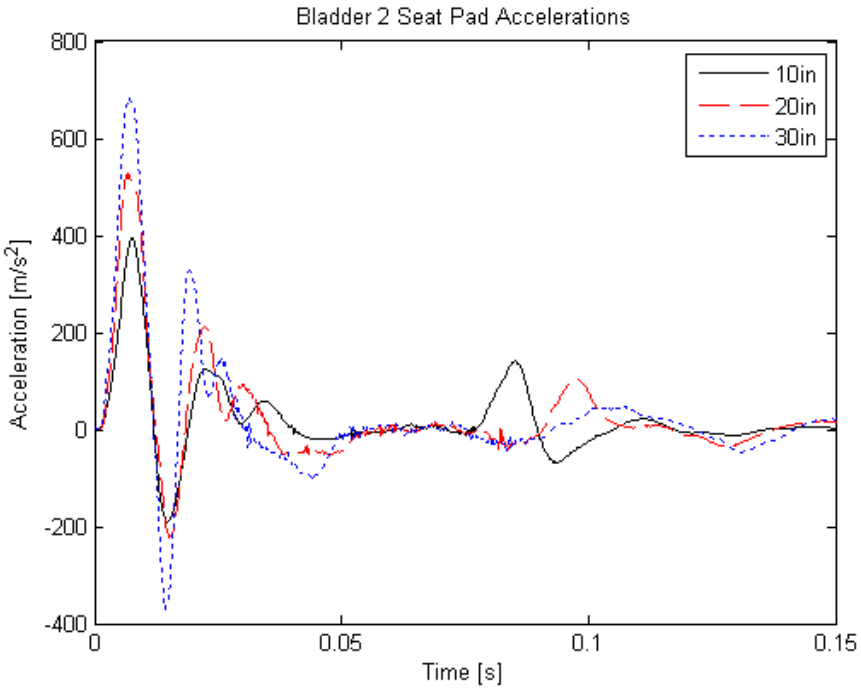

Figure 7.8 Bladder 2 Seat-pad Accelerations – All Drop Heights

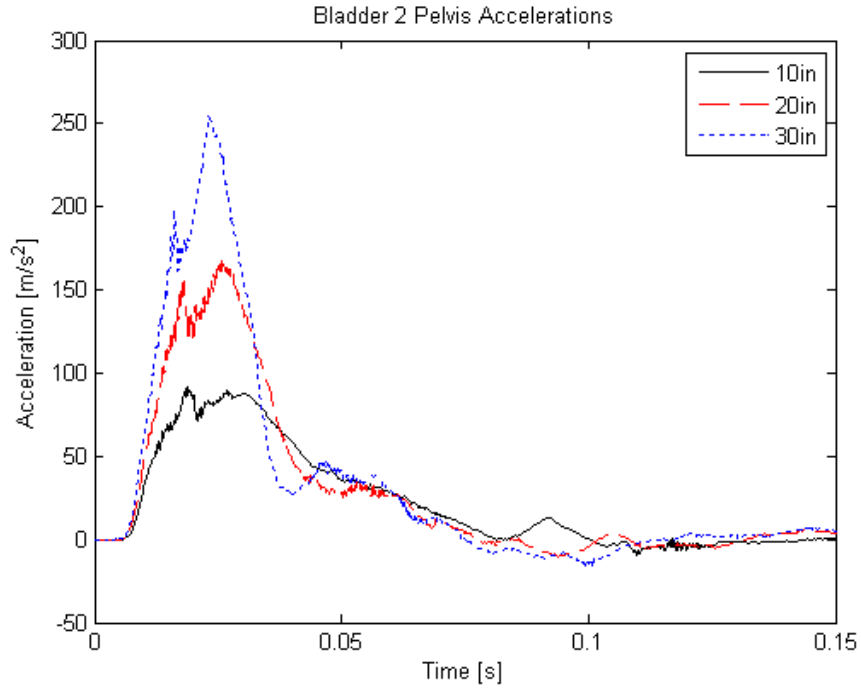

Figure 7.9 Bladder 2 Pelvic Accelerations – All Drop Heights

7.3.5 Bladder 3 Acceleration Performance – ARL

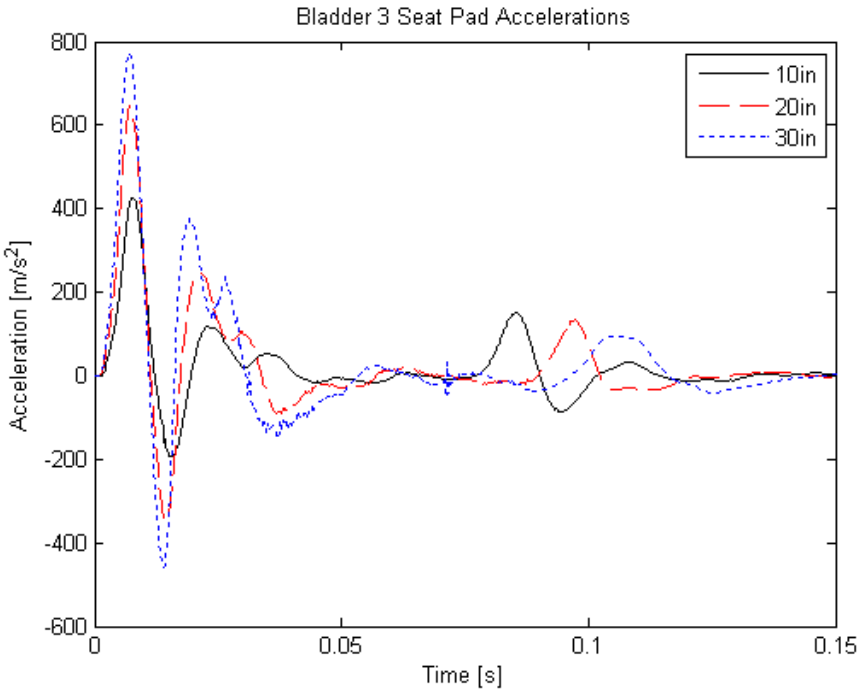

Figure 7.10 Bladder 3 Seat-pad Accelerations – All Drop Heights

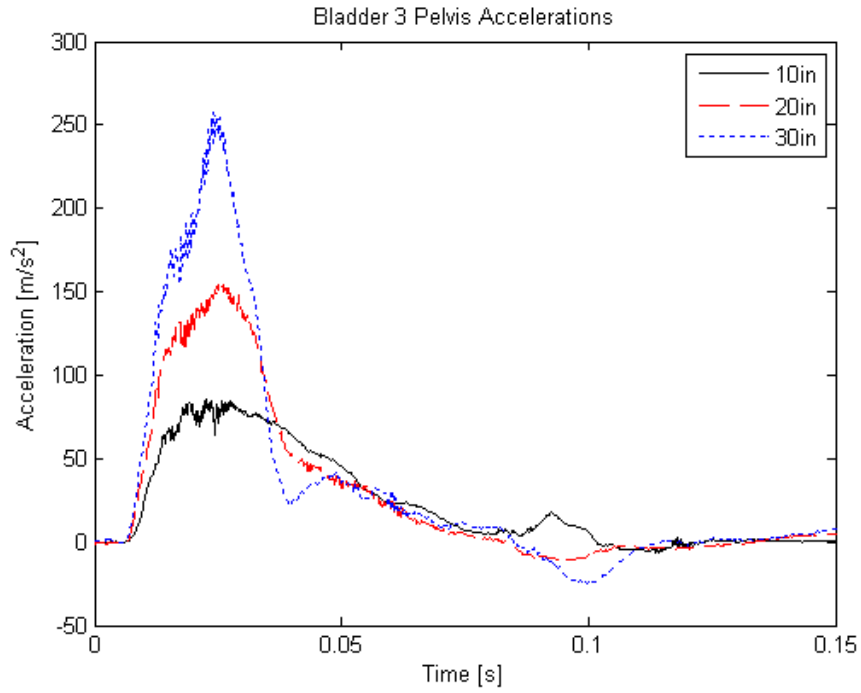

Figure 7.11 Bladder 3 Pelvic Accelerations – All Drop Heights

7.3.6 Bladder 4 Acceleration Performance – ARL

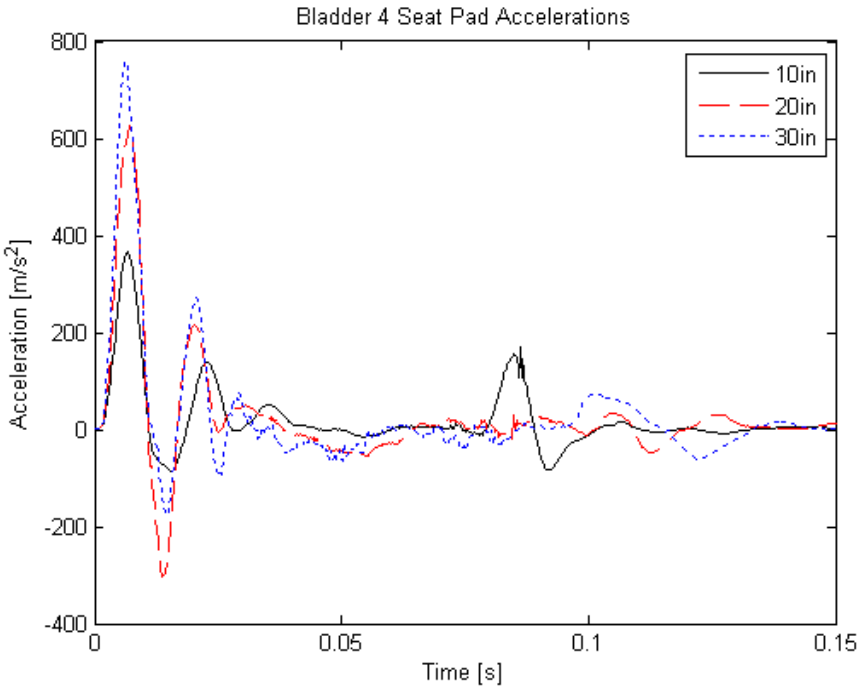

Figure 7.12 Bladder 4 Seat-pad Accelerations – All Drop Heights

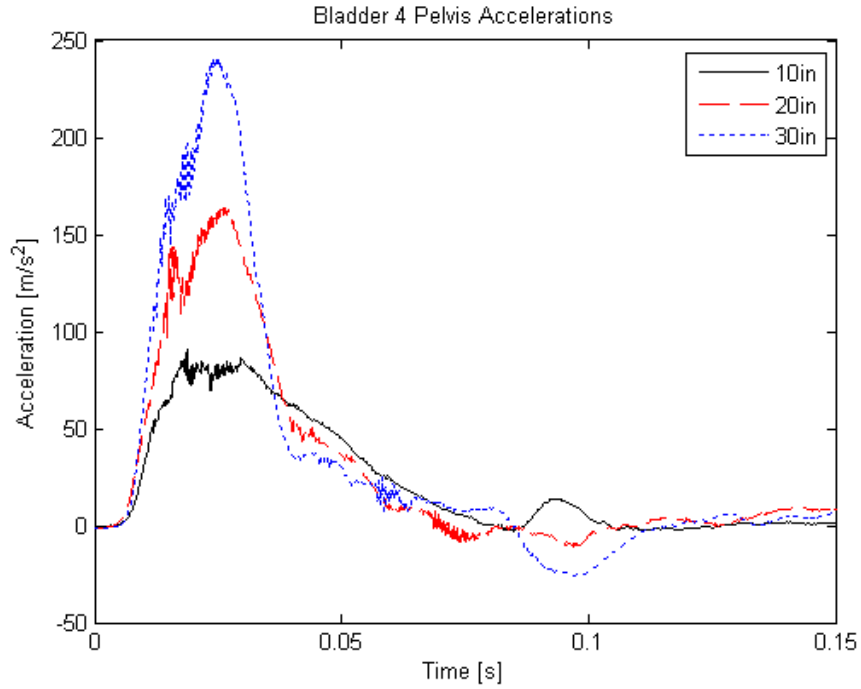

Figure 7.13 Bladder 4 Pelvic Accelerations – All Drop Heights

7.4 Spine Load Performance – ARL

One major issue to be discussed, in hopes of future research, is the validity of the Dynamic Response Index as a true measure for injury criteria. The measured spine loads from the ATD are presented here. Future reference will be made in comparing the reduction of measured spine load, as compared to the calculated reduction in DRI which is designed to be a predictor of spine load damage.

7.4.1 Combined Spine Load Performance by Drop Height - ARL

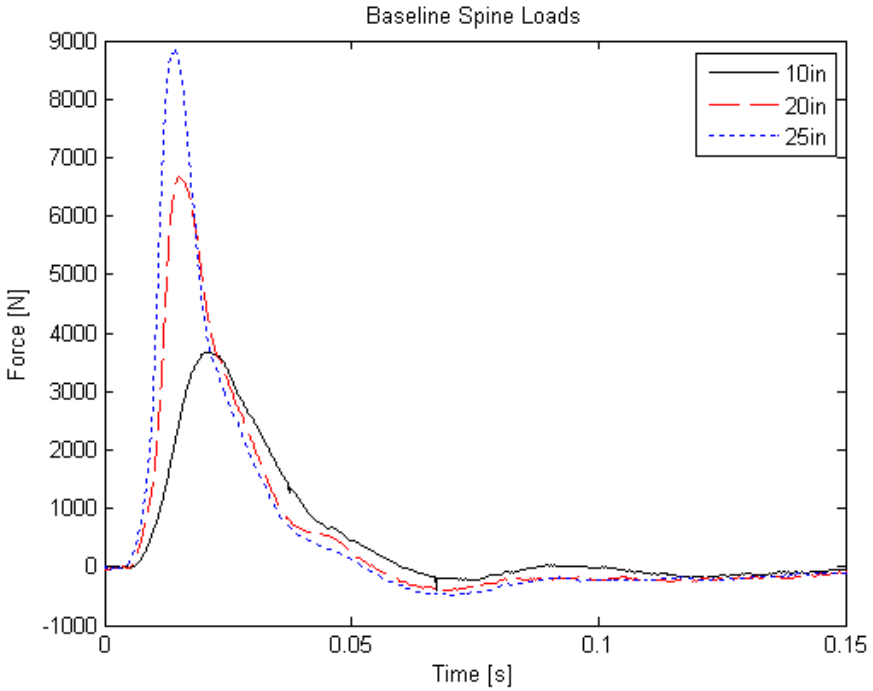

Figure 7.14 Baseline/Dummy Spine Loads – All Drop Heights

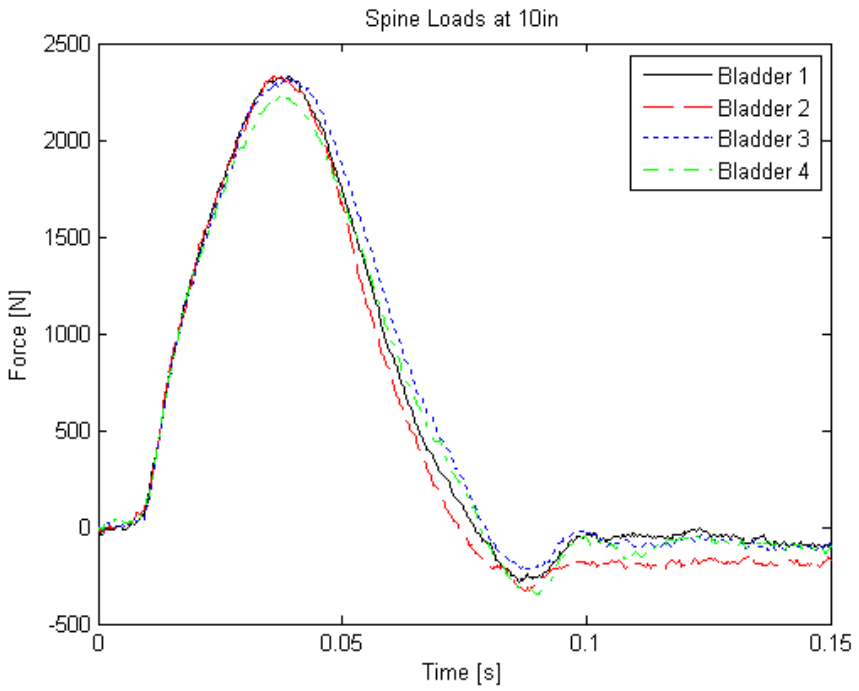

Figure 7.15 Spine Loads all Bladders– 10in Drop Height

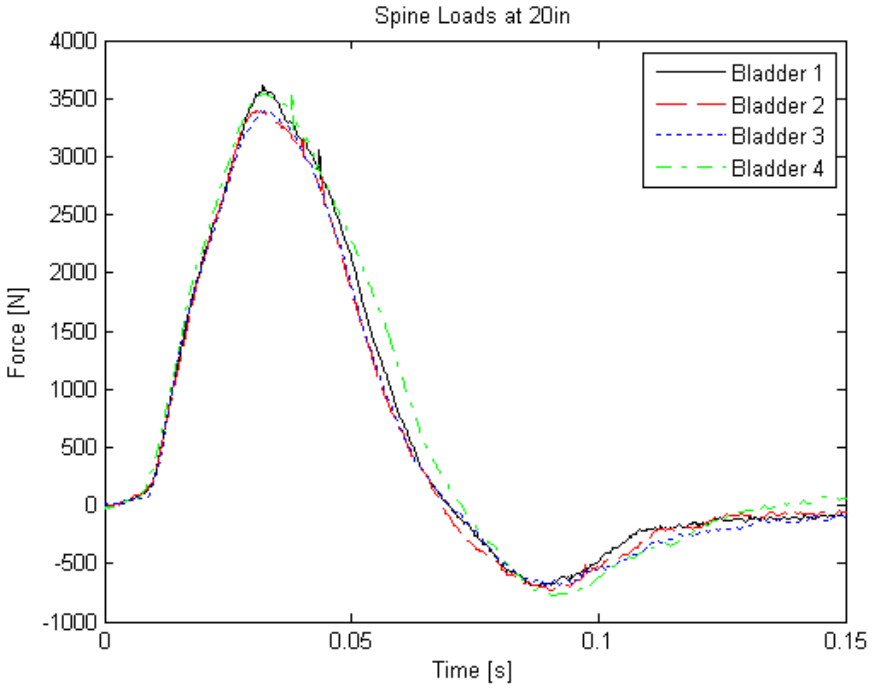

Figure 7.16 Spine Loads all Bladders– 20in Drop Height

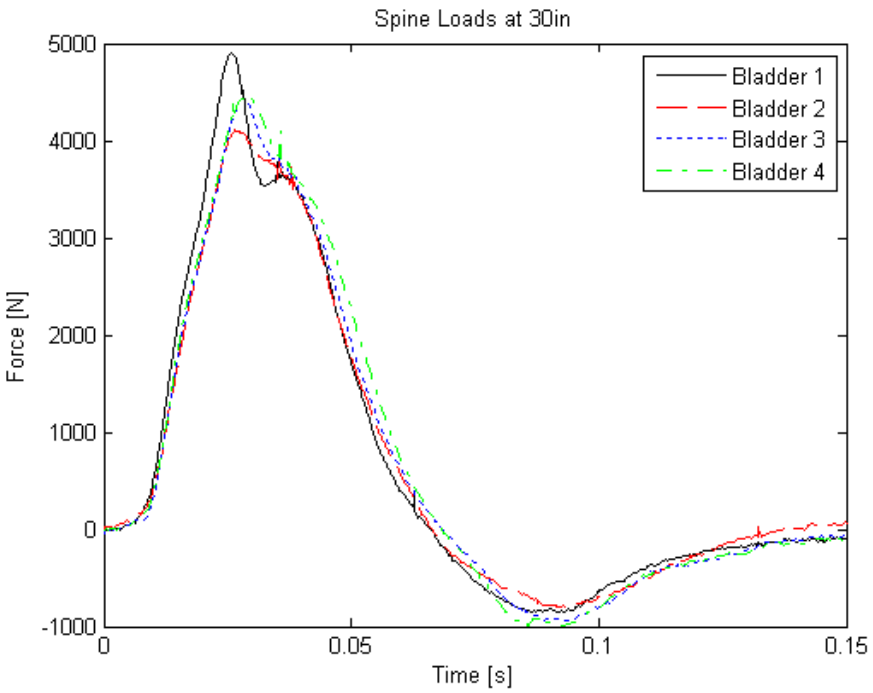

Figure 7.17 Spine Loads all Bladders– 30in Drop Height

7.4.2 Spine Load Performance by Bladder

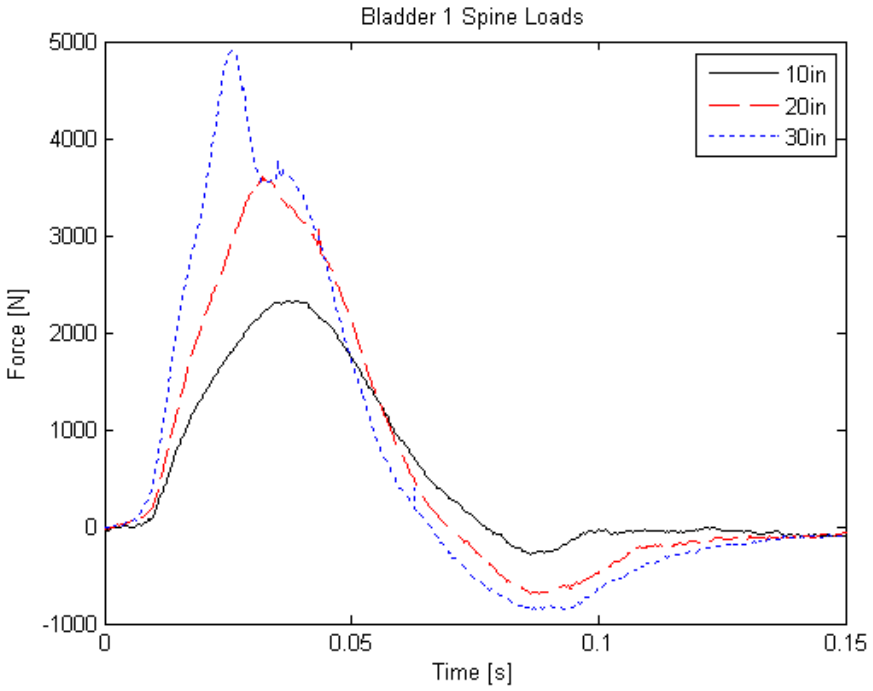

Figure 7.18 Bladder 1 Spine Loads – All Drop Heights

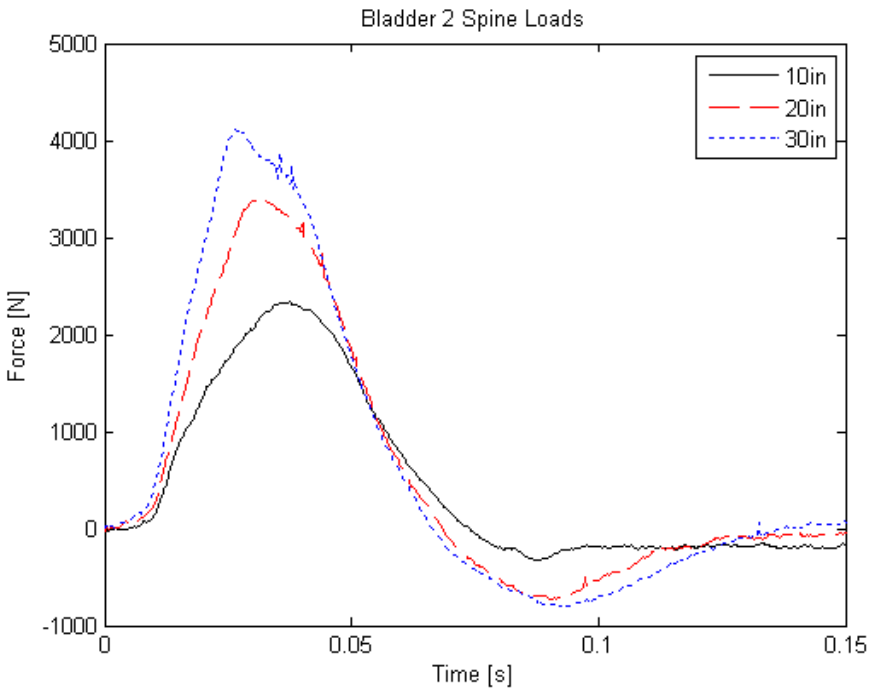

Figure 7.19 Bladder 2 Spine Loads – All Drop Heights

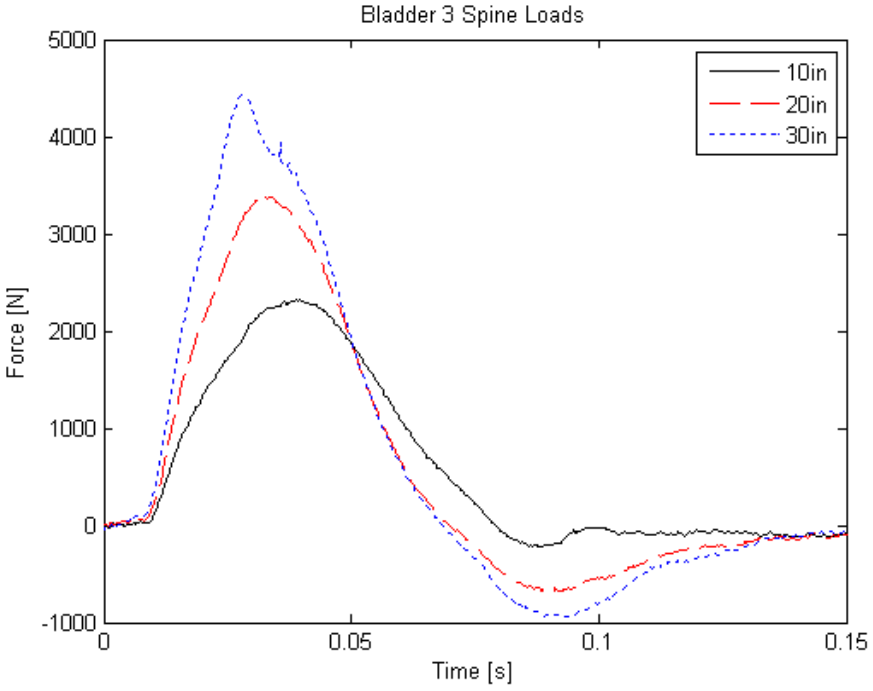

Figure 7.20 Bladder 3 Spine Loads – All Drop Heights

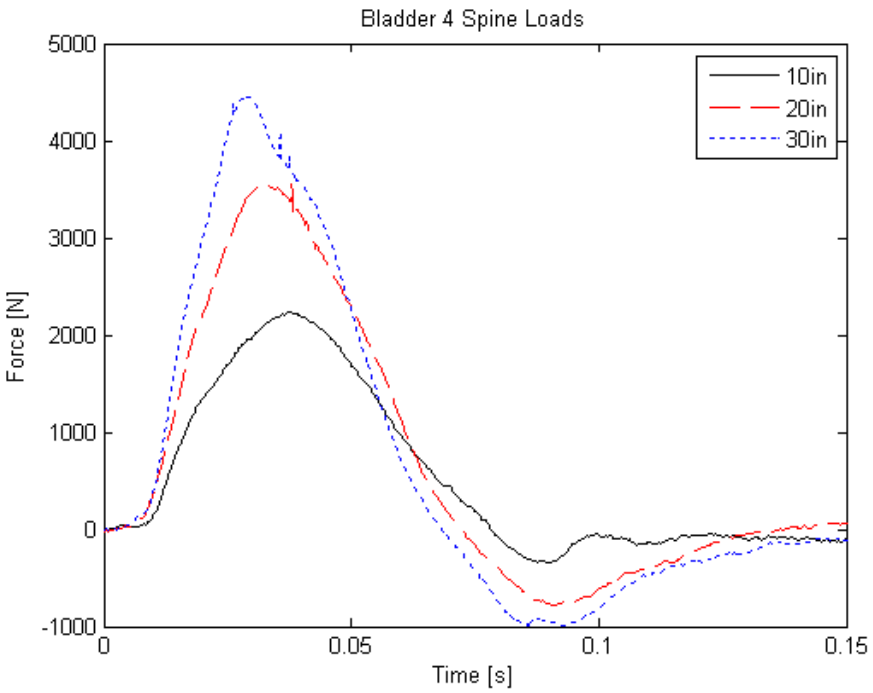

Figure 7.21 Bladder 4 Spine Loads – All Drop Heights

7.5 Dynamic Response Index Performance

7.5.1 DRI for Each Bladder from 30 in. Drop Height- ARL

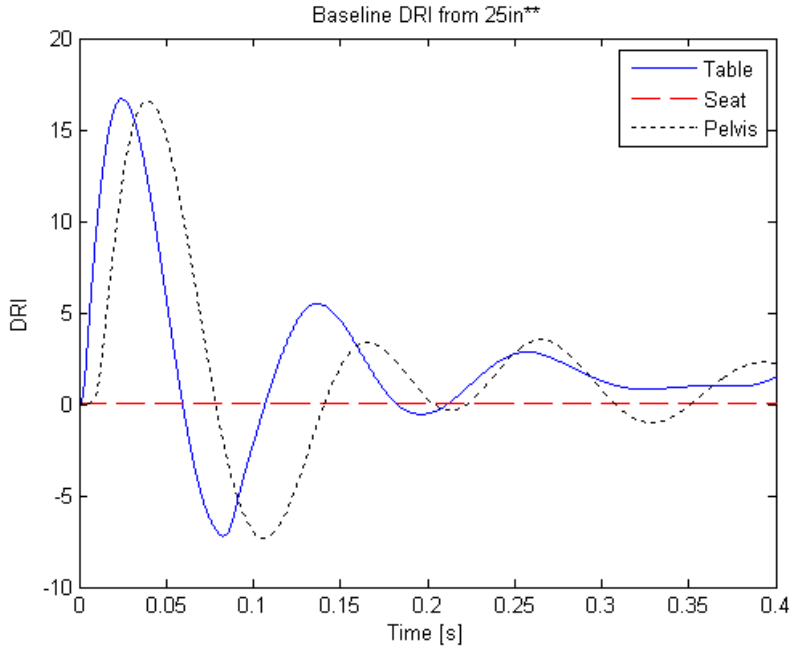

Figure 7.22 Baseline/Dummy DRIs – 25 in. Drop Height

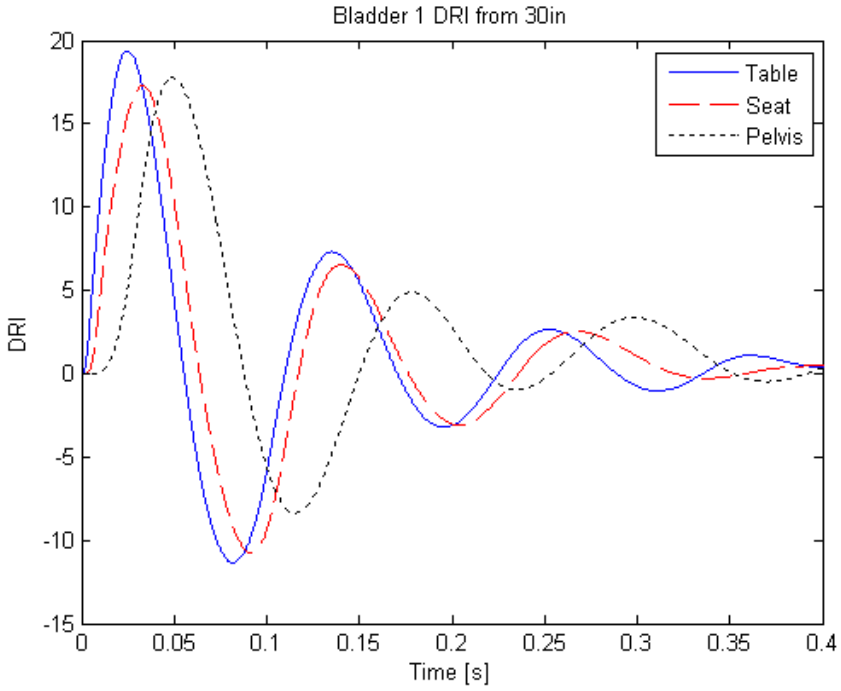

Figure 7.23 Bladder 1 DRI – 30 in. Drop Height

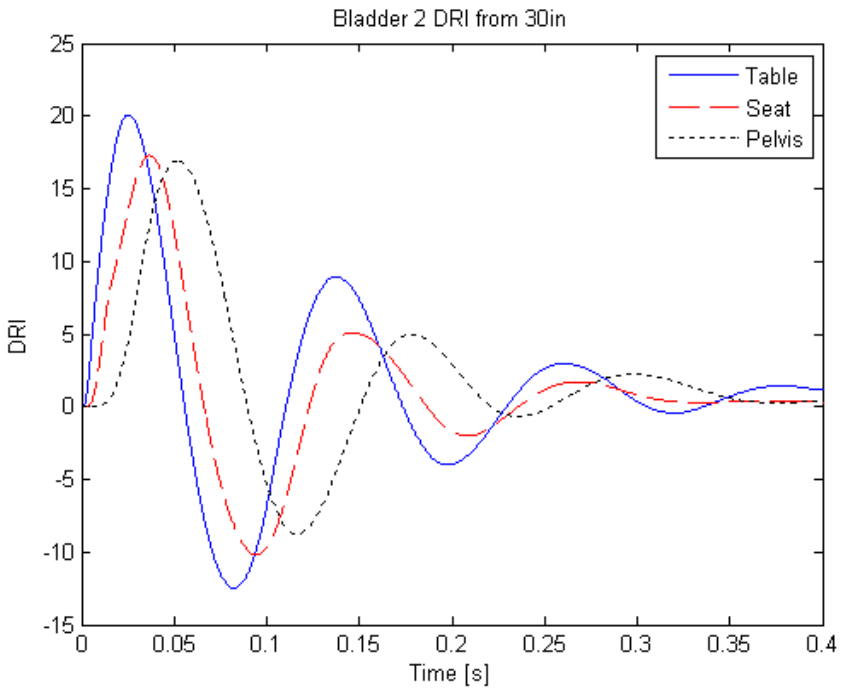

Figure 7.24 Bladder 2 DRI – 30in Drop Height

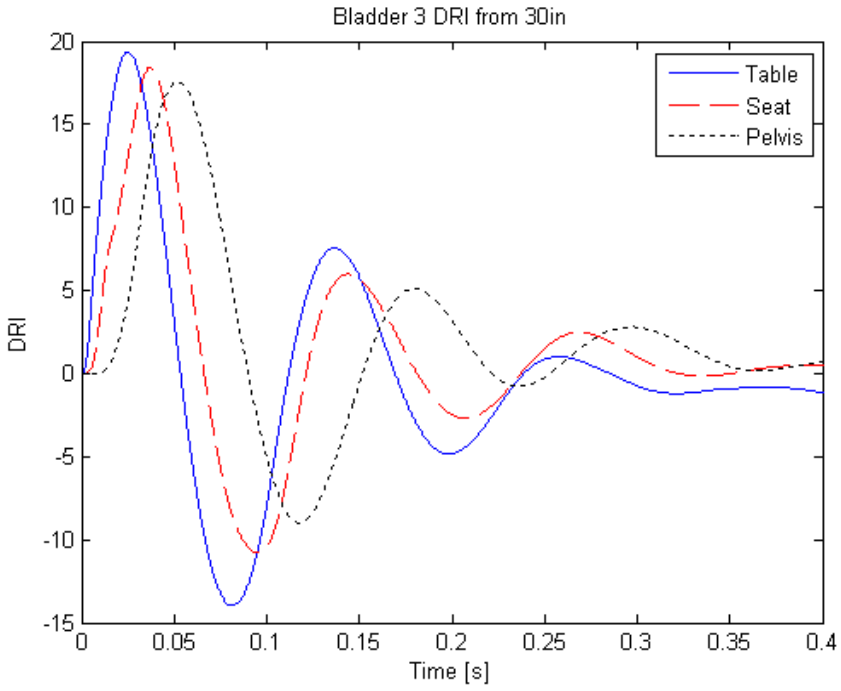

Figure 7.25 Bladder 3 DRI – 30in Drop Height

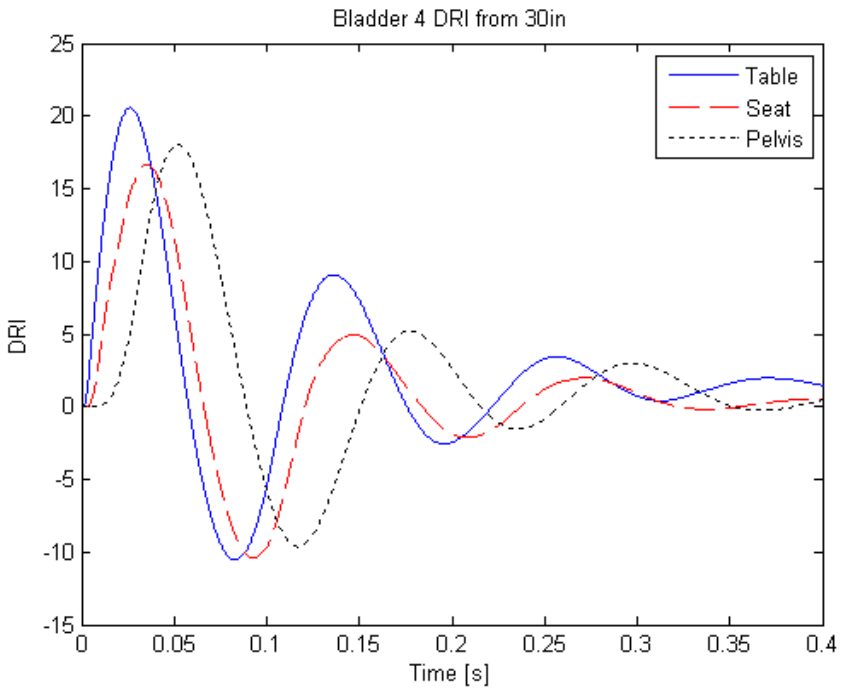

Figure 7.26 Bladder 4 DRI – 30in Drop Height

7.5.2 Combined DRI Performance of the Seat Pad from all heights

The SAE seat-pad accelerometer was not used during baseline testing. In the following figures to more accurately compare the Bladders performance, the figures have been zoomed to the area of interest near the peak DRI value. While the scale in each figure might differ, the range was maintained to give the reader an accurate perspective. Also this was necessary because the difference in peak DRIs were not overly significant from bladder to bladder.

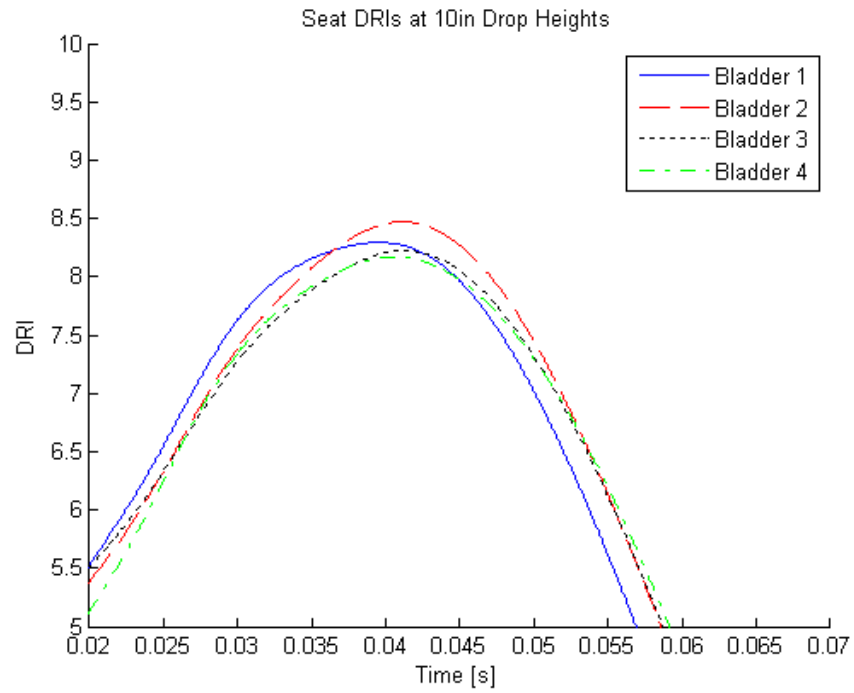

Figure 7.27 Seat-pad DRIs All Bladders – 10 in. Drop Height

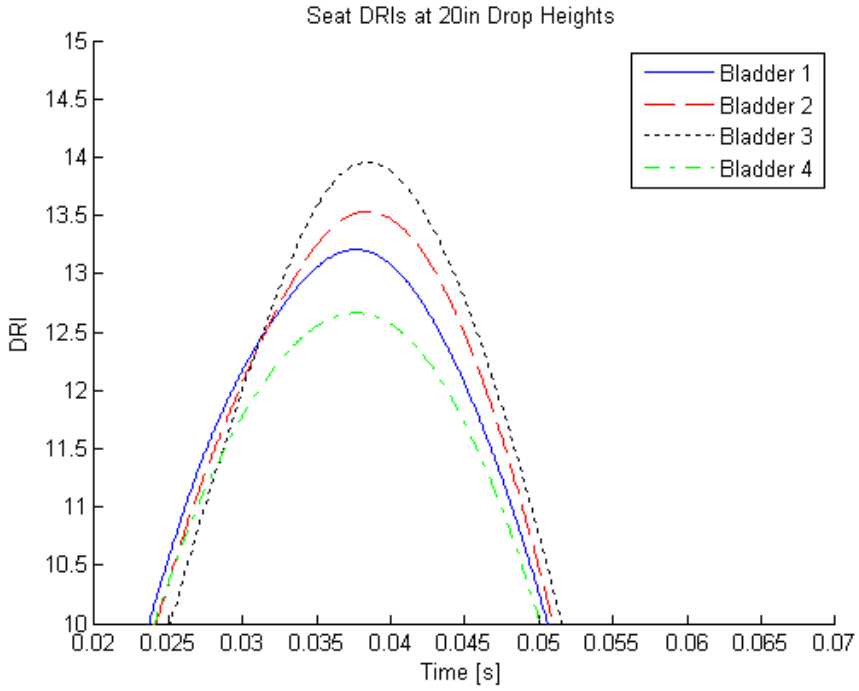

Figure 7.28 Seat-pad DRIs All Bladders – 20 in. Drop Height

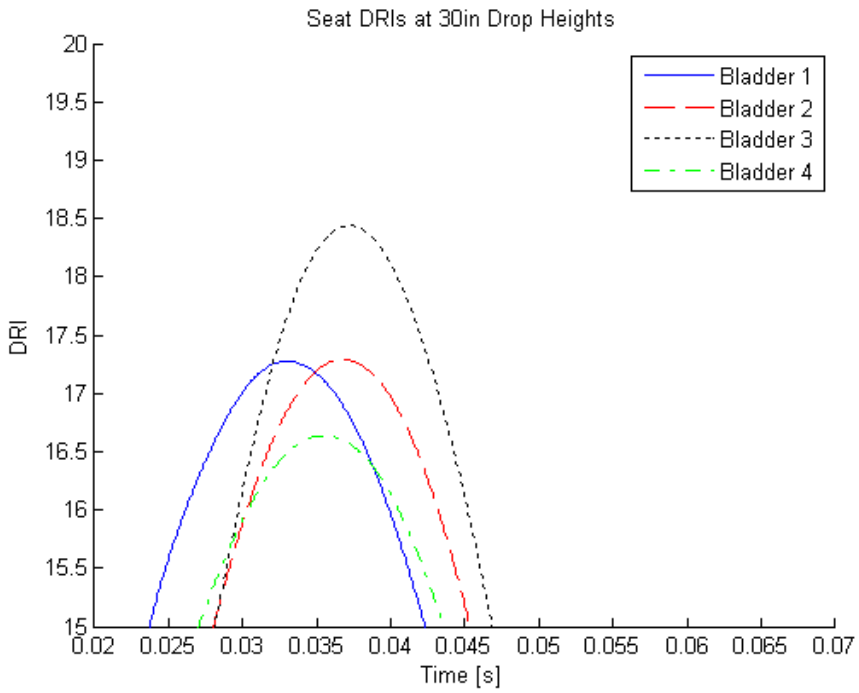

Figure 7.29 Seat-pad DRIs All Bladders – 30in Drop Height

7.5.3 Combined DRI Performance of the Pelvis from all heights

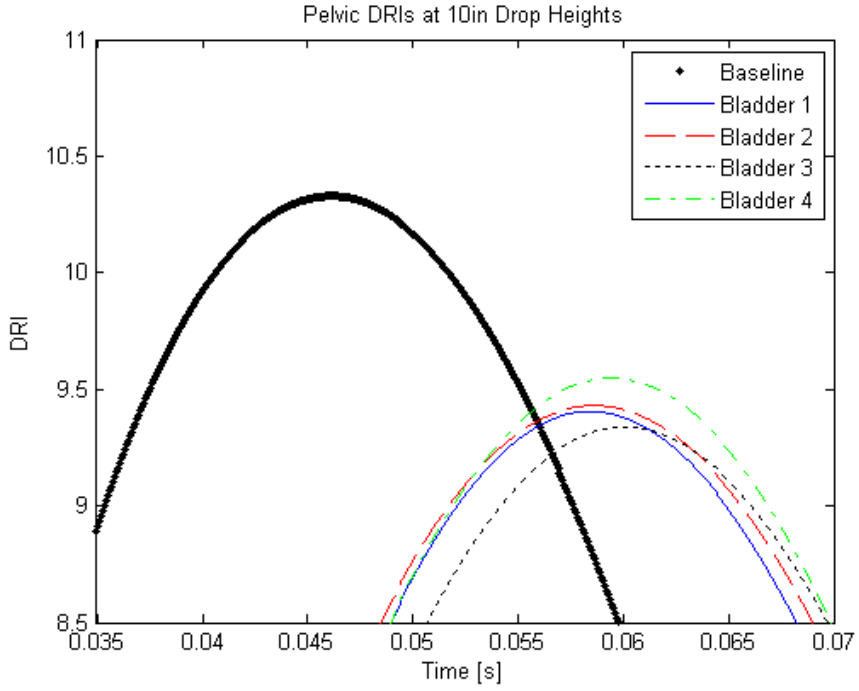

Figure 7.30 Pelvic DRIs All Bladders – 10in Drop Height

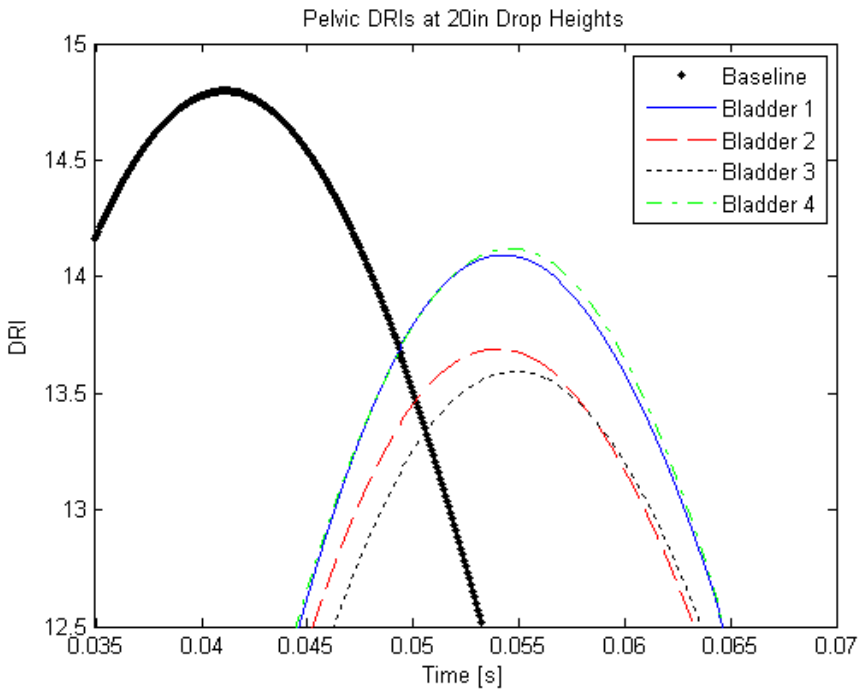

Figure 7.31 Pelvic DRIs All Bladders – 20in Drop Height

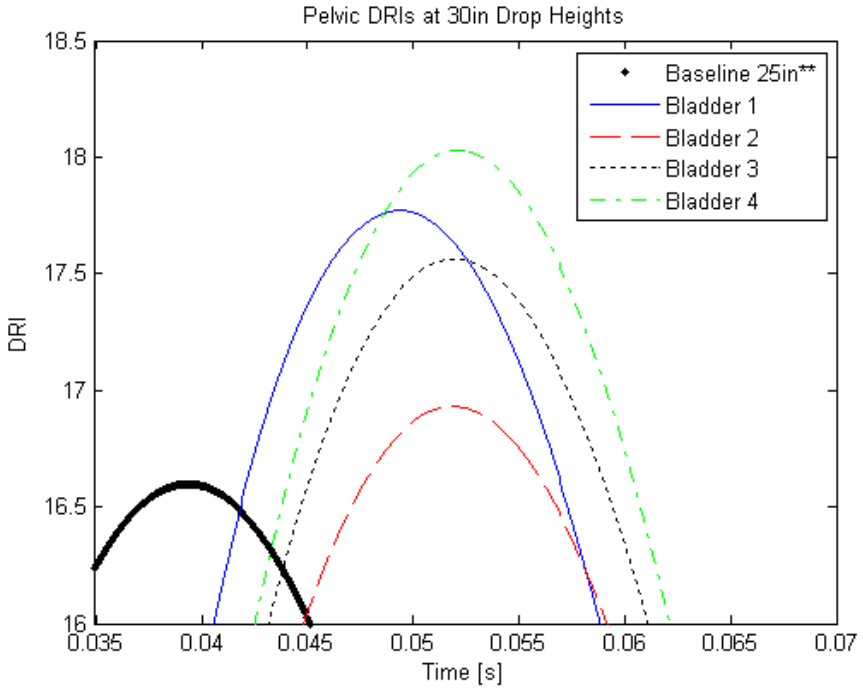

Figure 7.32 Pelvic DRIs All Bladders – 30in Drop Height

CHAPTER 8

UNLV SHOCK TESTING RESPONSE RESULTS

8.1 UNLV Shock Characterization

The shocks produced by the UNLV drop tower consistently have multiple pulses with approximately 2-5 millisecond pulse widths. This is different than the pulse produced by the Army Research Lab which are simple shocks consisting of half-sine pulses of approximately 5 milliseconds. The complete discussion and analysis of the data presented here can be found in Chapter 9.

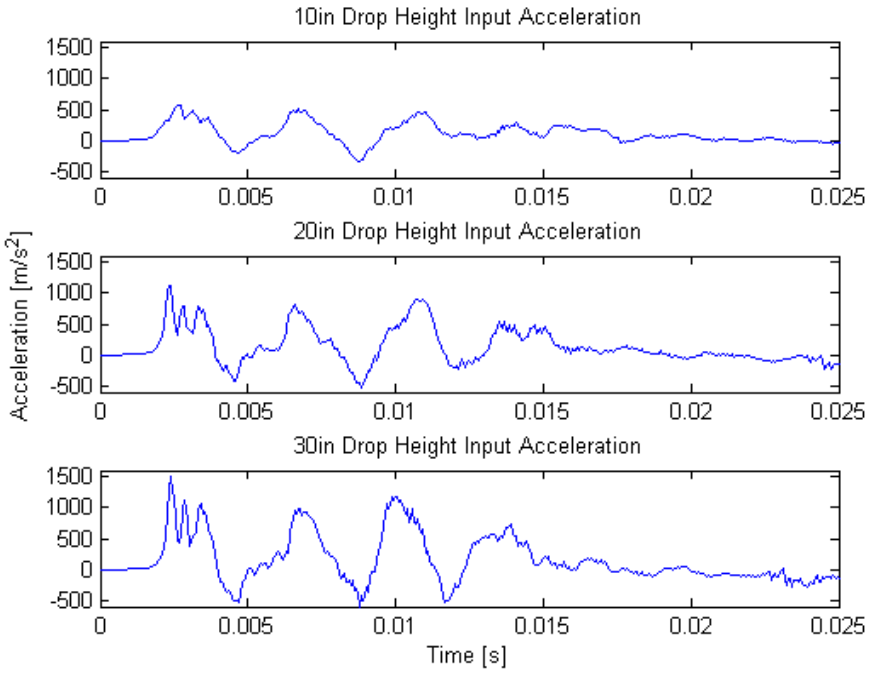

Figure 8.1 UNLV Input Shock Profiles from All Drop Heights

The UNLV shock pulses do not resemble classic shocks such as ARL's half-sine; rather they more resemble a pyrotechnic shock even though peak accelerations were reasonably similar. However the peak-peak values are greater when the positive-to-

negative peak values are taken into account. It should be noted that both shock types are considered zero-mean shocks because their velocities begin and end at zero.

A summary of the peak input accelerations from both ARL and UNLV is provided below. The UNLV accelerations are characterized in two ways here, first only its maximum positive acceleration is noted, while the "max peak-to-peak" is the total magnitude from the first positive peak to the first negative peak. This is shown here because, unlike the ARL shock profiles, the UNLV shock profiles do rebound producing negative accelerations.

	PEAK ACCELERATIONS [m/s^2]		
Height	**UNLV (max peak)**	**UNLV (max peak-to-peak)**	**ARL**
10in	582	916	885
20in	1120	1647	1437
30in	1496	2114	1847

Table 8.1 Summary of Peak Input Acceleration Values

8.2 Typical Signal Filtering Results

The UNLV signal's minimum pulse width of approximately 2ms, causes a fundamental pulse frequency to be:

$$f_{pulse} = \frac{1}{2\Delta t_{pulse}} \qquad \textbf{Equation 8.1}$$

Where the sampling rate should equal

$$f_{sampling} \geq 10 f_{pulse} \qquad \textbf{Equation 8.2}$$

And the filter-frequency 3dB cutoff point for a low-pass filter to be:

$$f_{filter} \geq 5f_{pulse}$$ **Equation 8.3**

Both of these conditions are satisfied and a filter frequency of 1250Hz is applied to all the following acceleration signals, regardless of their individual pulse width (as in the case of the seat-pad acceleration).

An example of each the raw and filtered input shock acceleration and the raw and filtered seat-pad acceleration are provided below with a summary of their percentage of peak-reduction from filtering which follows.

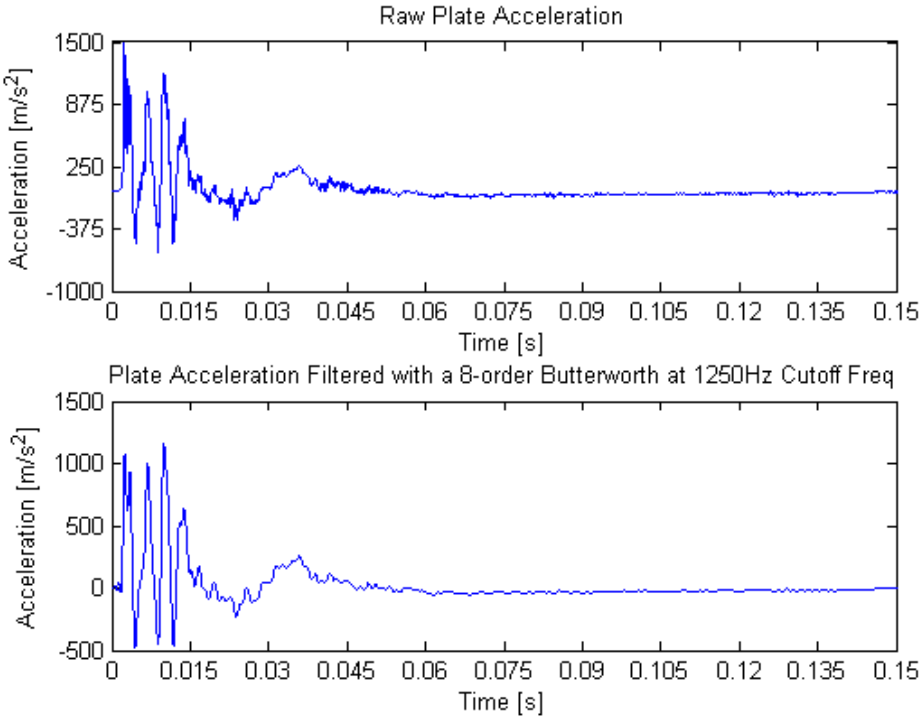

Figure 8.2 Typical Raw and Filtered Plate Accelerations - 30in Drop Height

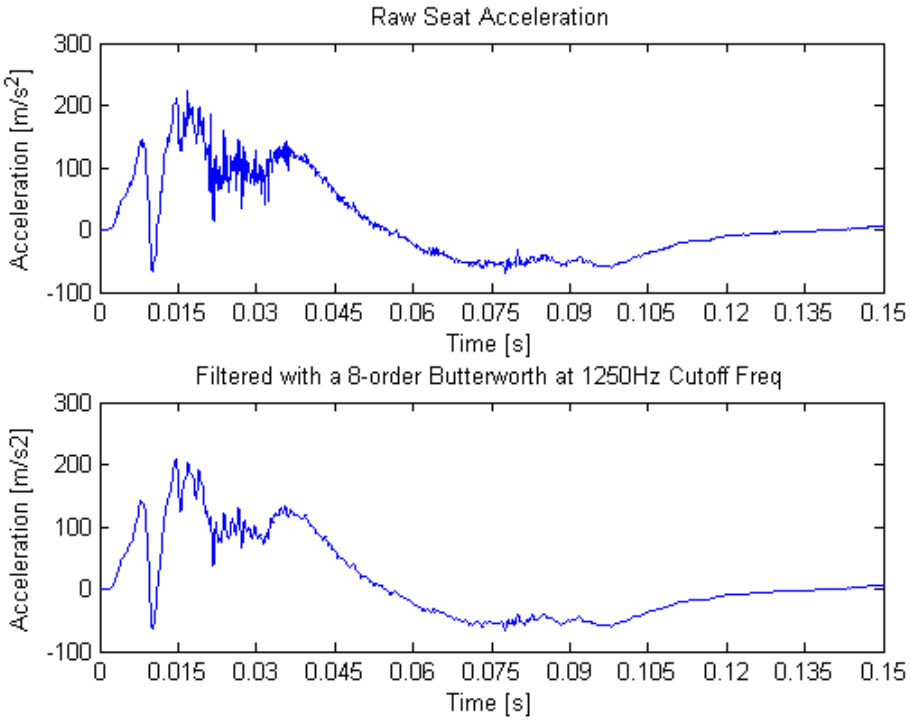

Figure 8.3 Typical Raw and Filtered Seat Accelerations - 30in Drop Height

	Input Acceleration	**Seat-Pad Acceleration**
Maximum Filtered Peak Value	1156 m/s^2	209 m/s^2
Percentage Filtered Peak Reduction	22.8%	6.5%

Table 8.2 Filtered Acceleration Peak Reduction

8.3 Combined Acceleration Performance Plots for all Drop Heights - UNLV

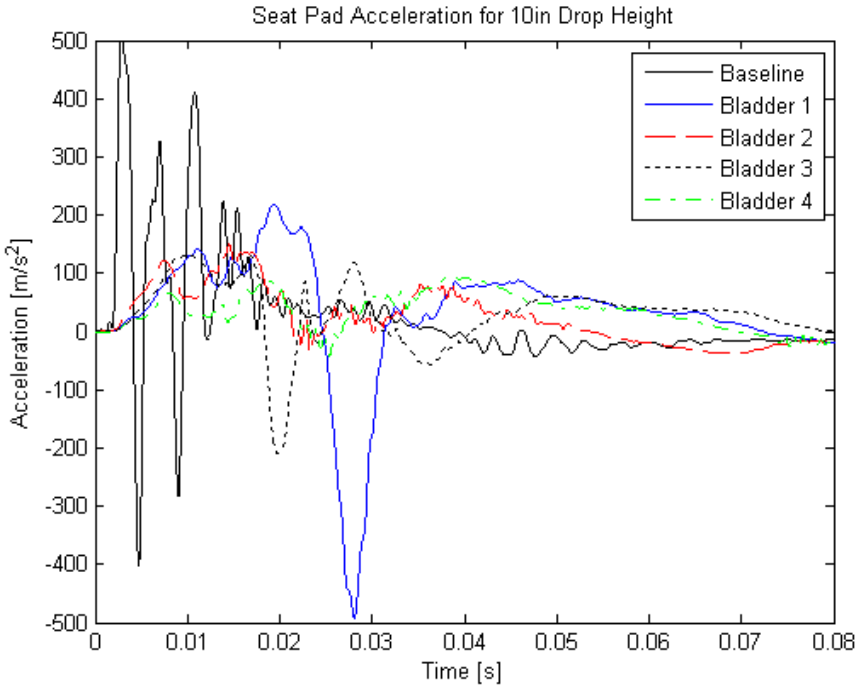

Figure 8.4 Seat Pad Acceleration - 10 in. Drop Height

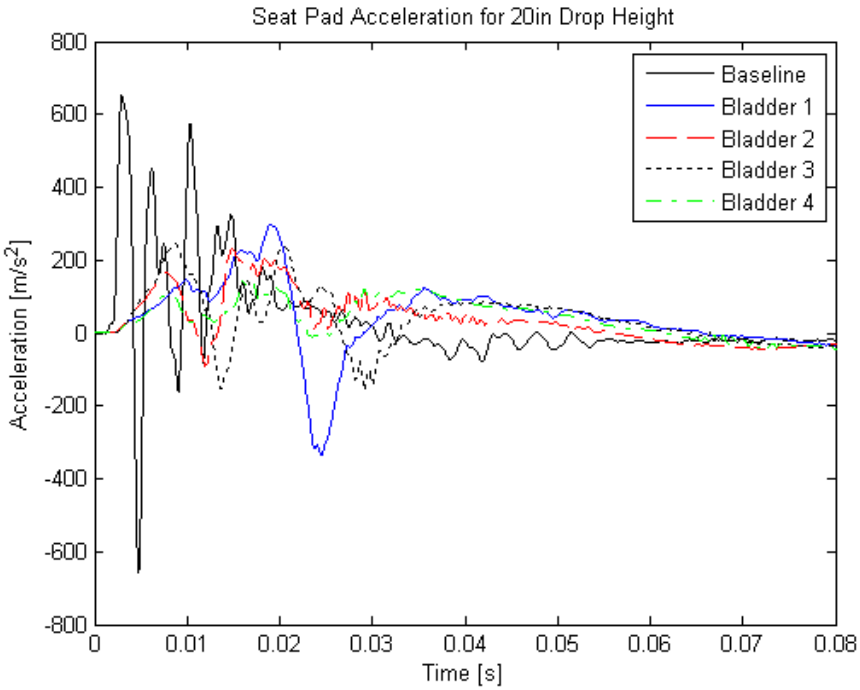

Figure 8.5 Seat Pad Acceleration - 20 in. Drop Height

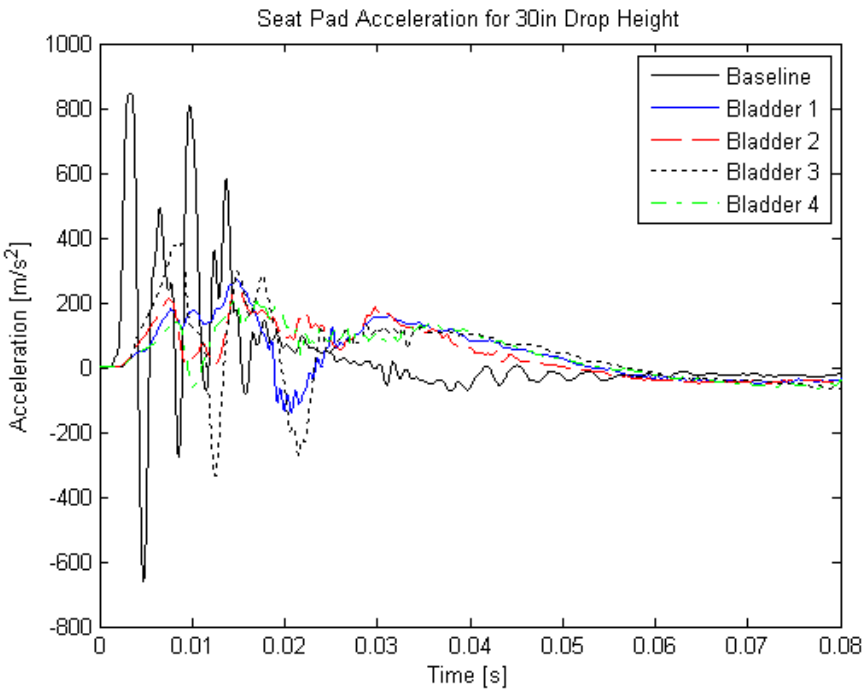

Figure 8.6 Seat Pad Acceleration - 30in Drop Height

8.4 Seat Acceleration Performance and Kinematics by Bladder for 30in Drop – UNLV

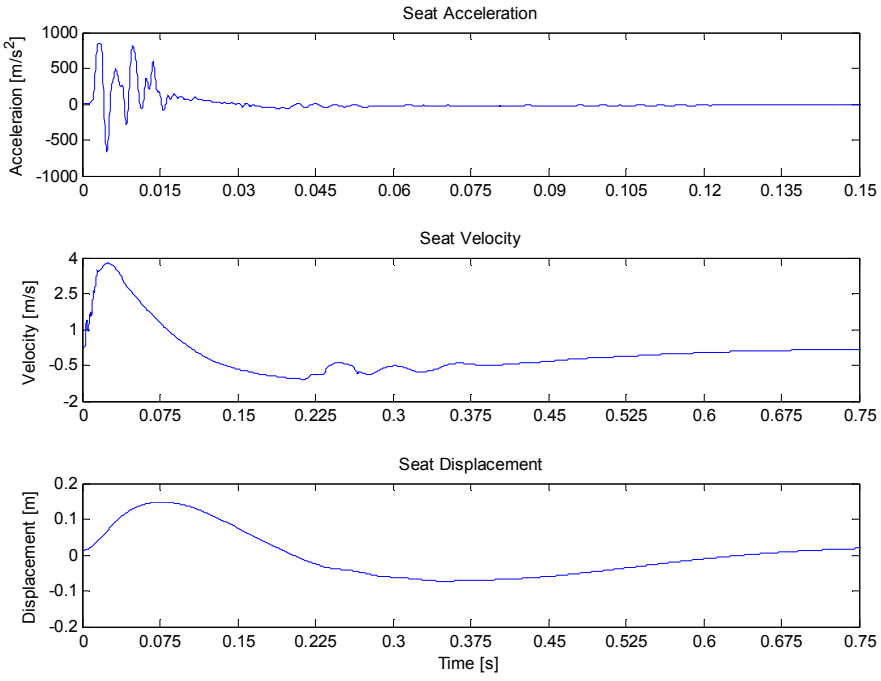

Figure 8.7 Baseline Seat Pad Response - 30 in. Drop Height

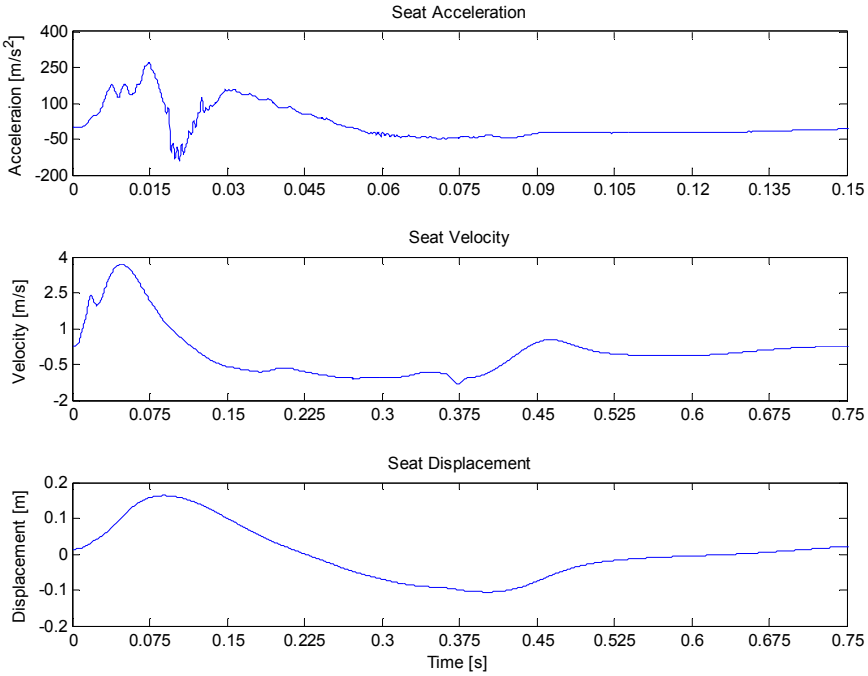

Figure 8.8 Bladder 1 Seat Pad Response - 30 in. Drop Height

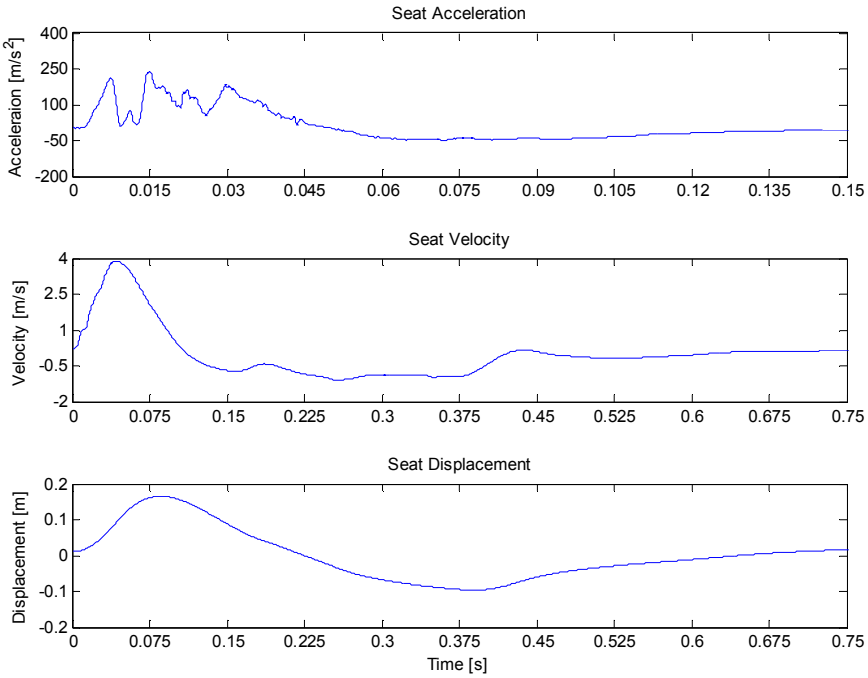

Figure 8.9 Bladder 2 Seat Pad Response - 30 in. Drop Height

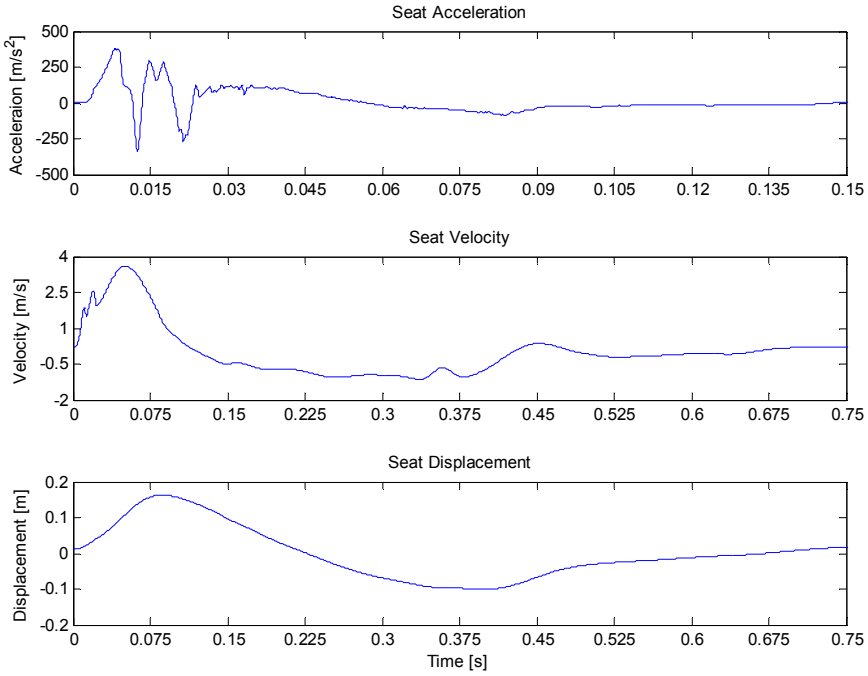

Figure 8.10 Bladder 3 Seat Pad Response - 30 in. Drop Height

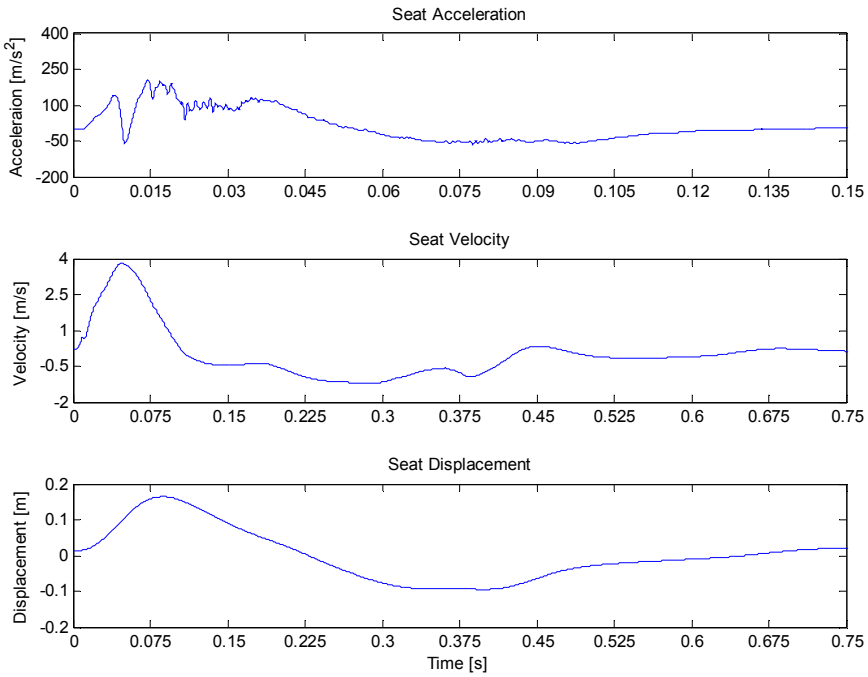

Figure 8.11 Bladder 4 Seat Pad Response - 30 in. Drop Height

8.5 Dynamic Response Index Performance - UNLV

A major difference in this analysis to the one conducted for ARL was the usage of the ATD. Without the ATD and the direct pelvis acceleration measurement, an actual Pelvic-DRI cannot be calculated. While observations will be made to the possible DRI for this battery of tests based on correlations from the ARL Drop tests, it is more likely that future work including repeat tests with an instrumented ATD and numerical analyses would be necessary to develop any relevant correlations.

8.5.1 DRI for 30in Drop Heights – UNLV

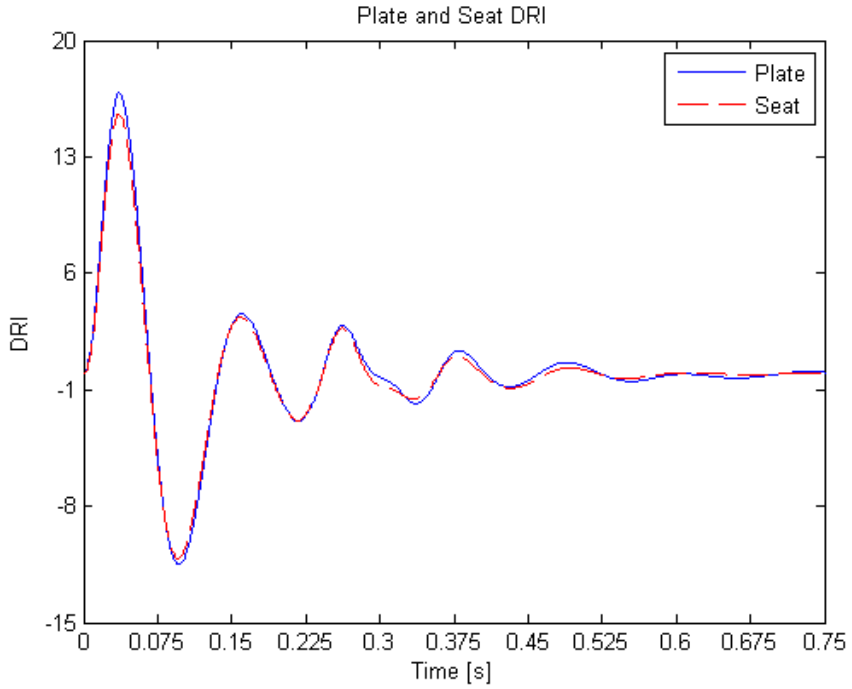

Figure 8.12 Baseline DRI - 30 in. Drop Height

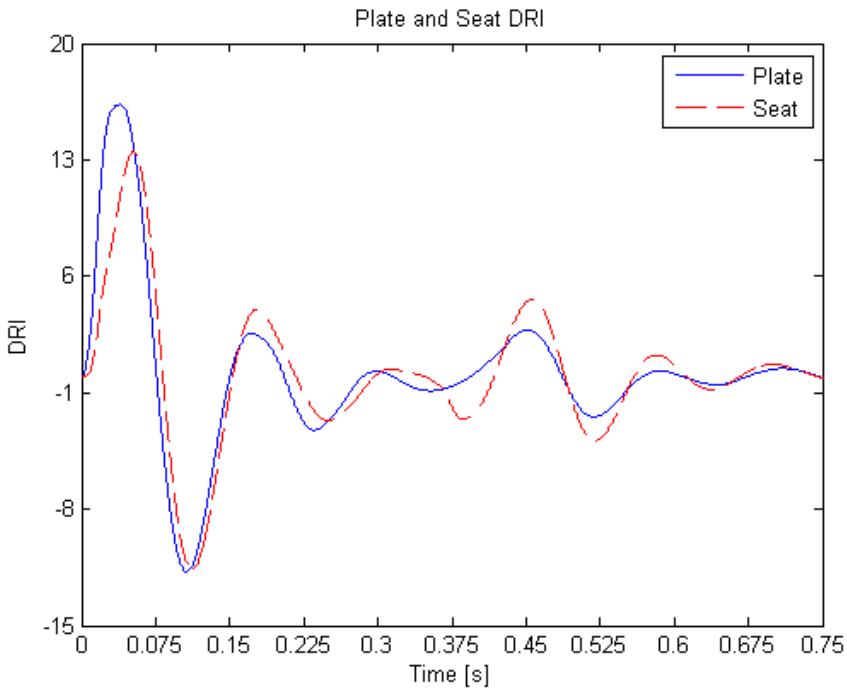

Figure 8.13 Bladder 1 DRI - 30 in. Drop Height

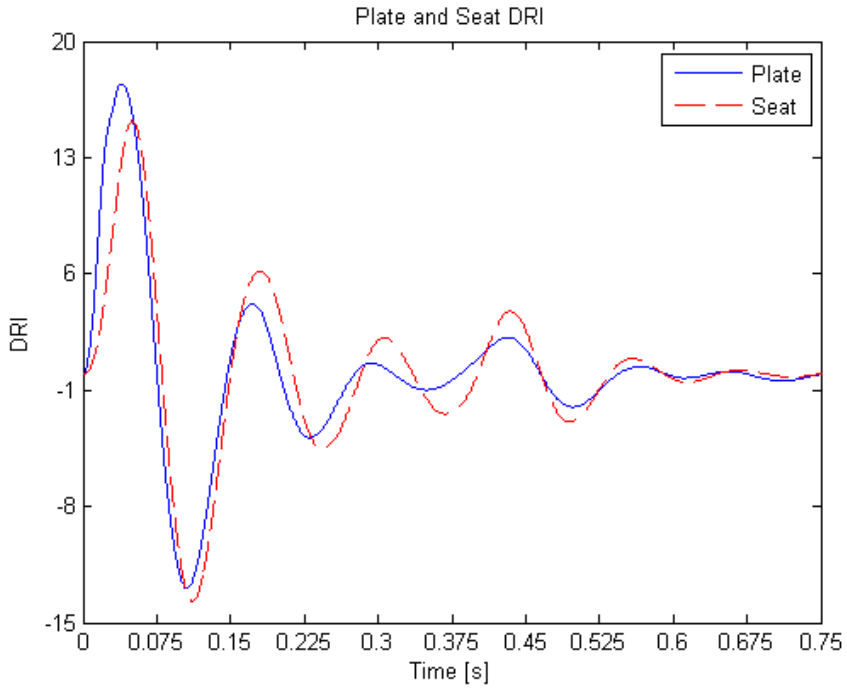

Figure 8.14 Bladder 2 DRI - 30 in. Drop Height

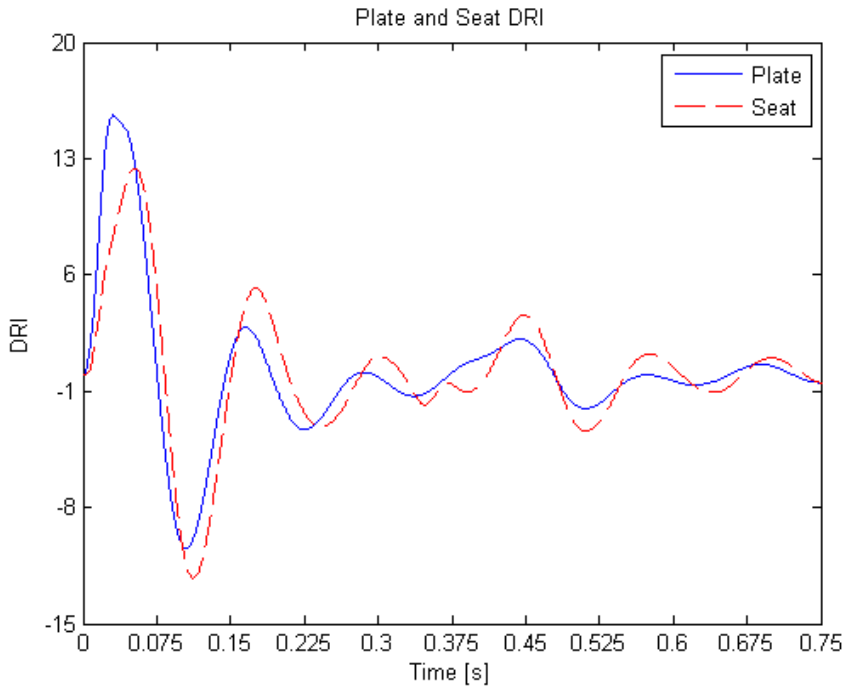

Figure 8.15 Bladder 3 DRI - 30 in. Drop Height

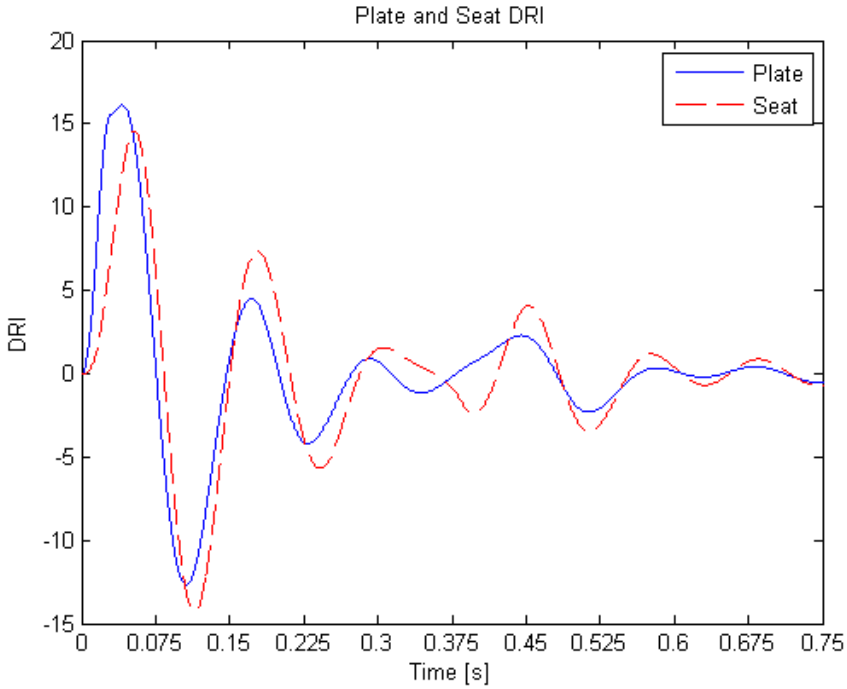

Figure 8.16 Bladder 4 DRI - 30in Drop Height

8.5.2 Combined DRI Performance for 30in Drop Heights – UNLV

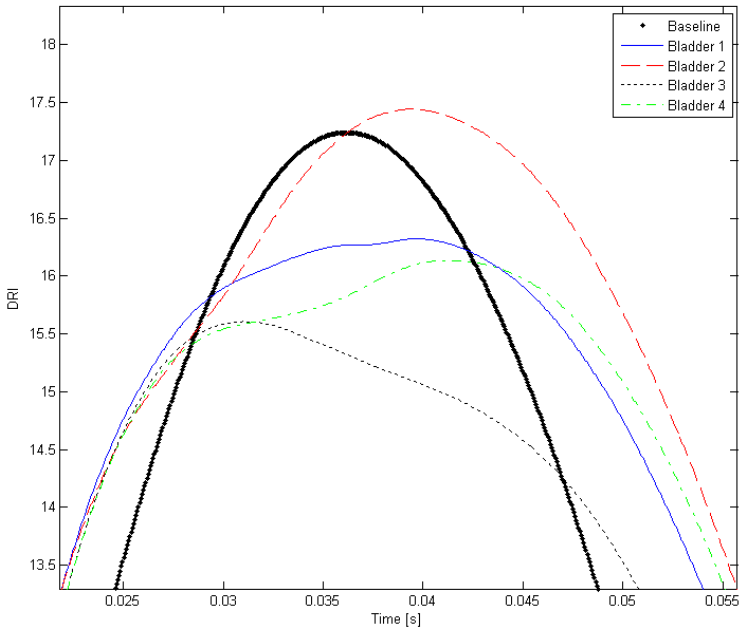

Figure 8.17 Plate DRI for all Bladders - 30in Drop Height

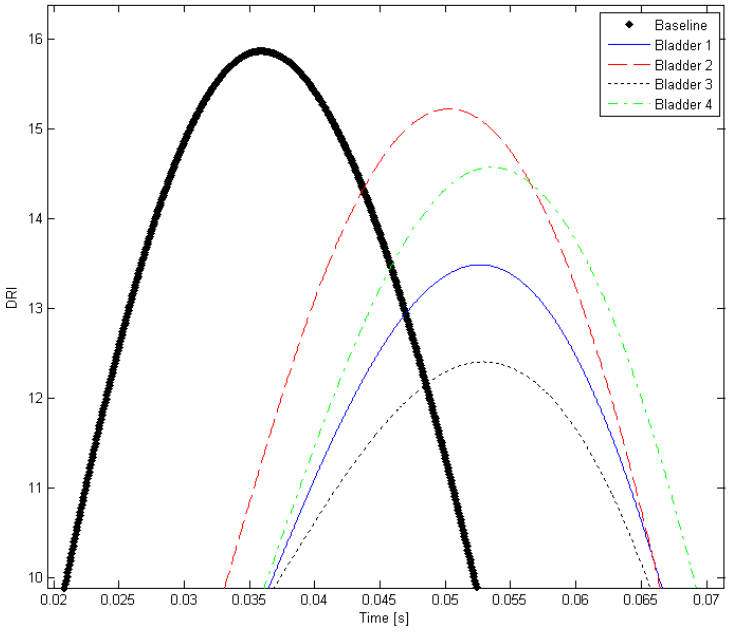

Figure 8.18 Seat DRI for all Bladders from 30in Drop Height

CHAPTER 9

DISCUSSION AND ANALYSIS OF RESULTS

The data developed during this study will be analyzed in this chapter both by section and by making comparisons across chapters. The investigation of air bladder seat cushion performance in reducing whole body shock and vibration exposure was a major objective of this project. Therefore, the relevant design parameters of the air bladder seat cushion that were investigated are provided in Table 9.1.

Bladder Number	Foam Density	Foam Hole Diameter	Internal Tube Diameter
1	1 lb/ft^3	0.5 in.	0.375 in.
2	1 lb/ft^3	1 in.	0.25 in.
3	2 lb/ft^3	0.5 in.	0.25 in.
4	2 lb/ft^3	1 in.	0.375 in.

Table 9.1 Review of Bladder Parameter Configurations

9.1 Discussion of Seat Vibration Results

9.1.1 Vibration Signal Comparison

As discussed in Chapter 5.1.3, the Warrior ride scenario signal and the constant r.m.s velocity signal have their own strengths and weaknesses and are expected to reveal different properties of the air bladder seat cushions. The warrior signal contains a significant amount of energy at the lower frequencies, but it has near negligible energy as frequencies approach 100 Hz (Figure 5.1 and Figure 5.2). The constant-RMS velocity signal was used for this reason. The constant velocity signal has low energy values at low frequencies and energy increase as frequency increases (Figure 5.3 and Figure 5.4). The energy levels as a function of frequency in each signal affected the coherence between the vibration inputs and outputs associated with each air bladder seat cushion. By using

the two signals, the entire frequency range of interest from 1-100Hz was excited with significant energy by at least one, if not both, of the signals.

9.1.2 Coherence, Frequency Response Function and Transmissibility Function

The amount of energy contained in both the Warrior and constant r.m.s velocity input signals within each of the 1/3-octave bandwidths directly affected the coherence of the input-output relationships associated with the different air bladder seat cushion configurations. The seat cushion is inherently a "soft" system that contrasts with a rigid structure where energy-transmissibility more readily occurs. The coherence function is defined as:

$$\text{Coherence} = \gamma^2_{xy}(f) = \frac{\left|G_{xy}(f)\right|^2}{G_{xx}(f)G_{yy}(f)} \qquad \textbf{Equation 9.1}$$

where $\gamma^2_{xy}(f) \leq 1$ and

G_{xy} = Cross-Power Spectral Density of the Input and Ouput

G_{xx} = Auto-Power Spectral Density of the Input

G_{yy} = Auto-Power Spectral Density of the Output

Figure 5.5 shows the coherence of the Warrior signal. The coherence for all seat bladder configurations dropped off drastically after the 10 Hz 1/3 octave band. The FFT of the input Warrior Signal (Figure 5.2), indicates that the magnitude of the individual frequencies dropped below 0.100 m/s^2 above the 10 Hz 1/3 octave band, contributing to the poor coherence.

The coherence of the constant-velocity signal (Figure 5.6) was satisfactory for all seat bladder configurations above 1.6 Hz 1/3 octave band and strong at frequencies above the 2 Hz 1/3 octave band. Bladder 1, which is the "softest" of all the air bladder seat cushion configurations, was the only bladder to suffer from a poor coherence above the 40 Hz 1/3

octave band. This was possibly associated with the low stiffness of this cushion configuration, resulting in less energy transfer.

The frequency response, FRF(f), and transmissibility, TR(f), functions are calculated differently. The frequency response function, FRF(f), which is a function of the coherence function, γ^2_{xy}, is obtained from:

$$FRF(f) = |G(jf)| = \frac{G_{xx(out)}(f)\,\gamma^2_{xy}(f)}{G_{yy(in)}(f)} \qquad \textbf{Equation 9.2}$$

where:

$\gamma_{xy}(f)$ = coherence function between the output, $G_{xx(out)}(f)$, and the input, $G_{yy(in)}$

$G_{xx(out)}$ = Auto-Power Spectral Density of the Ouput

$G_{yy(in)}$ = Auto-Power Spectral Density of the Input

The transmissibility function, TR(f), is obtained from:

$$TR(f) = \frac{|G_{xx}(f)|}{|G_{yy}(f)|} \qquad \textbf{Equation 9.3}$$

where:

G_{yy} = Auto-Power Spectral Density of the Input

G_{xx} = Auto-Power Spectral Density of the Output

Figures 5.15 and 5.17 show the magnitudes of the frequency response functions for the air bladder seat configurations for the Warrior and constant velocity signals, respectively, at frequencies where $\gamma^2_{xy} > 0.9$. Figures 5.13 and 5.14 show the magnitudes of the transmissibility functions for the air bladder seat configurations for the Warrior and constant velocity signals, respectively, at frequencies where $\gamma^2_{xy} > 0.9$.

9.1.3 Seat Cushion Input Autospectra

The 1/3 octave band autospectra of the vibration response of the different air bladder seat cushions associated with the Warrior excitation signal (Figures 5.7 and 5.9) peaked between the 3.15 - 5 Hz 1/3 octave bands. This implies a system resonance within this frequency range. The coherence associated with the seat cushion responses to the Warrior signal was very low at frequencies above the 10 Hz 1/3 octave band (Figure 5.5). This indicates the measured autospectra were not or were weakly associated with the Warrior excitation signal. The lack of coherence at frequencies at frequencies above the 10 Hz 1/3 octave band is due in part to the very low vibration values at these higher frequencies (Figure 5.2) Also, the one-degree-of-freedom antropodynamic dummy that was placed on the seat cushions rattled during the Warrior signal tests. Therefore, it is speculated that the measured autospectra of the vibration response of the seat cushions at frequencies above the 10 Hz 1/3 octave band were mainly associated with vibration within the antropodynamic dummy.

The 1/3 octave band autospectra of the vibration response of the different air bladder seat cushions associated with the constant velocity excitation signal (Figures 5.8 and 5.10) shows a slight peak between the 3.15 - 5 Hz 1/3 octave bands. This is associated with the system resonance that was identified with the Warrior signal. The seat cushion 1/3 octave band autospecta values continue to increase at frequencies above the 5 Hz 1/3 octave band because the corresponding 1/3 octave band levels associated with the constant velocity input also increase (Figure 5.3). The coherence associated with the seat cushion responses to the constant velocity signal became low at 1/3 octave band frequencies below 2 Hz and above 40 Hz for seat cushion configuration1and above 63 Hz

for seat cushion configurations 2 - 4 (Figure 5.6). This indicates the measured autospectra values were not or were weakly associated with the constant velocity excitation signal at these frequencies.

9.1.4 ISO Weighted Seat Pad Autospectra Analyses

The frequency weighting (W_k) for a seated human defined by ISO 2631 (Table 5.1) emphasizes the effects of whole body vibration exposure at frequencies between the 4 to 12 Hz 1/3-octave band frequencies by giving then weighting factors between 0.9 and 1.06. This is associated with the fact that the seated human body has resonance frequencies at around 5.8 and 8 Hz. Although it is not common to plot the ISO 1/3 octave band autospectra, it is interesting to note the effects of the ISO 2631 weighting factors on the measured air bladder seat cushion acceleration values. Figure 5.11 and Figure 5.12 show the effects of the resonant peak within the 4 and 5 Hz 1/3 octave bands.

9.1.5 ISO Weighted r.m.s. Acceleration and Vibration Dosage Values

The ISO weighted r.m.s. acceleration (a_W) and the fourth-power vibration dose values (VDV) were calculated as a single value that represented the overall exposure to the Warrior and constant velocity excitation signals. While the weighted r.m.s acceleration is inherently corrected for time, the VDV value is a factor of the exposure time. When whole body vibration signal is continuous with time, the a_W and VDV values are given by:

$$a_W = \left[\frac{1}{T} \int_0^T \left(a_w(t)\right)^2 dt \right]^{1/2} \quad [m/s^2]$$ **Equation 9.4**

$$VDV = \left[\int_0^T \left(a_w(t)\right)^4 dt \right]^{1/4} \quad [m/s^{1.75}]$$ **Equation 9.5**

where:

$a_w(t)$ = weighted r.m.s acceleration as a function of time history

T= duration of measurement [s]

However, when vibration spectra are given as 1/3 octave band values, the a_w and *VDV* values can be calculated by:

$$a_W = \left[\sum_i (W_i a_i)^2 \right]^{1/2} \quad [m/s^2]$$ **Equation 9.6**

where:

W_i = the weighting factor for the i-th 1/3-octave band

a_i = the r.m.s acceleration for the i-th 1/3-octave band

and VDV is estimated by:

$$eVDV = 1.4 a_W T^{1/4} \quad [m/s^{1.75}]$$ **Equation 9.7**

where:

eVDV = estimated Vibration Dosage Value

T = Duration of Measurement [s]

A summary of the measured a_W and eVDV values are provided below:

	Bladder 1		**Bladder 2**		**Bladder 3**		**Bladder 4**	
	Plate	**Seat Pad**	**Plate**	**Seat Pad**	**Plate**	**Seat Pad**	**Plate**	**Seat Pad**
a_W (m/s^2)	1.75	1.51	1.82	1.65	1.72	1.70	1.74	1.63
eVDV ($m/s^{1.75}$)	6.83	5.90	7.09	6.45	6.69	6.64	6.79	6.36
Output/Input Ratio	**0.86**		**0.91**		**0.99**		**0.94**	

Table 9.2 Warrior Signal Weighted R.M.S Acceleration and eVDV

	Bladder 1		Bladder 2		Bladder 3		Bladder 4	
	Plate	**Seat Pad**	**Plate**	**Seat Pad**	**Plate**	**Seat Pad**	**Plate**	**Seat Pad**
a_W (m/s^2)	1.73	0.78	2.07	0.81	2.05	1.07	2.07	0.84
eVDV ($m/s^{1.75}$)	6.72	3.04	8.06	3.15	7.97	4.18	8.06	3.29
Output/Input Ratio	**0.45**		**0.39**		**0.52**		**0.41**	

Table 9.3 Constant Velocity Signal Weighted R.M.S Acceleration and eVDV

The output/input ratios associated with the air bladder seat cushions were close to one when they were excited with the Warrior signal because the majority of the vibration energy in the signal was between the 2 to 16 Hz 1/3 octave bands. This is the region where the ISO weighing is near unity and the region where the vibration transmissibility of the seat cushions are near or slightly greater than unity. The output/input ratios associated with the seat cushions were significantly less than one when they were excited by the constant velocity signal because the majority of the vibration energy in the signal was in the higher 1/3 octave bands where the vibration transmissibility of the seat cushions were significantly less than one. Tables 9.2 and 9.3 indicates that seat cushion configuration 1 performed best for the Warrior signal and seat cushion configuration 3 performed the worst. Seat cushion configuration 2 performed the best for the constant velocity signal and seat cushion configuration 3 performed the worst.

9.1.6 Overall Air Bladder Seat Cushion Performance Comparison for Vibration Transmissibility

The 1/3 octave band frequency response magnitudes were used to compare the performances of the four air bladder seat cushion configurations. Both Figure 5.15 for the Warrior input signal and Figure 5.17 for the constant velocity input signal showed the

same frequency response trends. Seat cushion configurations 1 and 2 demonstrated a better performance in the critical 1/3 octave bands between 2.5 and 8 Hz.

For both the ISO weighted acceleration values, a_W, and the vibration dose values, eVDV, the output/input ratios associated with the air bladder seat cushions were close to one when they were excited with the Warrior signal because the majority of the vibration energy in the signal was between the 2 to 16 Hz 1/3 octave bands. This is the region where the ISO weighing is near unity and the region where the vibration transmissibility of the seat cushions are near or slightly greater than one. The output/input ratios associated with the seat cushions were significantly less than one when they were excited by the constant velocity signal because the majority of the vibration energy in the signal was in the higher 1/3 octave bands where the vibration transmissibility of the seat cushions were significantly less than one. Tables 9.2 and 9.3 indicates that seat cushion configuration 1 performed best for the Warrior signal and seat cushion configuration 3 performed the worst. Seat cushion configuration 2 performed the best for the constant velocity signal and seat cushion configuration 3 performed the worst.

9.2 Discussion of Pressure Testing Results

Figure 6.2 represents a typical plot of the internal pressure of the seat bottom with respect to percent-compression of the seat cushion air bladder. This compression test was performed with a seat-butt attached to the MTS system in order to simulate the compression that would occur by a human subject compression during a shock event, such as a mine blast. It shows that the internal pressure reaches approximately 2.0 psi.

However, this these quasi-static test results are of less interest when relating internal seat cushion air bladder pressure to an extreme shock event, such as a mine blast.

Internal dynamic pressures measured simultaneously in the seat-bottom and seat-back during drop tower tests indicate that the peak pressures reached in the seat-bottom during a shock event were much greater than those experienced on the MTS machine at a crush speed of 2 in./s. Seat bottom pressures for the MTS tests ranged from 0 to 2.5 psi as the seat bottom was compressed. Pressure pulse that were observed in the seat bottom during drop tower tests were roughly shaped as a half-sine with a pulse width that ranged from around 7.5 to 10 ms and a pulse height that ranged from around 3 to 8 psi, depending on drop height and air bladder seat cushion configurations.

Many of the pressure-pulses in the seatback appeared to be affected by electronic noise or another type of electronic disturbance. This was a transducer anomaly that appeared at an early stage in the testing program and that could not be removed. The problem could have been associated with the fact that the measured pressure values were close to the noise floor of the transducer. It was not possible to purchase a replacement pressure transducer, nor was there time to switch the pressure transducers between the seat bottom and seatback and repeat the drop tower tests. Therefore, the seatback pressure data were considered to be useful only for providing an understanding of the approximate peak-pressures in the seatback, as well as, the time delay between the peak pressures in the seat-bottom and the seatback.

Table 9.4 shows a summary of the seat bottom peak pressures, and Table 9.5 shows a summary of the seatback peak pressures.

Pressure in Seat-Bottom [psi]				
	Bladder 1	**Bladder 2**	**Bladder 3**	**Bladder 4**
10in	3.45	4.30	3.00	4.24
20in	5.46	6.00	5.12	5.99
30in	7.73	7.50	5.97	7.35

Table 9.4 Pressure in Seat Bottom for all Drop Heights

Pressure in Seat-Back [psi]				
	Bladder 1	**Bladder 2**	**Bladder 3**	**Bladder 4**
10in	0.49	0.71	0.54	0.53
20in	1.25	0.97	0.78	0.91
30in	1.11	1.25	1.55	1.18

Table 9.5 Pressure in Seat Back for all Drop Heights

The area of a human butt form is 167 in.^{2}. Therefore, the seat-bottom peak pressure can be converted to an applied force on the seated-human. This assumes constant contact between the seated human and the seat bottom. The seated applied force can provide an interesting insight to the design of future air bladder seat cushions. Table 9.6 shows a summary of the calculated peak forces applied to a seated occupant by the seat bottom.

Force Applied to Seated Occupant by Seat Bottom [N]				
	Bladder 1	**Bladder 2**	**Bladder 3**	**Bladder 4**
10in	129.5	161.4	112.6	159.2
20in	205.0	225.2	192.2	224.9
30in	290.2	281.6	224.1	275.9

Table 9.6 Calculated Force Applied to Seated Occupant by Internal Bladder Pressure

As a final comparison, the bladders are ranked by least amount of applied force to the seated occupant by drop height. This ranking is summarized in Table 9.7. Bladder 3 delivered the least amount of force to the occupant across all drop heights and Bladder 1

delivered the most greatest amount at 30in while Bladder 2 did so for 10 and 20in heights..

Ranking by Force Applied per Drop Height				
	Bladder 1	**Bladder 2**	**Bladder 3**	**Bladder 4**
10in	2nd	4th	1st	3rd
20in	2nd	4th	1st	3rd
30in	4th	3rd	1st	2nd

Table 9.7 Rankings of Bladders by Applied Force to Seated Occupant of all Drop Heights

9.3 Discussion of ARL Shock Testing and ATD Performance Results

The shock pulses produced the drop tower at the U.S. Army Applied Research Laboratory (USARL) were consistently simple, zero-mean, half-sine pulses with approximately 5 ms pulse widths (Figures 7.1 and 7.2). Table 9.8 shows a summary of the peak acceleration amplitudes measured on the mounting plate of the USARL drop tower as a function of drop height

AVERAGE USARL SHOCK PEAK ACCELERATIONS [m/s^2]	
10 in. Drop Height	913
20 in. Drop Height	1,464
30 in. Drop Height	1,848

Table 9.8 Average USARL Shock Input Peak Accelerations

9.3.1 Anthropomorphic Dummy/Baseline Testing

Initially the anthropodynamic shock dummy (ATSD) was tested at three drop heights when seated directly on the drop tower platform: 10 in., 20 in., and 25 in. The ATSD was not tested at a drop height of 30 in. because of a fear of damaging the internal sensors in

the dummy. Table 9.9 shows baseline pelvis acceleration, DRI and spine load for the three drop heights. The values for the 30 in. drop height were obtained from a 2nd order polynomial regression equation of the respective data.

USARL ATSD Baseline Values					
Drop Height (in.)	Platform Peak Accel. (m/s^2)	Pelvis Peak Accel. (m/s^2)	Pelvis Peak Accel./ Platform Peak Accel.	DRI	Spine Load (N)
10	942	257	0.27	10.5	3,674
20	1,472	647	0.44	14.8	6,672
25	1,677	851	0.51	16.6	8,852
(30)	1,844	(1,030)	0.56	(17.9)	(10,087)

Table 9.9 Summary of USARL ATSD Baseline Values

Just by analyzing the pelvic acceleration variation from height to height, we see that as the drop height, and impact velocity increase, the dummy's natural damping decreases. If it performed linearly in this range of inputs, then theoretically the pelvic acceleration would increase by a factor of $\sqrt{2}$ for every doubling of drop height, simply by considering the change in impact velocity.

While the dummy reduces the peak acceleration in the pelvis in the 10in drop to nearly 75% of the input, that number drops to 57% in the 20in, and 53% in the 30in. The seat-pad accelerometer was not used in this series of measurements.

9.3.2 Typical Bladder Acceleration and Plate Kinematics

Due to the large number of recorded measurements, and in order to reduce to total volume of figures presented in the main body of the text, additional drop heights performances will be presented in the Appendices.

Figure 7.4 shows the performance of the seat-pad accelerometer for each of the bladders. Again the dummy could not be compared in these figures because no seat-pad accelerometer was used in the dummy's baseline testing.

We can see a recurring theme that Bladder 1 will respond with a larger acceleration magnitude. Bladders 2, 3 and 4 have seat pad acceleration responses that do resemble each other. However Figure 7.4 interestingly shows that rebound acceleration increases for each of the remaining bladders. Also where Bladder 3 has the largest overall peak-peak acceleration Bladder 1 actually has the lowest. However Bladder 1 still produces the highest Pelvic acceleration (Figure 7.5) and even the highest Spinal Load nearing almost 5000N Figure 7.17 (Section 7.4.1 and 7.4.2). Bladder 2 had the lowest spine load.

Figures 9.1-9.4 review the acceleration, and kinematic platform profiles for Bladder 2 30in drop as typical profiles for all bladders.

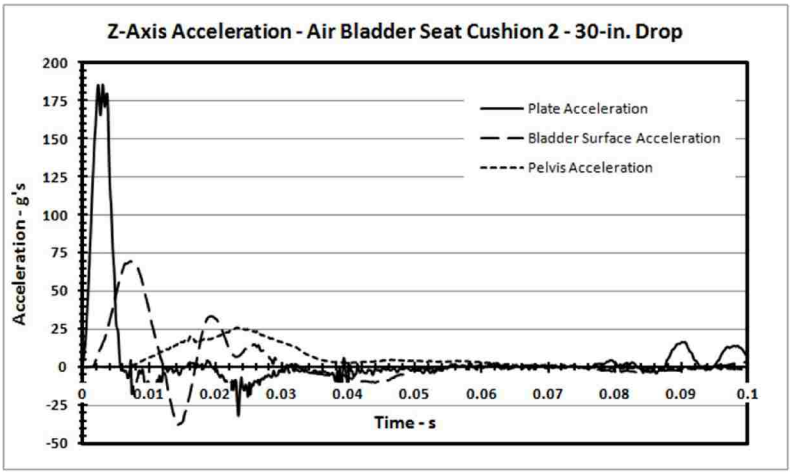

Figure 9.1 Review of Bladder 2 Acceleration – 30in Drop Height

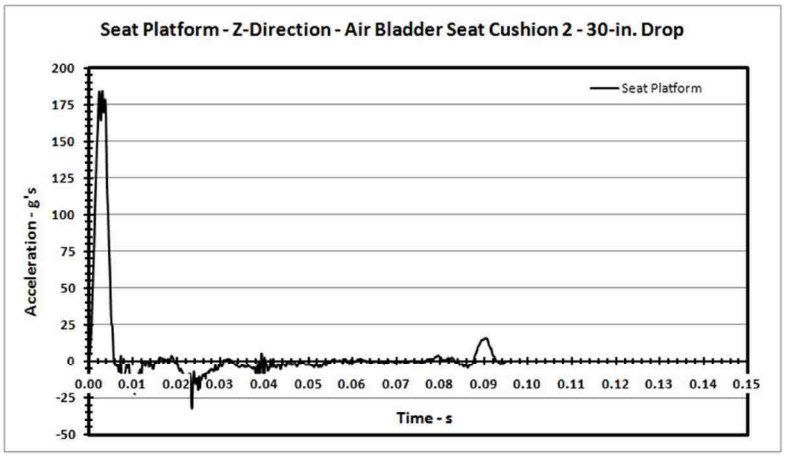

Figure 9.2 Bladder 2 Platform Acceleration – 30in Drop Height

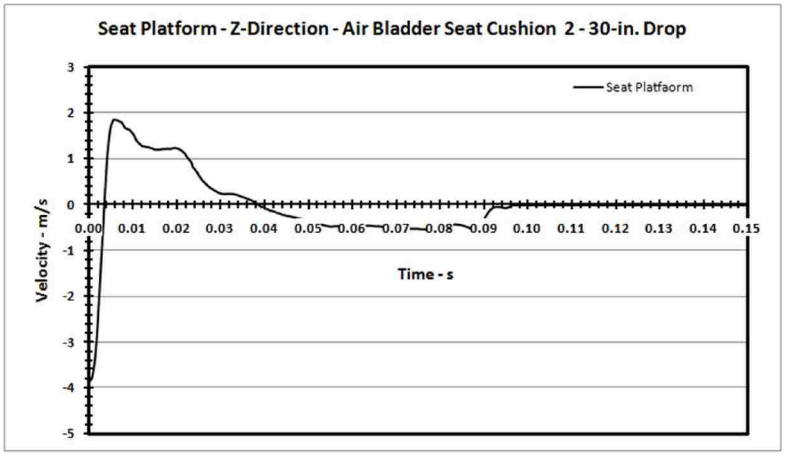

Figure 9.3 Bladder 2 Platform Velocity – 30in Drop Height

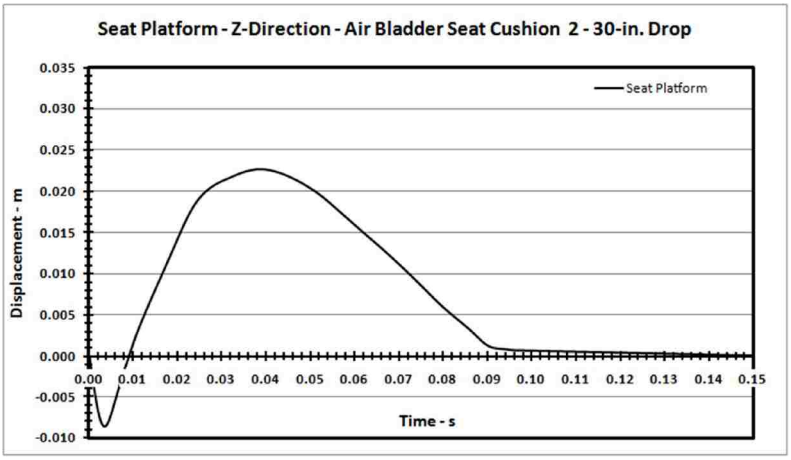

Figure 9.4 Bladder 2 Platform Displacement – 30in Drop Height

9.3.3 Individual Bladder Acceleration Performance

Each of the bladders is characterized and presented individually from section 7.3.2 to 7.3.6. Looking at Bladder 1 independently in Figure 7.4 and Figure 7.6, remembering the 1lb bladder with the largest internal tube diameter, is structurally stiffer than the 0.5in foam hole diameter of Bladder 2, it appears that Bladder 2 smaller orifice diameter allowed slower back flow of air from the seat-back to the seat-bottom, possibly accounting for the noticeably larger negative-rebound acceleration. This property again becomes apparent when comparing Bladder 3 and 4; Bladder 3 having larger orifice-diameter, has larger negative acceleration.

The interesting difference between the peak negative acceleration between Bladder 1 and Bladder 2, and then again between Bladder 3 and 4, are nearly the same for both sets. This possibly presents the idea that the increase in negative rebound-acceleration can be calculated by knowing the increase in orifice-diameter. Predicting response by changing orifice diameter is a prime topic for future study.

While the differences in Pelvic accelerations are actually low, Bladder 1 does have the largest magnitude, but only within the range of $50m/s^2$, slightly more than 5 g's. And while the remaining bladders are within approximately $10m/s^2$ of eachother, Bladder 4 does have the lowest response by a slim margin.

By looking at all of the individual bladder performances, sorted by drop height we also see an expected result that as the drop height, and impact velocity increase, the pulse width decreases and any peak magnitudes, both positive and negative, also increase.

9.3.4 Spine Load Performance

The spinal load injury criteria discussed in Chapter 2, and presented in Table 2.6 shows that the lumbar-spine limit in the vertical direction is between 6672-8007N. Figure 7.14 shows the spinal-loads in the vertical direction for all three of the dummy's drop heights [10, 20, 25in]. At the lowest height, the baseline 10in drop already produces a load of nearly half the tolerance limit, the 20in drop does fall within the tolerance range and the 30in exceeds it.

For both the 20 and 30in drops Bladder 2 had the lowest response in terms of spine loading. At the 20in drop, Figure 7.16, we see that there are two groupings Bladder 1/Bladder 4 and Bladder2/Bladder 3. Again these two groupings only have internal-tube/orifice diameter in common. The lower spine-load response coming from the bladder grouping with the *smaller* of the two tube diameters at 0.25in.

At 30in however, while Bladder 1 still had the worst response and Bladder 2 had the best, Bladders 3 and 4 had nearly identical responses and peaks.

Table 9.7 summarizes the baseline/dummy response including predicted values for a 30in drop. Table 9.8 shows spinal load reduction.

Spinal Load and Percent Reduction from 30in Drop Height		
	Spinal Load (N)	Spinal Peak Reduction
Baseline/Dummy	10,087	N/A
Bladder 1	4,893	51.49%
Bladder 2	4,119	59.17%
Bladder 3	4,425	56.13%
Bladder 4	4,448	55.90%

Table 9.10 Spinal Load Reductions at 30in Drop Height

9.3.5 Summary of all USARL Peak Values

Tables 9.10-9.14 review the peak values for platform acceleration, pelvic acceleration and their ratio, spine load, and DRI. Figures 9.5-9.16 show the trends, versus peak plate acceleration, for all collected data (ranging from 5-30 in. drop heights) for peak pelvic acceleration, DRI, and spine load. The figures emphasize a major issue discussed here: that while DRI values can remain relatively unchanged, peak pelvic accelerations and spine load are significantly and drastically reduced.

USARL ATSD Air Bladder Seat Cushion 1 Values					
Drop Height (in.)	Platform Peak Accel. (m/s^2)	Pelvis Peak Accel. (m/s^2)	Pelvis Peak Accel./ Platform Peak Accel.	DRI	Spine Load (N)
10	907	89	0.10	9.4	2,330
20	1,467	167	0.11	14.1	3,612
30	1,859	310	0.17	17.8	4,893

Table 9.11 USARL ATSD Air Bladder Seat Cushion 1 Values

USARL ATSD Air Bladder Seat Cushion 2 Values					
Drop Height (in.)	Platform Peak Accel. (m/s^2)	Pelvis Peak Accel. (m/s^2)	Pelvis Peak Accel./ Platform Peak Accel.	DRI	Spine Load (N)
10	899	92	0.10	9.4	2,335
20	1,447	167	0.12	13.7	3,394
30	1,854	255	0.13	17.0	4,119

Table 9. 12 USARL ATSD Air Bladder Seat Cushion 2 Values

USARL ATSD Air Bladder Seat Cushion 3 Values					
Drop Height (in.)	Platform Peak Accel. (m/s^2)	Pelvis Peak Accel. (m/s^2)	Pelvis Peak Accel./ Platform Peak Accel.	DRI	Spine Load (N)
10	927	85	0.09	9.3	2,317
20	1,472	154	0.11	13.7	3,389
30	1,839	258	0.14	17.5	4,425

Table 9.13 USARL ATSD Air Bladder Seat Cushion 3 Values

USARL ATSD Air Bladder Seat Cushion 4 Values					
Drop Height (in.)	Platform Peak Accel. (m/s^2)	Pelvis Peak Accel. (m/s^2)	Pelvis Peak Accel./ Platform Peak Accel.	DRI	Spine Load (N)
10	893	91	0.10	9.6	2,242
20	1,462	163	0.11	14.2	3,536
30	1,844	241	0.13	18.1	4,448

Table 9.14 USARL ATSD Air Bladder Seat Cushion 4 Values

9.3.6 Dynamic Response Index Performance - ARL

The DRI model was developed to characterize the response of the spinal column to short duration accelerations. Its parameters have been validated through aircraft ejection seat studies, catapult tests, and drop tests [20,21]. However its validity from predicting injury sustained from blast loading has actually not been validated [22]. To review, the DRI formulation is based on a 1-D Lumped Parameter model of the spine based on the maximum displacement of that 1-D model, equation Chapter 2.9, with natural frequency of $\omega = 52.9 rad/s$ and damping ratio of $\zeta = 0.224$ [12].

The DRI lumped parameter model and equation are based upon an acceleration input. Therefore theoretical DRI of any shock pulse can be calculated by applying any acceleration profile as the 2nd order linear differential equation's forcing function. In the case of ARL requirements, the pelvic accelerations are used as the primary input. However, for the sake of comparison, all acceleration values were used as inputs. This was done so that the amount of theoretical "DRI-reduction" can be calculated.

Figure 7.22 shows that from pelvic DRI nearly matches that Table based DRI. Figures 7.22-7.26 show each bladder's DRI performance for the 30in drop height. While all of the bladders produced a reduction in input-to-pelvic-DRI at 30in, none produced a reduction above 3-DRI values.

In the context of an injury likelihood, Figure 2.5 shows the spinal injury rate as a function of DRI for Aircraft Seat Ejection Events, a DRI of 16 is considered to have 1% spinal injury rate, while a DRI of 20 would result in a 10% spinal injury rate. This number is in contrast to NATOs value of 17.7 as a 10% spinal injury level. Thus a difference of 3 DRI can be considered significant.

When comparing the pelvic-DRI for each of the bladder in Figures 7.30-7.32 we see that in the 10in Drop height all of the bladders have a DRI near or below 9.5 resulting in essentially no risk for spinal-injury, although the baseline DRI for this test was only in the range of 10.5 DRI. At 20in the difference is more pronounced. While Bladder 3 had the lowest DRI value near 13.5 and Bladder 4 had the highest at nearly 14, the familiar grouping of Bladder 2/3 and Bladder 1/4 appeared again, showing that the bladders with the smaller internal diameter ports to have the better performance. This trend is repeated at 30in (Figure 7.32), except Bladder 2 coming out to be the clear winner, with the only bladder producing a pelvic-DRI of less than 17. Bladder 3, the stiffer of the smaller internal-tubed bladders rating at 17.5. Bladders 1 and 4, both of which have the larger 0.375in internal-tube diameter performed worse, where Bladder 1 bordered the 17.7 DRI limit for injury and Bladder 4 failed that criteria. Figure 7.32 and Table 9.1 show the bladders with the smaller internal diameter ports have the better performance than their larger ported counterparts.

Table 9.13 lists the apparent ranking of the bladder performance, by DRI, for the 30in drop height. While this rank was not the case through all drop heights, 30in was the first height to produce clear and significant differences. This ranking assumes that same trend will continue for greater drop heights and only absolute magnitude of the Pelvic-DRI.

Rank	Bladder
1st	**Bladder 2** [0.25in Internal Tube Diameter, 1lb Density Foam]
2nd	**Bladder 3** [0.25in Internal Tube Diameter, 2lb Density Foam]
3rd	**Bladder 1** [0.375in Internal Tube Diameter, 1lb Density Foam]
4th	**Bladder 4** [0.375in Internal Tube Diameter, 2lb Density Foam]

Table 9.15 Summary of Bladder Configuration Performance Rankings by DRI

9.4 Discussion of UNLV Shock Performance

The difference in the UNLV and the ARL drop tests are the absence of an instrumented anthropomorphic dummy and the non-simple shock profile used. While ARL's profile was a classic half-sine pulse with essentially zero-negative acceleration or rebound, UNLV's profile is believed to more resemble data showing actual blast profiles. The discussion of severity of shocks is an ongoing one in the study of vibrations, and the variety of injury metrics and shock-characterization tools show that there is no clear solution. The characterization of a shock severity, particularly in reference to induction of human injury, will hopefully be discussed in future studies.

Table 8.1 shows a summary of all of the peak acceleration value of both the UNLV and ARL drop tests. And Figures 7.1 and 8.1 show a summary of the shock profiles, zoomed to the fundamental pulses. While the UNLV shock pulses appear more violent and dynamic, they still had overall smaller peak acceleration. Table 8.1 also shows the maximum peak values of UNLV's drop tests when measured from maximum peak-to-negative peak. However if only initial peak acceleration is considered then the ARL pulse peaks were on average 324m/s^2 (33 g's) greater than the UNLV pulses.

Drop Height	ARL-UNLV Peak Input Acceleration Difference
10in	303 m/s^2
20in	317 m/s^2
30in	351 m/s^2

Table 9.4 Difference in Raw Peak Acceleration Values from ARL to UNLV

The recommended values for sampling and filtering data are 10-times fundamental pulse width and 5-times fundamental pulse widths respectively, Equations 8.1-8.3. While the data was oversampled, the filtering frequency suggestion was met exactly. While the UNLV pulse consisted of pulse widths of up to 5ms, the primary pulses were from 2-3ms in width, so a filtering frequency of 1250Hz was applied to all subsequent shock data, including the seat-pad acceleration even though its pulse widths were much greater. Figure 8.2-8.3 shows baseline raw and filtered acceleration for both the input plate and seat-pad respectively. Table 8.2 shows a summary of the peak reduction by filtering; while the seat-pad during baseline tests only saw a 6.46% reduction, the input acceleration saw a 22.76% reduction.

9.4.1 Seat Pad Acceleration Discussion

The usage of a sandbag dummy will affect the overall impedance of the system, and therefore the acceleration profile of the seat-pad. However usage of such a dummy is largely preferred to that of a rigid mass when comparisons to the ATD used at ARL are desired. Yet without a direct comparison of the sandbag-dummy and the THOR III ATD using the same input signal, it would be difficult to state any conclusive differences. Such a study would also be future goal.

Figures 8.4-8.6 showcase the unique performance of the seat-pad acceleration under the UNLV shock pulse. All of the bladders exhibit an interesting negative acceleration

after their initial positive-peak. The negative peak decreases for all bladders as the drop height and input acceleration magnitudes increase, while the initial positive peaks continue to increase. Because of the convention used in the acceleration direction the negative acceleration is essentially the rebound, or the motion and acceleration in the positive vertical direction. This feature is most prominently displayed in the 10in drop height where Bladder 1 has a negative peak approximately 2.5-times greater than its positive peak and Bladder 3 displays a similar behavior at a negative peak at approximately 2-times its positive peak. It is believed that the reduced internal-tube diameter of Bladders 2/3 are effectively decreasing this spring-back effect by increasing the damping of the system by slowing the air flow from the seat bottom to the seat back, also slowing the decent of the seat/butt surface.

9.4.2 Dynamic Response Index Discussion – UNLV

Again, two important piece of information that cannot be gathered from the series of tests conducted at UNLV are the pelvic-acceleration and the spine-load because of the lack of an instrumented-ATD. However, as in the ARL-DRI analysis, DRI values can be calculated from the available acceleration data, and compared to the ARLresults.

A discussion of the combined analysis of the DRI values from both testing facilities is presented in section 9.5.

Regardless of the more dynamic nature of UNLV's shock input, the DRI plots from ARL (Figures 7.22-7.26) and UNLV (8.12-8.16) look strikingly similar. This is due to the nature of the DRI calculation; DRI is directly proportional to the displacement output of a 2^{nd} order underdamped system and therefore less sensitive to minor changes in the shape of the input acceleration profile. Where ARL input acceleration produces a DRI of

nearly 20 from a 30in drop height, UNLV input DRIs range from 15.8-17.4 with an average DRI of 16.4. This is due to the smaller UNLV peak acceleration.

Where ARL input acceleration profiles resulted in essentially identical max DRI values, the UNLV input profiles did result in slightly different DRI values per-drop occurrence. The differences are enough to require the peak values of the input and seat-pad output DRIs for accurate comparison as can be seen in Figure 8.17. Figure 8.18 shows all of the bladders and the baseline DRIs for the seat-pad output.

If we compare these bladders using only peak DRI value, in this case the seat-pad accelerometer is the highest level of measurement available. At first glance we see that Bladder 3 has the lowest DRI with Bladder 1 ranking second. Bladder 2 which was the leader in the ARL test group ranked last. However because this DRI ranking is based on the seat-pad acceleration and not the pelvic-acceleration the two series of tests must be compared in a different fashion.

9.5 Comparison of ARL and UNLV DRI Performances

We see a deviation from the previous pattern observed in the DRI performance at ARL. In the ARL testing the bladders with the smaller, 0.25in internal tube diameter were the clear winners, with the lighter density foam bladders performing better within each grouping of internal-tube diameters, see Table 9.9. However no such clear pattern was seen for the UNLV tests.

9.5.1 Peak DRI Rankings

A ranking system based purely on peak DRIs may not be sufficient, especially since Pelvic-DRIs were not available during the UNLV testing. The next section compares the testing series by looking at the magnitudes of DRI reduction in each bladder configuration.

Peak DRI Magnitudes – 30in UNLV		
	Input DRI	**Seat Pad DRI**
Bladder 1	16.32	13.49
Bladder 2	17.44	15.23
Bladder 3	15.60	12.41
Bladder 4	16.13	14.58
Baseline/Sandbag Dummy	17.24	15.87

Table 9.5 Magnitudes of DRIs from UNLV Testing

Peak DRI Magnitudes – 30in ARL			
	Input DRI	**Seatpad DRI**	**Pelvic DRI**
Bladder 1	19.38	17.27	17.77
Bladder 2	20.05	17.29	16.93
Bladder 3	19.37	18.84	17.56
Bladder 4	20.35	16.64	18.03
Baseline/Dummy(25in)	16.69	N/A	16.54

Table 9.6 Magnitudes of DRIs from ARL Testing

Table 9.16 shows that in some cases seatpad DRI to be unexpectedly lower than pelvic DRI. Minor variations in the dummy placement, its movement during the drop and even during rebound will affect the seat-pad accelerations and thus DRI. Mathematically the only way the seat-pad DRI can be lower than that of the pelvis is if the pelvic acceleration profile would cause the 1-D to undergo a greater maximum displacement than that of the seat-pad, even though the peak seat pad acceleration can be up to 3-times

as high as that of the pelvic acceleration. This can only be caused by the significant increase of the pelvic acceleration pulse width in comparison to the seatpad's.

Peak DRI Rankings - UNLV and ARL			
	ARL *Pelvic* DRI	ARL *Seatpad DRI*	UNLV *Seatpad* DRI
Bladder 1	3rd	2nd	2nd
Bladder 2	1st	3rd	4th
Bladder 3	2nd	4th	1st
Bladder 4	4th	1st	3rd

Table 9.7 Rankings based on Peak DRIs from UNLV and ARL Testing

9.5.2 Peak Difference DRI Analysis

Ranking based purely on DRI is obviously not sufficient. This section compares testing series by looking at an artificially calculated "DRI reduction" in each bladder configuration.

Peak DRI Magnitude Differences – 30in ARL			
	Input – Seatpad	Seatpad – Pelvic	Input – Pelvic
Bladder 1	2.11	-0.50	1.61
Bladder 2	2.76	0.36	3.12
Bladder 3	0.53	1.28	1.81
Bladder 4	3.71	-1.39	2.32
Baseline/Dummy	N/A	N/A	0.45

Table 9.20 Magnitude Differences of DRIs from ARL Testing

Rankings by Input – Pelvic DRI ARL	
1st	Bladder 2
2nd	Bladder 4
3rd	Bladder 3
4th	Bladder 1

Table 9.21 Magnitude Differences of DRIs from UNLV Testing

This ranking, Table 9.20, which shows DRI-differences may be more meaningful than Table 9.17 which ranks the ARL DRI based purely on peak DRI. While this takes into account the difference between the input and the output DRIs. While Bladder 4 performed the worst in overall pelvic DRI, when considering this metric its ranking increases to second place. The relative order of the remaining bladders did not change.

Peak DRI Magnitude Differences – UNLV		
	Input – Seatpad DRI	Seatpad – Pelvic DRI
Bladder 1	2.83	N/A
Bladder 2	2.21	
Bladder 3	3.20	
Bladder 4	1.56	
Baseline/Sandbag Dummy	1.26	

Table 9.8 Magnitude Differences of DRIs from UNLV Testing

Rankings by Input – Seatpad DRI		
	ARL	UNLV
1st	Bladder 4	Bladder 3
2nd	Bladder 2	Bladder 1
3rd	Bladder 1	Bladder 2
4th	Bladder 3	Bladder 4

Table 9.9 Magnitude Differences of DRIs from ARL and UNLV Testing

Notice that if the difference in DRI from the Input-to-Seatpad is used, then no clear pattern whatsoever is present. In fact the rankings have been completely reversed.

9.5.3 DRI Rankings Overview

Because of the large variety of ways that the bladders can be ranked, a summary of the rankings discussed above have been provided here. In some cases to see trends the

bladders have been organized by ranking rather than the other way around, as can be seen in some of the above figures.

	Pelvic DRI		**Seatpad DRI**		**Input – Seatpad DRI**		**Input – Pelvic DRI**	
	ARL	UNLV	ARL	UNLV	ARL	UNLV	ARL	UNLV
Bladder 1	3rd	N/A	2nd	2nd	3rd	2nd	4th	N/A
Bladder 2	1st		3rd	4th	2nd	3rd	1st	
Bladder 3	2nd		4th	1st	4th	1st	3rd	
Bladder 4	4th		1st	3rd	1st	4th	2nd	

Table 9.10 Summary of DRI Rankings by Criteria and Test Location

9.6 Review of Total Bladder Performance by Input Acceleration

The individual performance trends between bladders for the seatpad acceleration and the spinal load are discussed in detail in Section 9.3.3-9.3.4 for the ARL series of tests and in Section 9.4.1 for the UNLV series. This section provides an overview of the peak values of pelvic-acceleration and spine load throughout the ARL battery of tests and compares that information to the applied usage of DRI.

The following figures will show the relationship and the difference in magnitudes between each bladder and the baseline/dummy values for:

- Peak Pelvic Acceleration vs Peak Input Acceleration
- Peak DRI vs Peak Input Acceleration
- Peak Spine Load vs Peak Input Acceleration

Previously only three drop heights were used in the presentation of data, for consistency and as a sufficient representation. However, all available drop heights per bladder are represented in the following figures.

They consistently show that the bladders only marginally reduce the pelvic-DRI value when compared to the baseline test. However, in contrast they show that peak pelvic accelerations, and the potentially more important spine loads are significantly reduced.

Also the spine load never met or exceeded the maximum spine load limit of approximately 6,672N (1,500lbf); where it was regularly exceeded by the baseline tests. In fact the peak difference is typically on the order of 4,000N (900lbf). Moreover, the magnitude of the pelvic acceleration showed the typical peak difference to be on the order of 600m/s^2.

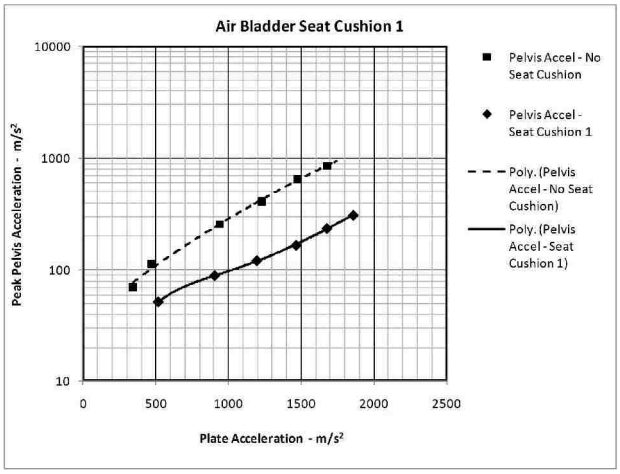

Figure 9.5 Bladder 1 Pelvic Acceleration versus Plate Acceleration – All Data

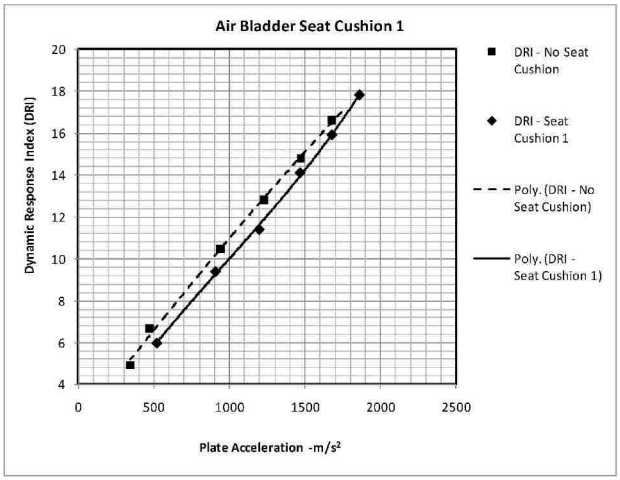

Figure 9.6 Bladder 1 DRI versus Plate Acceleration – All Data

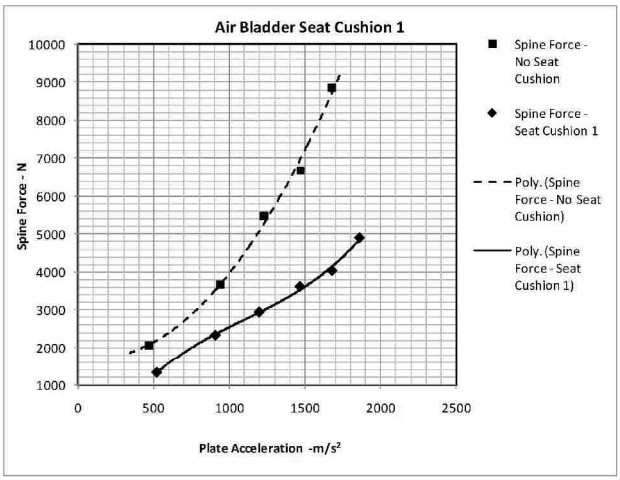

Figure 9.7 Bladder 1 Spine Load versus Plate Acceleration – All Data

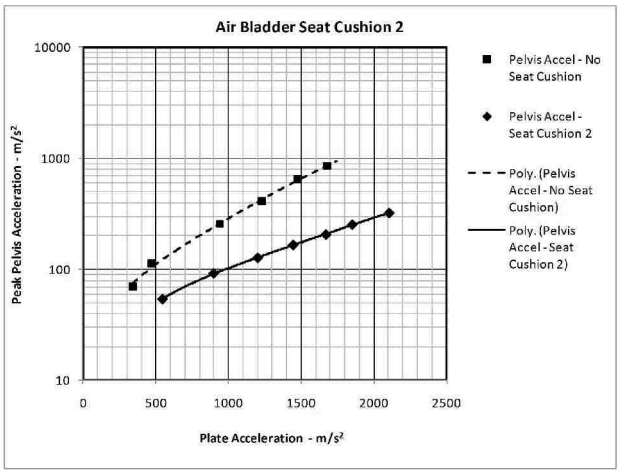

Figure 9.8 Bladder 2 Pelvic Acceleration versus Plate Acceleration – All Data

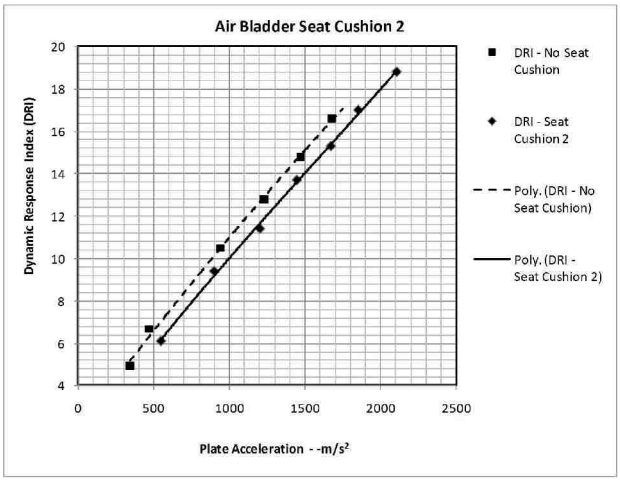

Figure 9.9 Bladder 2 DRI versus Plate Acceleration – All Data

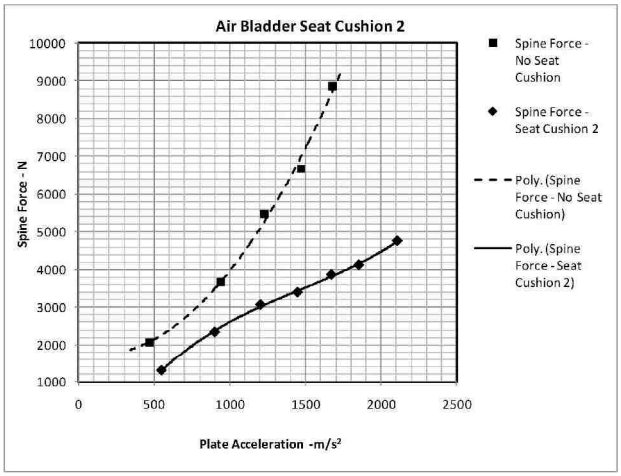

Figure 9.10 Bladder 2 Spine Load versus Plate Acceleration – All Data

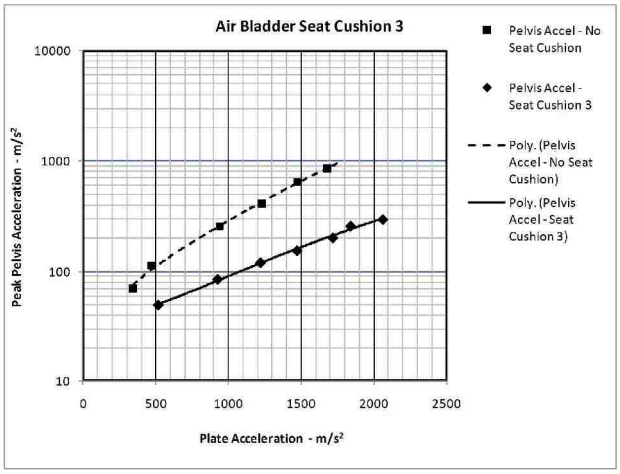

Figure 9.11 Bladder 3 Pelvic Acceleration versus Plate Acceleration – All Data

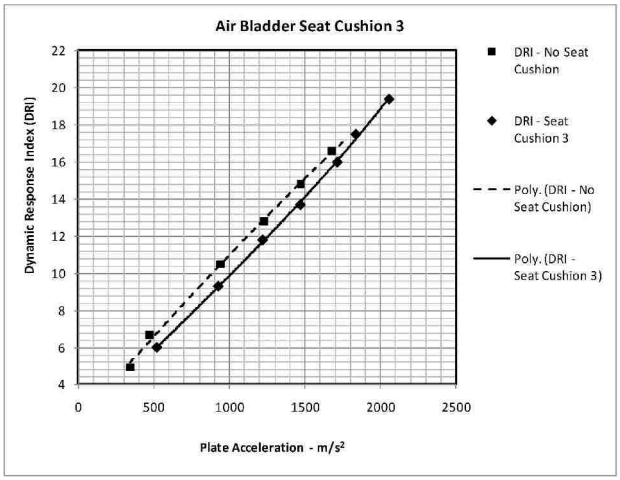

Figure 9.12 Bladder 3 DRI versus Plate Acceleration – All Data

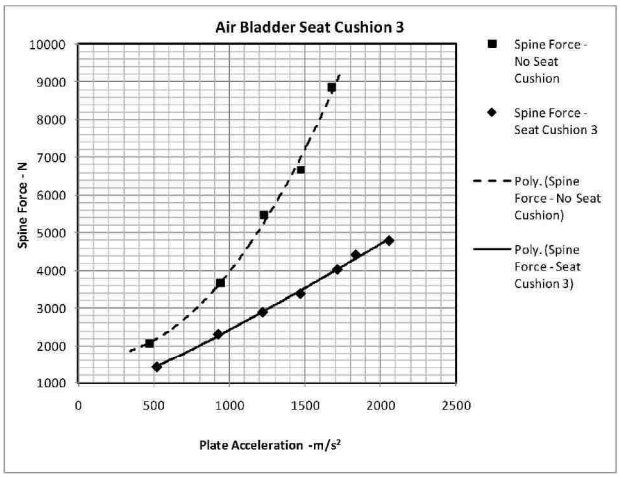

Figure 9.13 Bladder 3 Spine Load versus Plate Acceleration – All Data

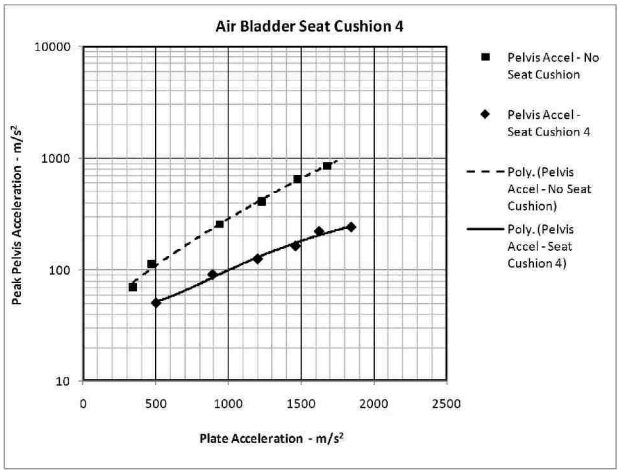

Figure 9.14 Bladder 4 Pelvic Acceleration versus Plate Acceleration – All Data

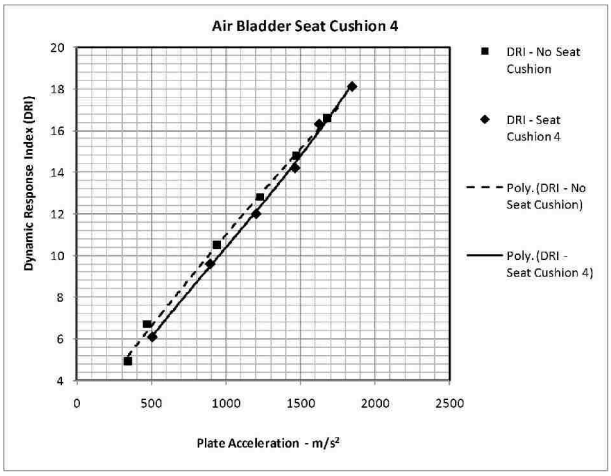

Figure 9.15 Bladder 4 DRI versus Plate Acceleration – All Data

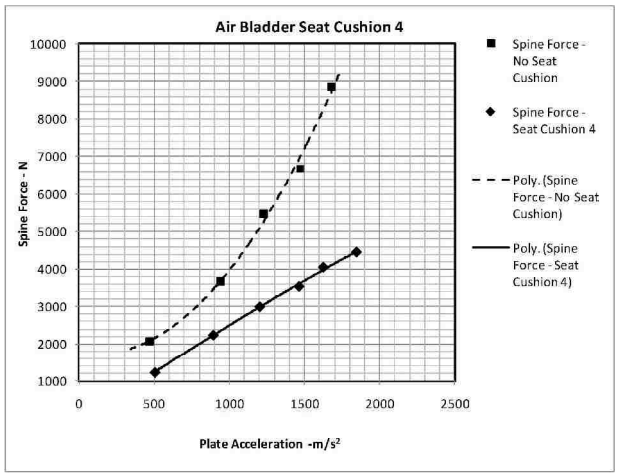

Figure 9.16 Bladder 4 Spine Load versus Plate Acceleration – All Data

9.7 Overall Performance Trends and Conclusions

By ARL standards and test methodology, which is based on the NATO standard, only the peak pelvic-DRI is considered. It is being used as the sole metric by which seat systems are evaluated. While Figures 9.5-9.16 show that drastic and significant reductions in pelvic accelerations and spinal loads, even when DRI values only see minor reductions. Since there are clear limits to spine load tolerance, DRI's sole usage has begun to be questioned.

As Table 9.18 shows, calculating the difference in Input-DRI and Pelvic-DRI from blast event to blast event helps to account for even minor differences in the blast event. This was shown that even with ARLs drop tower there were minor differences from drop to drop, even with identical massed objects being placed on the drop platform.

From the perspective of vibration transmissibility, Bladder 2 is the clear winner with Bladder 3 showing the greatest vibration-dosage and frequency weighted acceleration transmitted to the occupant over both input acceleration signals. Bladder 2 is chosen as the performance leader in this case because while Bladder 1 outperformed Bladder 2 in the Warrior signal by 5%, Bladder 2 outperformed Bladder 1 by 13.7% in the constant-velocity signal.

If the data gathered from ARL alone was used, then Bladder 2 would win on essentially all accounts, lowest peak-pelvic DRI, peak DRI reduction, and lowest peak spinal load. However, the UNLV data would suggest the usage of Bladder 3 by its greatest DRI-reduction and peak seat-pad accelerations; it also has the best performance in the calculated peak force transmitted by the pressure in the seat-bottom, where Bladder

2 interestingly has the worst performance in overall in that category and Bladder 1 had the worst for the 30in drop.

From the perspective of the configuration parameters of the prototypes, designed to satisfy a fractional factorial DOE in future studies, we see that while the bladders with the smaller of the internal tube diameters, Bladder 2 and 3, showed the overall lowest peak pelvic DRI at ARL, if the difference in Input-to-Output DRIs are considered, while Bladder 2 still remains the winner. Bladder 4, ranked last by peak-DRI, ranks second in performance if the DRI-difference is used instead.

It is the opinion of this study that the usage and analysis of spinal loading is underemphasized in several current standards. While two separate blasts events can produce nearly identical pelvic DRI, the reduction in pelvic acceleration, and the extremely important spinal load is drastic. Figures 9.17-9.19 show this fact using the 25in drop height, because it is the largest drop-event in which the baseline/dummy was used without a bladder.

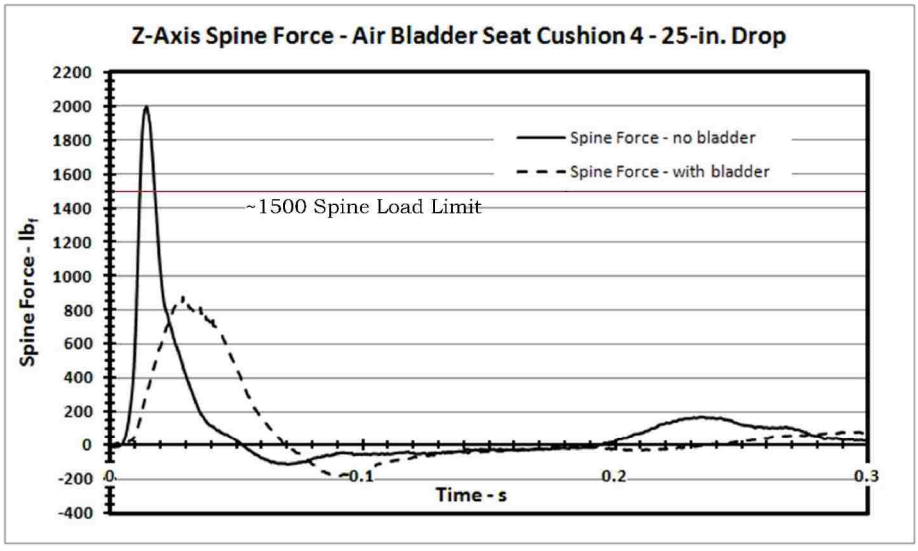

Figure 9.17 Comparing Baseline and Bladder 4 Spine Load – 25in Drop Height

Figure 9.17 clearly shows that spine load was significantly reduced when compared to the baseline spinal load. It also shows that even at 25in, the baseline spine load exceeds the upper allowable limit of 1,500lbf. From this standpoint even Bladder 4 (not the best performer) can be seen as a significant improvement. This is emphasized by Figure 9.18 which shows a reduction in pelvic acceleration greater than 70%. However the DRI (Figure 9.19) have nearly identical values, bringing DRI accuracy into question.

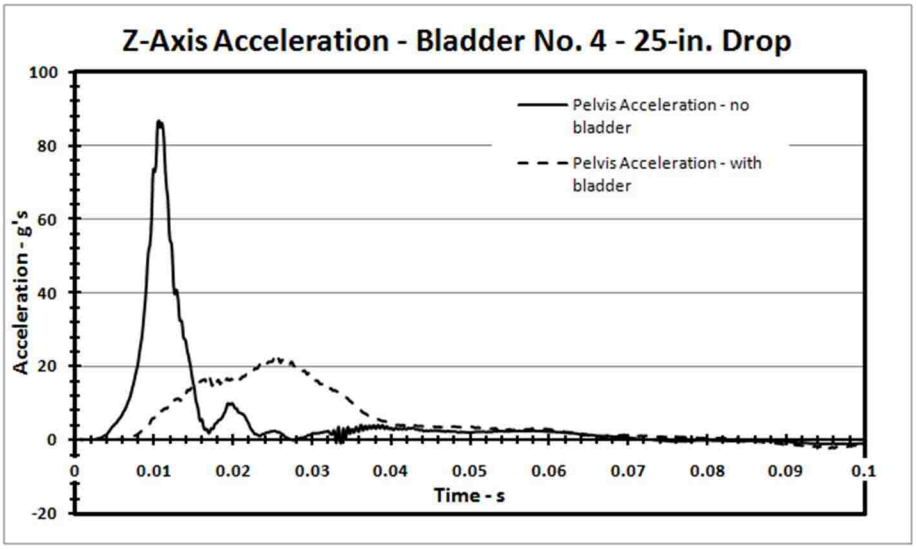

Figure 9.18 Comparing Baseline and Bladder 4 Pelvic Acceleration – 25in Drop Height

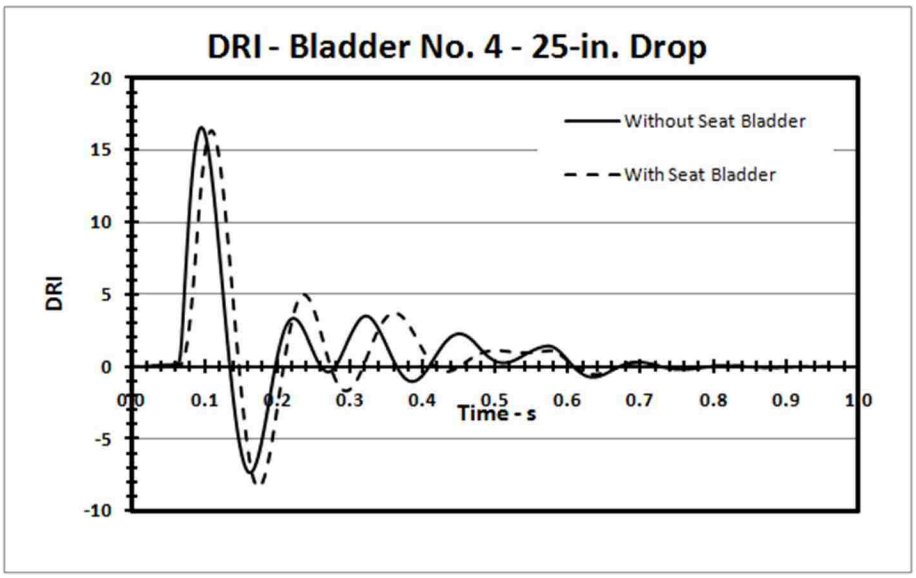

Figure 9.19 Comparing Baseline and Bladder 4 DRI – 25in Drop Height

Future models predicting an anthropomorphic-dummy response to a given seat-pad input would make comparison and analysis more direct, especially when data from multiple tests sites is available. However, given the available data, and the characterization tests performed it is suggested that for shock excitation events, decreasing the internal-tube/orifice diameter linking the seat bottom and seat back together creates an increase in damping. With that primary goal met, the seated occupant reaches his peak velocity more gradually, decreasing peak-DRI, and peak spinal load. From the current configurations, the bladders with the smaller, 0.25in internal-tube diameters, Bladders 2 and 3 are recommended for shock and blast events.

Given the current data and the overall performance of the bladders across both shock excitation testing series and their performances against two random and impulsive vibration profiles, Bladder 2 is considered to be the best performing bladder.

While this decision is given with respect to the current configurations, it should be remembered that the parameters chosen for each bladder configuration, satisfied a fractional-factorial taguchi test matrix, for a future design of experiment analyses. Doing so, with the large amount of available data compiled and analyzed by this work will help guide future iterations of research. And an understanding of the effects of individual parameters can allow tailoring of individual pneumatic air-bladders to specific vibration and shock environments.

CHAPTER 10

CONCLUSIONS AND RECCOMENDATIONS

The result of the extensive experimental testing, characterization and analyses of the pneumatic-seat bladder system has provided validation or previously untested theoretical work and valuable information for future work into application shock or vibration events.

The experimental focus of this work can be separated into five equally important, while principally independent categories: creation of four prototype bladder configurations, dynamic pressure consideration, vibration transmissibility, ARL shock testing, and shock testing conducted at UNLV.

This chapter will succinctly discuss the important aforementioned data and analyses including important trends occurring from design decisions. Recommendations and conclusions will be provided based on performance and internal design parameters of individual bladders. It will also make recommendations for the usage of current bladder configurations appropriate for immediate implementation and recommendations for future work.

10.1 Pneumatic Seat Cushion Overview

The air bladder system's properties and key features can be summarized as follows:

- Self contained shock and vibration attenuation system. Consists of two interconnected foam-air bladders making up the seat-bottom and seat-back.
- Easily deployable to any location or vibration application.
- Can be added as an addition to essentially any existing seat system.

- Does not contain any permanently-deforming energy absorbing device. Mitigation takes place internally within the air-bladder compartments. Bladder will return to original shape under most conditions.
- Deals with shock and vibration environments, where other shock mitigation systems are not also adept at simultaneously dealing with non-impulsive vibration.
- Major strength is that it is ideal for situations with multiple shock events because no permanent deformation takes place. This includes blast events with slam down, which is not easily dealt with current EA systems.

10.2 Previous Work

The design of the bladder and the previous work included:

- Designed the concept of the interconnected pneumatic seat bladder system.
- Limited to a single cushion configuration and data validation of the numerical model was only performed with a limited number of drop tests.
- Numerical agreement was only high for peak acceleration values at certain drop heights.
- Pressure information into the numerical model was done only quasi-statically.
- Numerical model was two-dimensional, five-degree-of-freedom, mass-spring-damper model of the upper legs, thighs, pelvis/lower-torso and upper torso coupled to seat shock isolation system.
- The model was robust and provides a strong construct for future work and modification based on this study's experimental results, analyses, and insights.

10.3 Overview of Current Work

- Four prototype bladders were constructed to fulfill future needs of a fractional taguchi test matrix. The bladder configurations can be reviewed in Table 9.1.
- Two vibration signals were used to test the vibration transmissibility of the bladder systems.
    - The Warrior Signal: A 20s real ride signal obtained from the seat-pan of the Warrior British military vehicle. This signal contains large amounts of energy in the lower frequency bands, and little at median and high frequencies.
    - The Constant rms-Velocity Signal: A random vibration signal designed to have a constant rms-velocity in each of the 1/3-octave bands.
    - A 1-D passive anthropomorphic dummy weighing 120lbs was used in this battery of tests.
- Shock testing was performed at both UNLV and ARL.
    - The tests conducted at ARL used an instrumented THOR III anthropomorphic dummy weighing 170lb.
    - The drop testing conducted at UNLV was performed on a lightweight drop tower designed and built on the premises.
    - The tests conducted at UNLV used a 150lb sandbag dummy with the weight distributed to better mimic an anthropomorphic dummy.
- During the UNLV series of drop tests pressure measurements were taken from both the seat-bottom and the seat-back.

10.4 Summary of Current Data and Results

Chapter 9 provided an in-depth discussion of the individual portions of the data, trends, and conclusions as to bladder configuration preferences.

Bladder Parameters
Bladder 1 [0.375in Internal Tube Diameter, 1lb Density Foam]
Bladder 2 [0.250in Internal Tube Diameter, 1lb Density Foam]
Bladder 3 [0.250in Internal Tube Diameter, 2lb Density Foam]
Bladder 4 [0.375in Internal Tube Diameter, 2lb Density Foam]

Table 10.1 Review of Bladder Configuration Parameters

- Quasi-static pressure testing showed peak pressures of only 2.5psi in the seat bottom. However dynamic pressure testing revealed that the pressure in the seat-bottom from 3psi at the lowest drop height to 7.73psi.
    - If the bladders are ranked by the amount of force delivered to the seated occupant, based on pressure in the seat-bottom, then Bladder 3 was the clear winner at all drop heights.
    - Bladder 2, which also had the smaller of the internal-tube diameters, performed the worst in this testing.
- While both random vibration signals delivered similar weighted acceleration and vibration dosage levels, the bladders were more effective at attenuating higher frequency energies.
    - Bladder 2 had the overall greatest reduction in rms weighted acceleration and VDV when both input signals are taken into account.
    - Bladder 3 had the worst performance.

    - The less-stiff Bladder 1 performed near that of Bladder 2 and performed better under the Warrior Signal.
- ARL drop testing with the THOR III dummy showed that Bladder 2 had the best performance, if only peak DRI was to be considered.
    - Bladder 2 also showed the greatest peak spine load reduction.
- The UNLV testing utilized a non-simple shock, resembling real blasts more so than a simple pulse would, providing added variety to the testing.
    - Because the UNLV drop tests lacked an instrumented ATD, direct comparison between UNLV and ARL testing is difficult.
    - Seat-pad acceleration data is difficult to draw conclusions with. No clear trends are apparent when attempting to relate seat-pad DRI or differences in DRI to pelvic-DRI.
    - However, by UNLV data alone, Bladder 3 showed the overall greatest reductions in seat-pad accelerations and relative DRIs.

10.5 Conclusions

- Performance and ranking of bladders were expected to differ depending on the application, whether shock or lower level random-vibration.
- The internal tube diameter, connecting the seat-bottom to the seat-back, was expected to have the greatest influence on performance, with foam density being the next most influential factor.
- For non-shock vibration events, the lower density foam pads outperformed the rest. While the stiffest bladder configuration, Bladder 3, performed the worst. The

implication is that the reduced stiffness was advantageous for this application. The effect of orifice-diameter is still unclear because Bladder 1 and Bladder 2 each out-performed the other in one of the input signals.

- The dynamic pressure results show entirely the opposite result of the vibration-transmissibility. Bladder 3, the stiffest of the configurations produced the lowest pressure peak, where Bladder 2 produced the highest peaks. The effects of internal pressure seem to be closely linked to seat-pad DRI and input-to-seat pad DRI differences.
- Shock testing at both locations provided a wealth of information, particularly DRIs summarized in Table 9.18. However, without an instrumented anthropomorphic dummy, conclusions on pelvic accelerations and spinal loads are difficult. However based on the available data from both centers Bladders 2 and 3 are considered to be the top performers.
    - The two bladders share the common smaller internal orifice diameter. The smaller orifice was originally chosen to increase the internal damping by slowing the flow of air into the seat back, slowing the overall decent of the occupant and reducing the transmitted load.
- The leading performer in essentially all tests was a bladder configuration with the smaller orifice-tube diameters: Bladder 2 and Bladder 3.

10.6 Future Work

- The drop tests conducted at UNLV would benefit most from the availability of an instrumented human dummy. It is suggested that both simple shocks, such as those produced at ARL, and non-classical blasts as seen at UNLV be used.
- While an ATD is considered more beneficial, a commercial drop tower with readily available pulse programmers would provide more consistent shock events and provide a greater variety of potential inputs.
- Rather than relying solely on DRI, other metrics relating input accelerations, velocities, and spinal load profiles to injury potential are hoped to be discussed in future works.
- Using the wealth of experimental data in this work, modifications and enhancements of the previously developed numerical model is to be performed.
    - A further advancement of this model by experimental validation will allow for future bladder systems to be tailored to their vibration environment.

10.7 Final Thoughts

The work conducted in this study is the result and proof of concept for the pneumatic seat-bladder system. While there are many avenues for future work and enhancement this phase has created and tested 4 prototype variations of the system and shown that it is effective at reducing random and impulsive vibration events. In some cases the same bladder is capable of performing well in both environments. The bladder systems benefit from being easily deployable or used as an addition to other current seat systems. It has

the advantage of not relying on permanently deforming EAs, providing continuous protection against repetitive impulses, a feature lacked by most seat systems.

At the time of this writing, the work conducted here has earned further funding by the Army Air Medical Research Lab for implementation of this technology in military stretcher systems exposed to a variety of shock and vibration events.

APPENDIX A

SUPPLEMENTAL PLOTS

A.1 Supplemental ARL Drop Test Plots

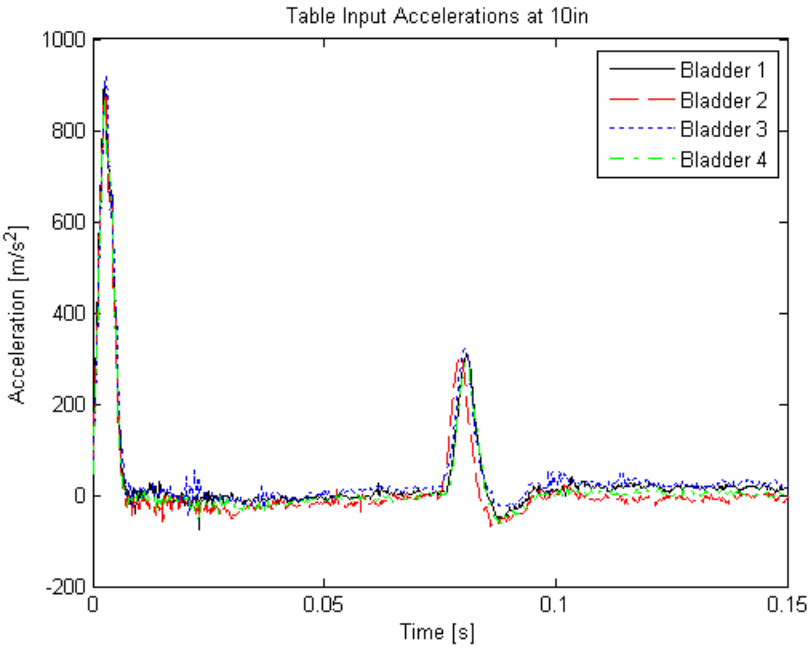

Figure A.1 Table Input Accelerations for 10 in. Drop Height-ARL

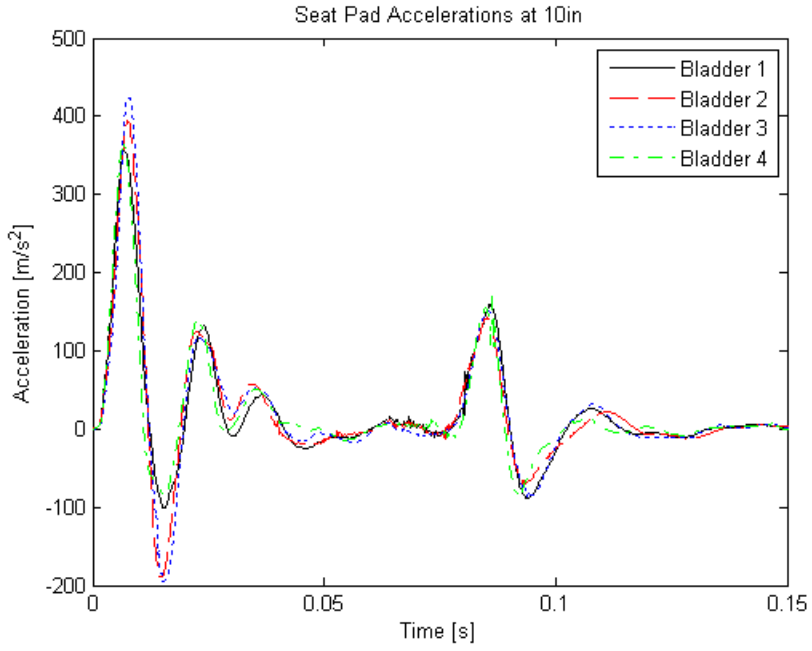

Figure A.2 Seat Pad Accelerations for 10 in Drop Height-ARL

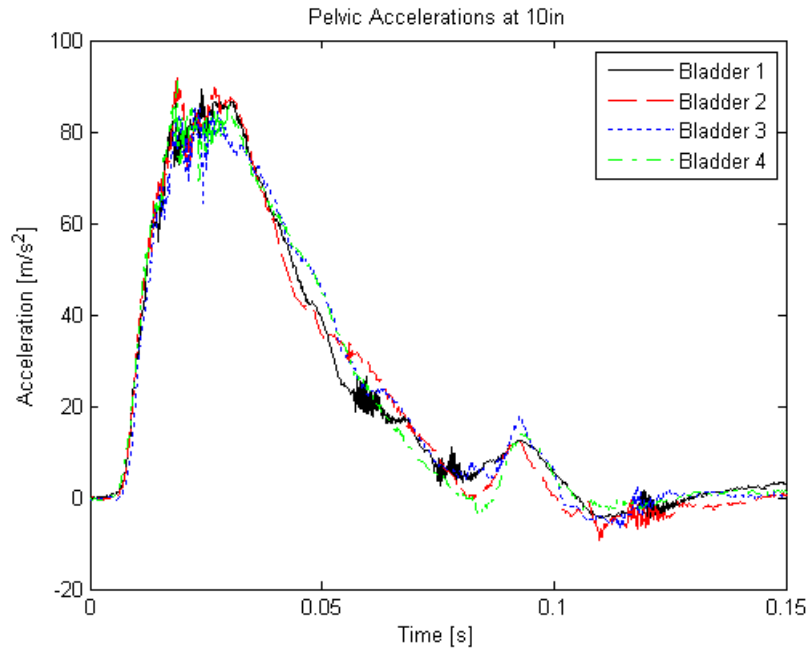

Figure A.3 Pelvic Accelerations for 10 in. Drop Height-ARL

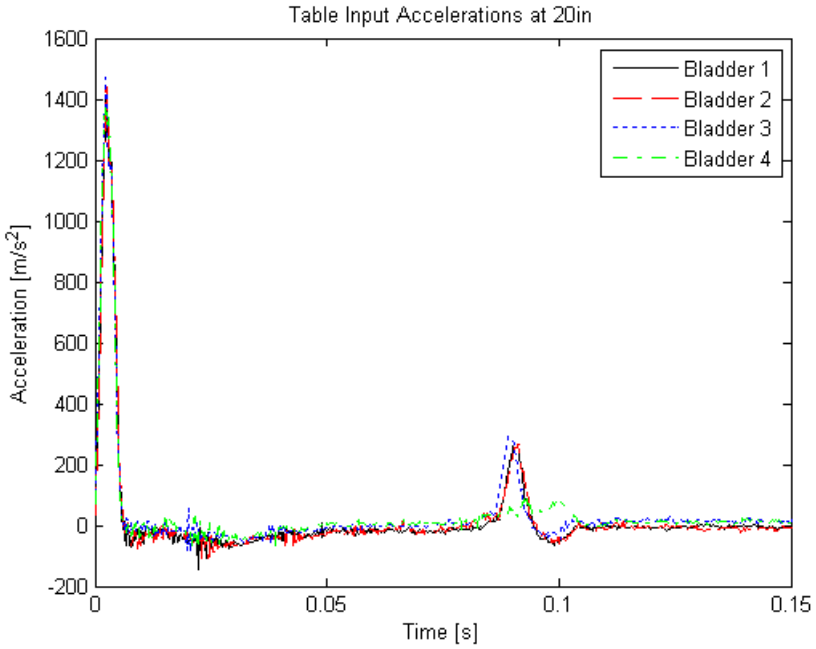

Figure A.4 Table Input Accelerations for 20 in. Drop Height-ARL

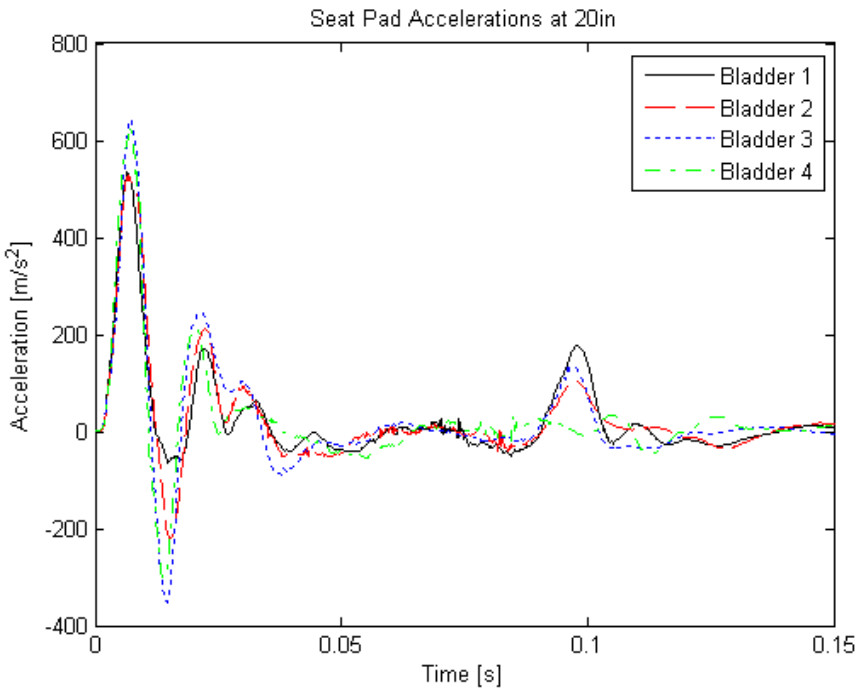

Figure A.5 Seat Pad Accelerations for 20 in. Drop Height-ARL

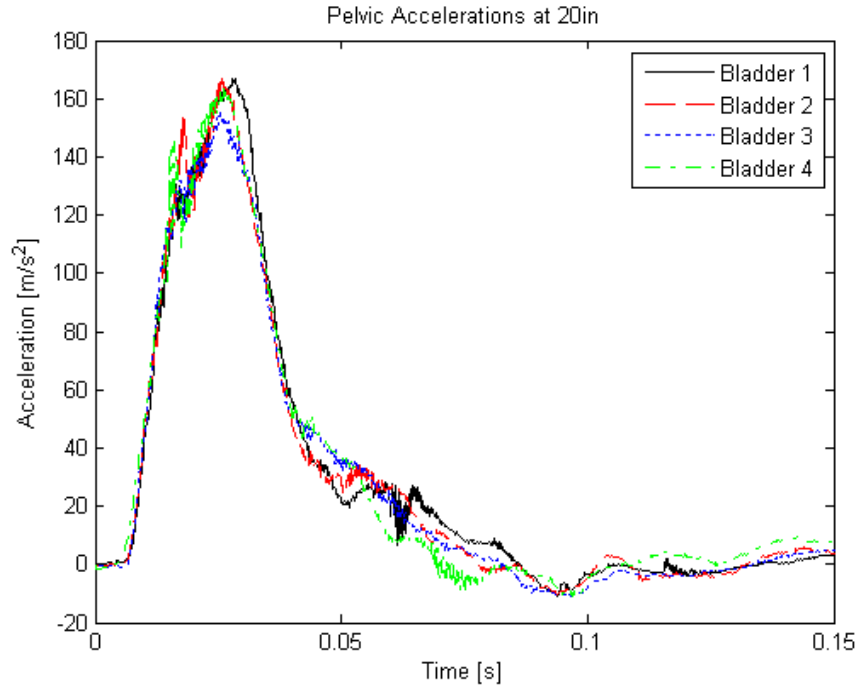

Figure A.6 Pelvic Accelerations for 20 in. Drop Height-ARL

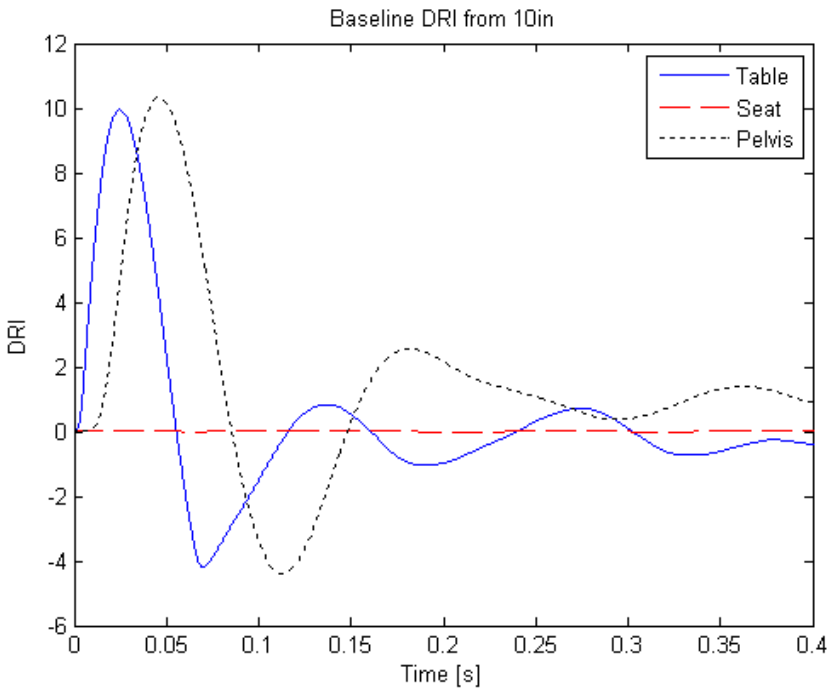

Figure A.7 Baseline DRI for 10 in. Drop Height-ARL

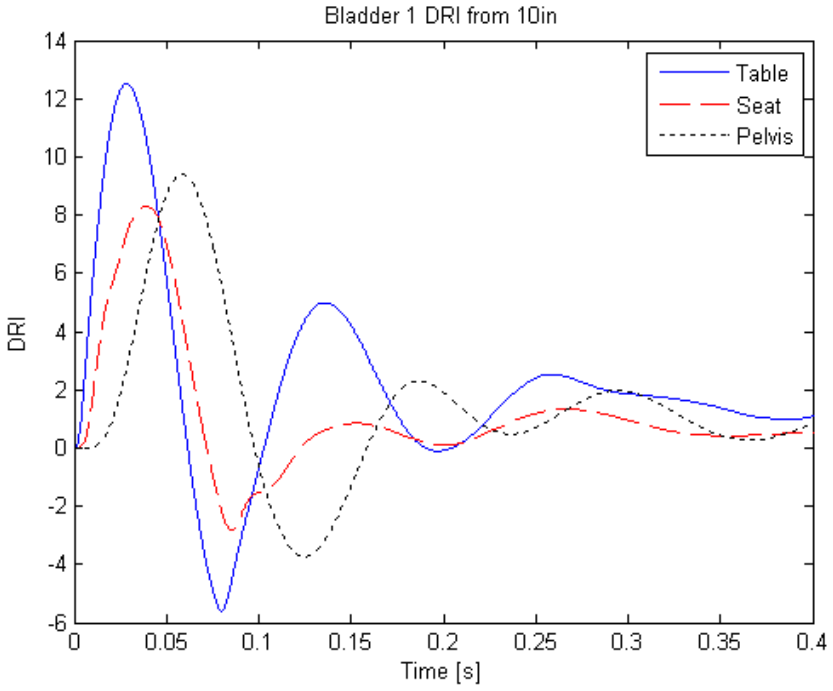

FigureA. 8 Bladder 1 DRI for 10 in. Drop Height-ARL

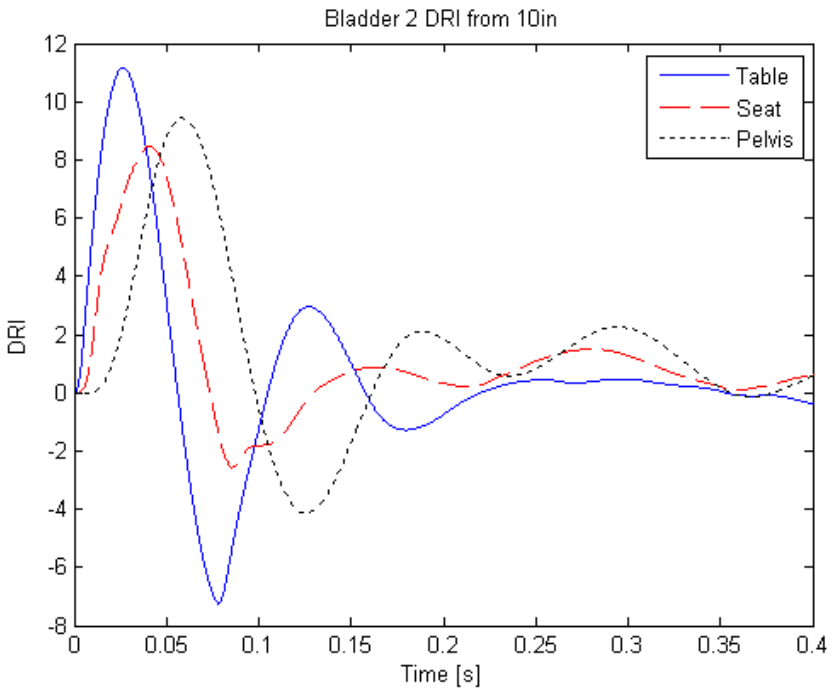

Figure A.9 Bladder 2 DRI for 10 in. Drop Height-ARL

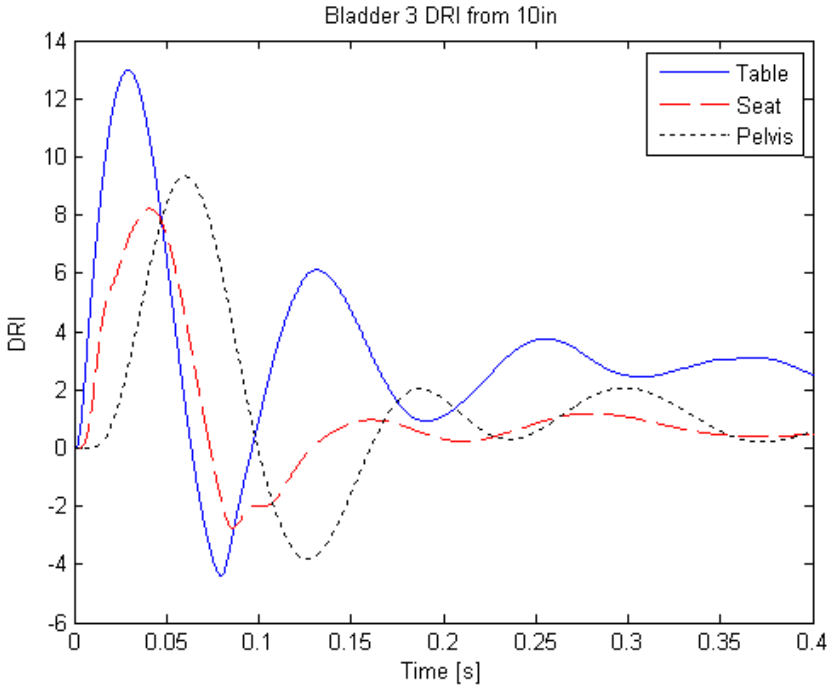

Figure A.10 Bladder 3 DRI for 10 in. Drop Height-ARL

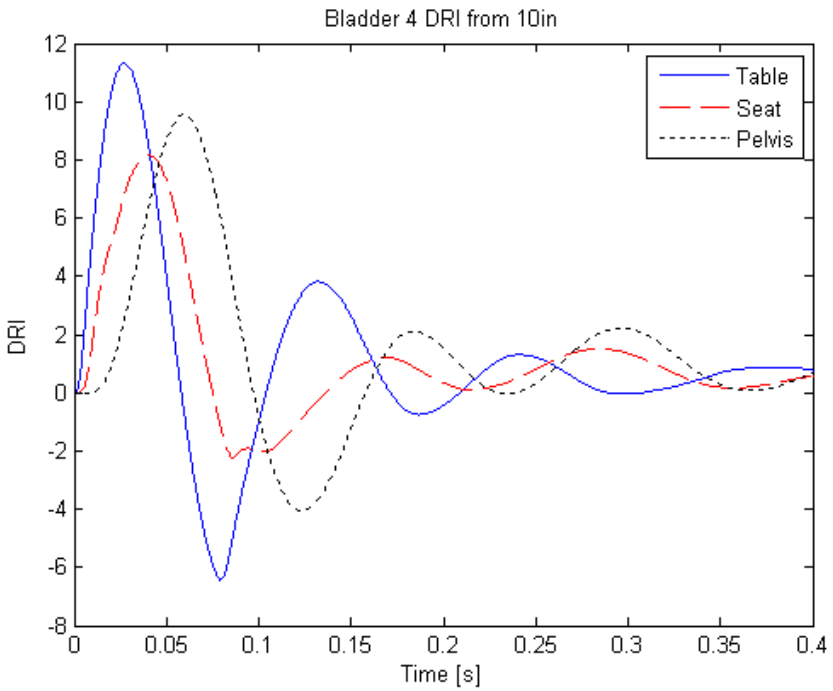

Figure A.11 Bladder 4 DRI for 10 in. Drop Height-ARL

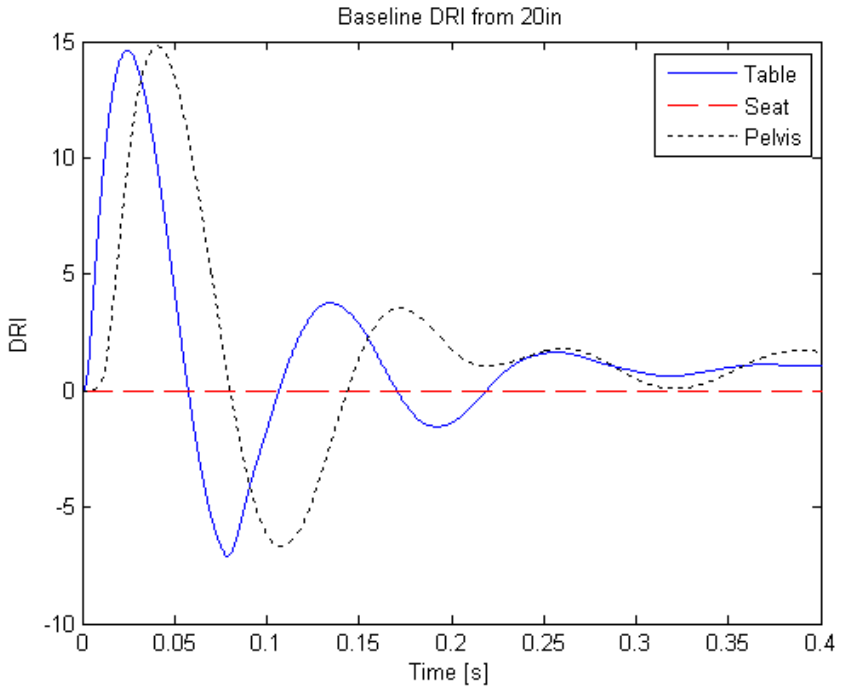

Figure A.12 Baseline DRI for 20 in. Drop Height-ARL

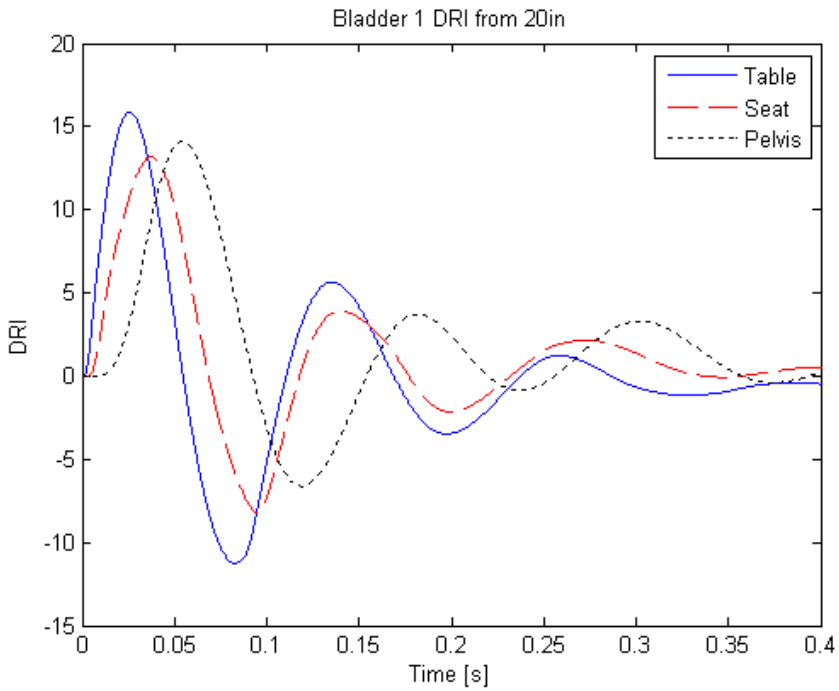

Figure A.13 Bladder 1 DRI for 20 in. Drop Height-ARL

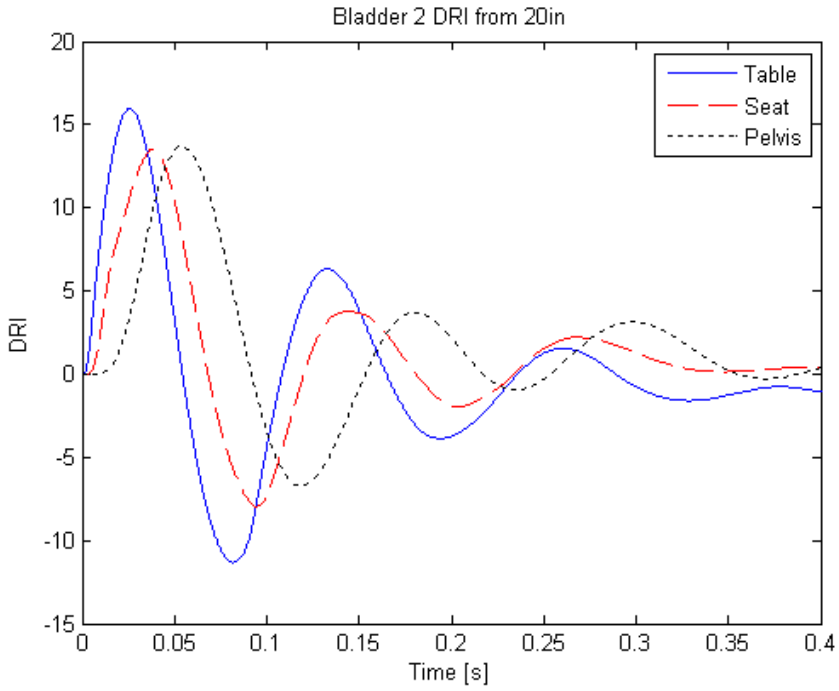

Figure A.14 Bladder 2 DRI for 20 in. Drop Height-ARL

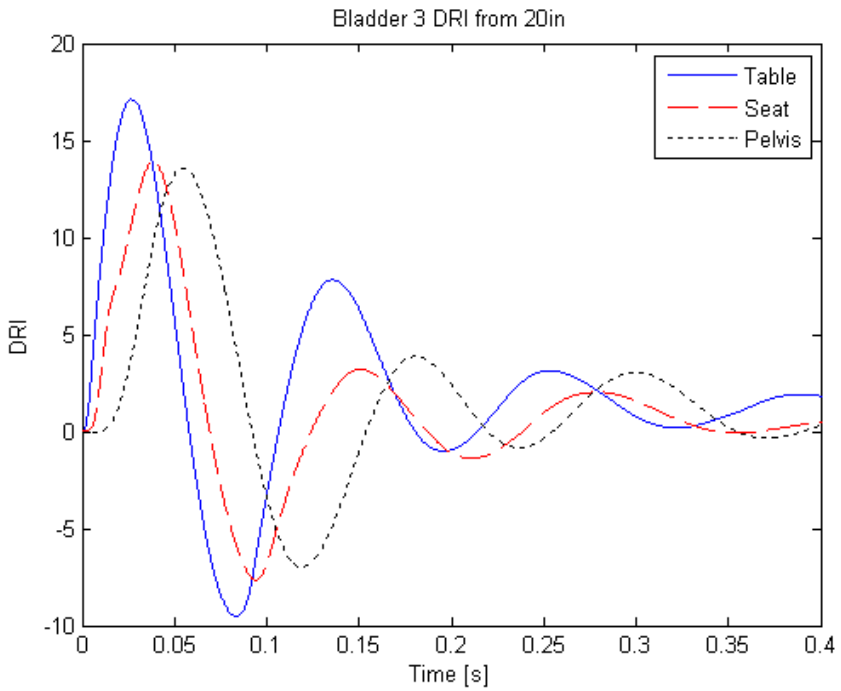

Figure A.15 Bladder 3 DRI for 20 in. Drop Height-ARL

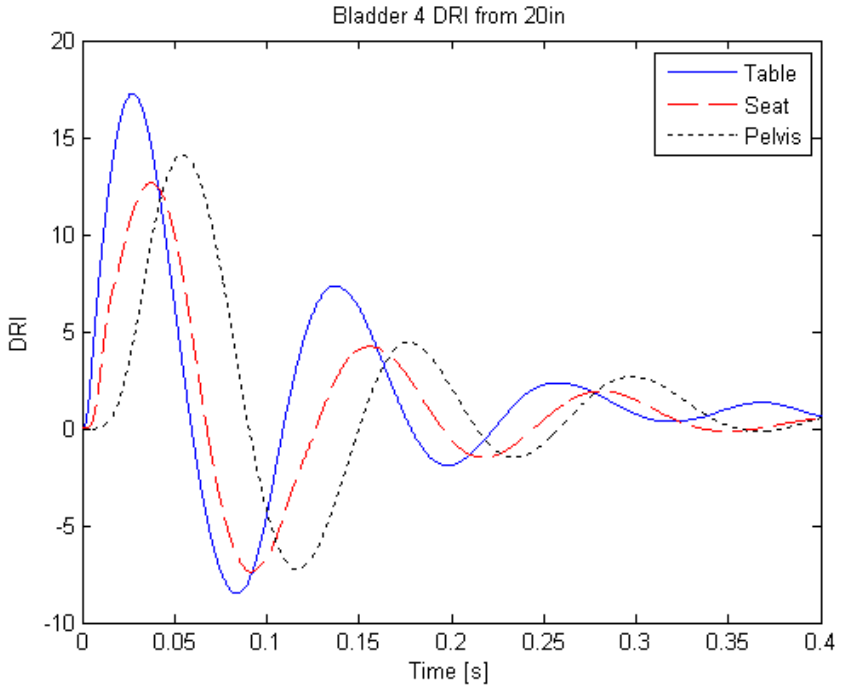

Figure A.16 Bladder 4 DRI for 20 in. Drop Height-ARL

A.2 Supplemental UNLV Drop Test Plots

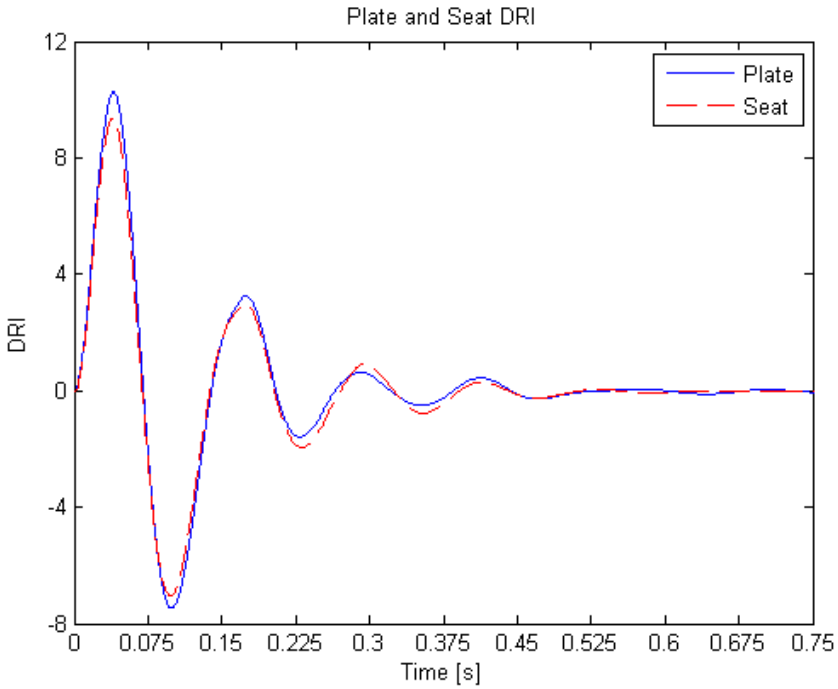

Figure 17 Baseline DRI for 10 in. Drop Height-UNLV

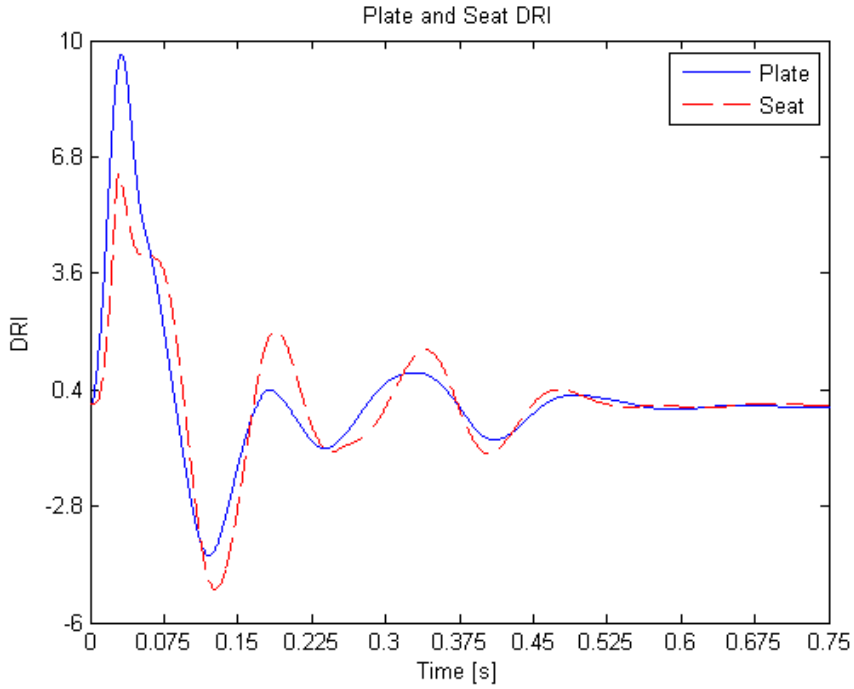

Figure A.18 Bladder 1 DRI for 10 in. Drop Height-UNLV

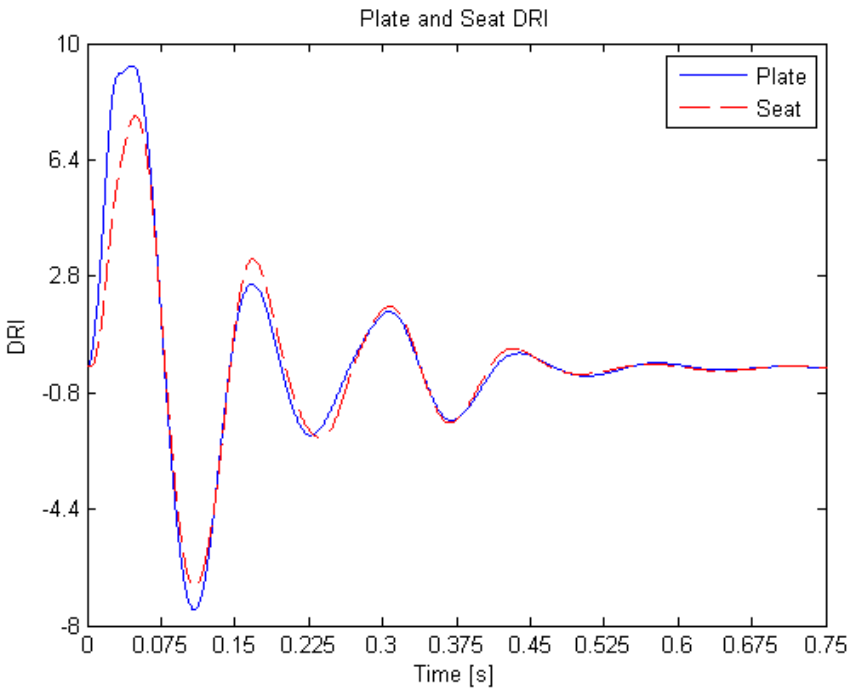

Figure A.19 Bladder 2 DRI for 10 in. Drop Height-UNLV

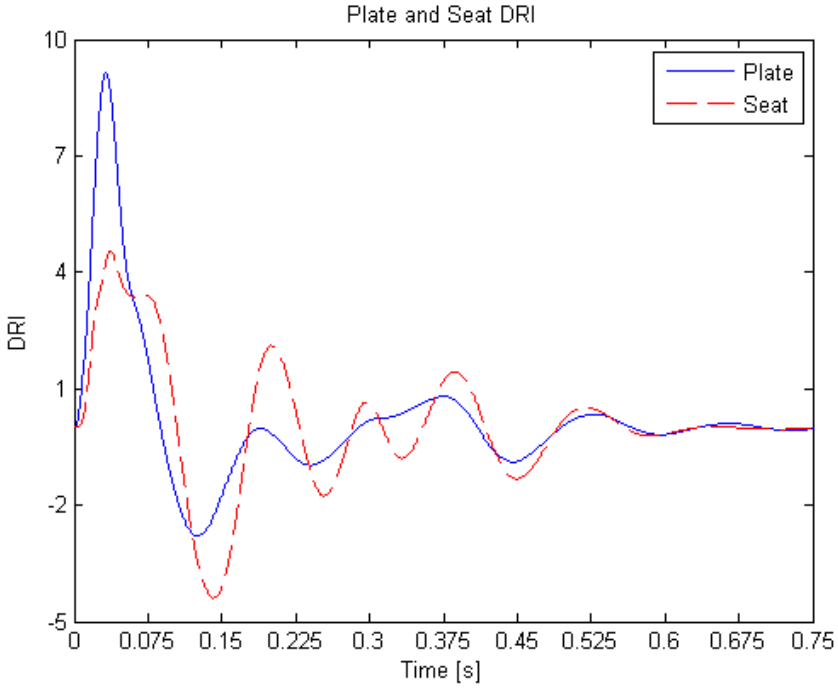

Figure A.20 Bladder 3 DRI for 10 in. Drop Height-UNLV

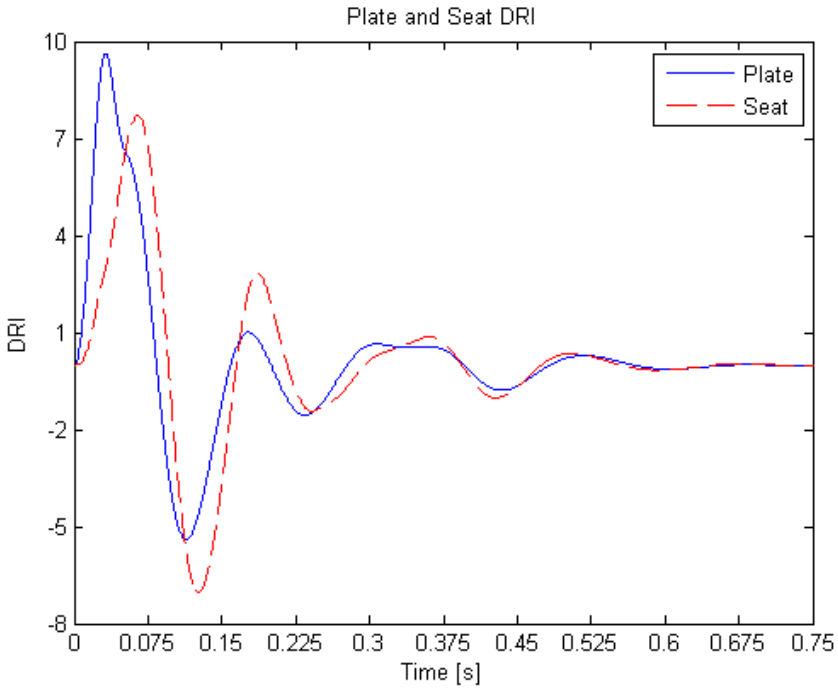

Figure A.21 Bladder 4 DRI for 10 in. Drop Height-UNLV

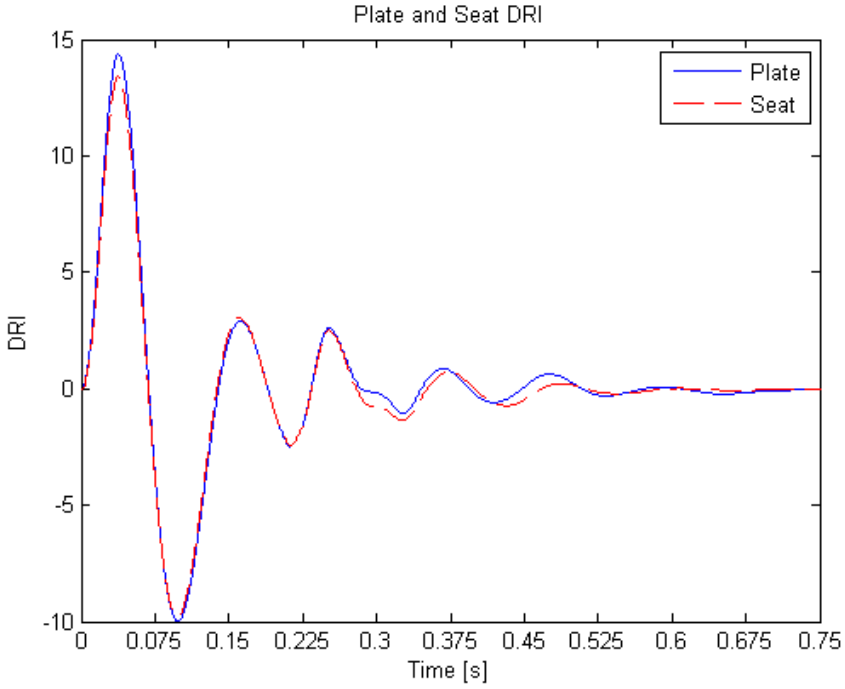

Figure A.22 Baseline DRI for 20in Drop Height-UNLV

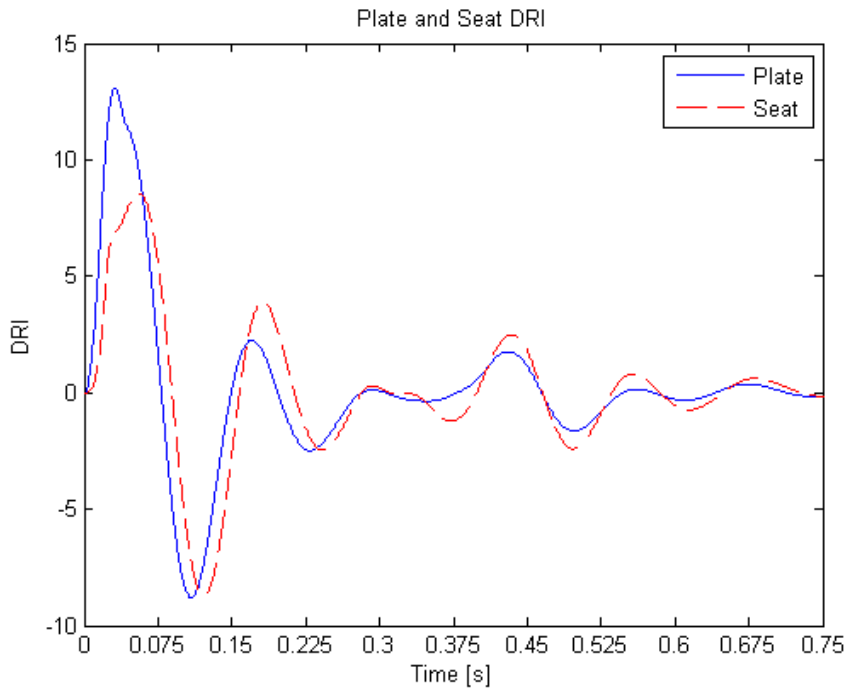

Figure A.23 Bladder 1 Baseline DRI for 20in Drop Height-UNLV

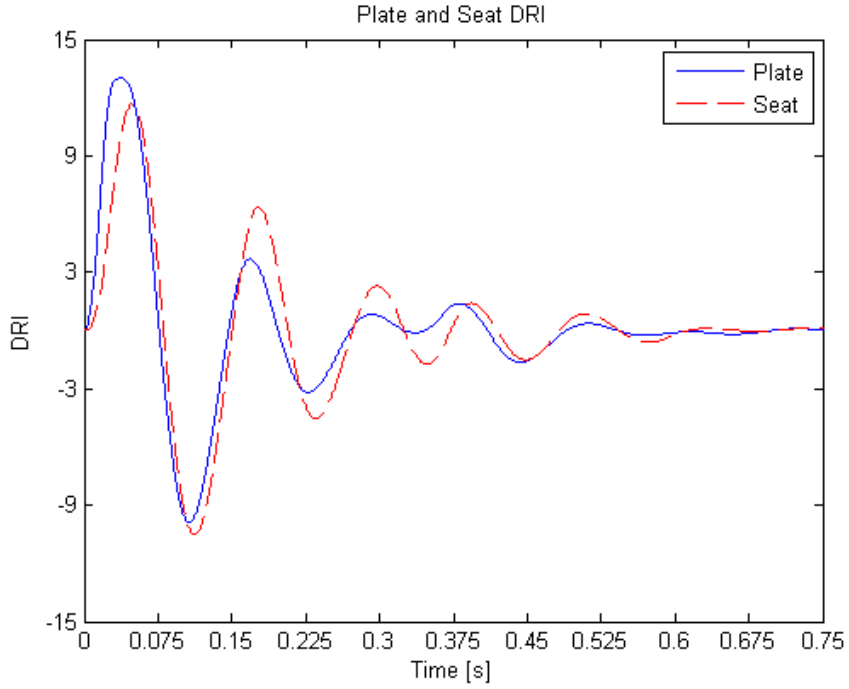

Figure A.24 Bladder 2 Baseline DRI for 20in Drop Height-UNLV

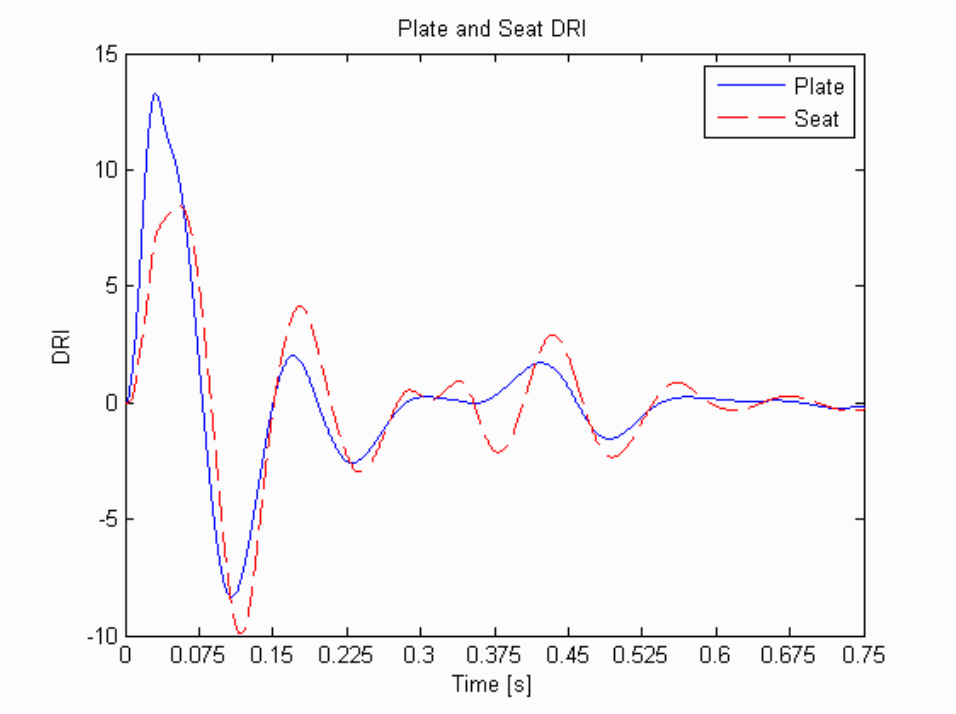

Figure A.25 Bladder 3 DRI for 20in Drop Height-UNLV

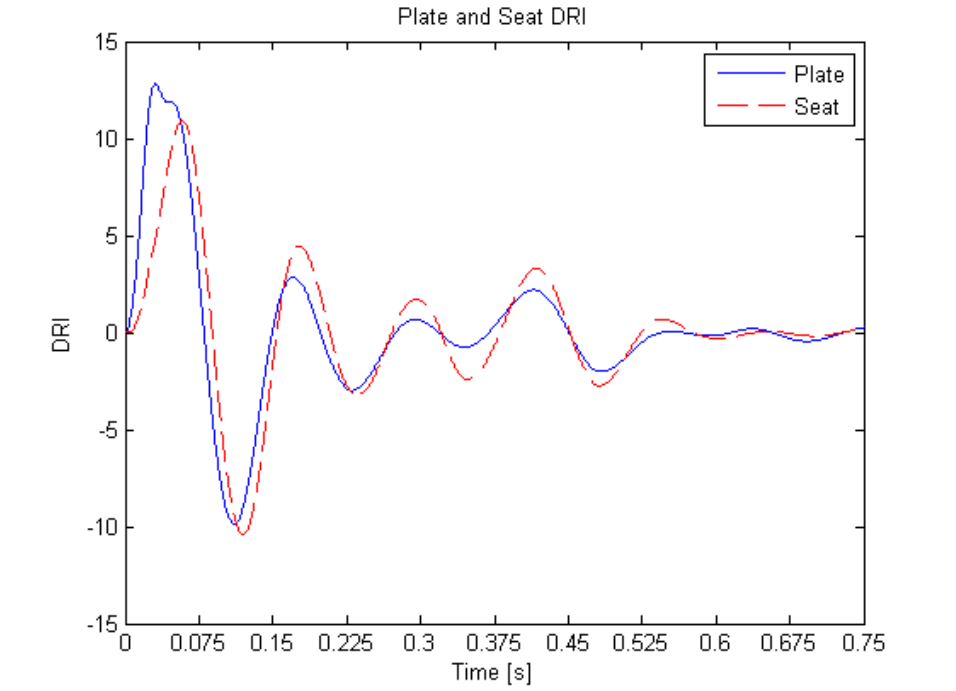

Figure A.26 Bladder 4 DRI for 20in Drop Height-UNLV

REFERENCES

[1] Lafrance, L.P., "Mine Blast Protection System for Military Support Vehicles", American Society of Mechanical Engineers PVP, Vol. 361, c1998, pg 305-309

[2] Axelsson, H. and Odd S., January 2003. "Mine Clearance Vehicles, Crew Safety Standard." The Swedish Defense Material Administration, Test Range Karlsborg 8.

[3] ISO 2631-1:1997, "Mechanical Vibration and Shock-Evaluation of human exposure to whole-body vibration-Part 1:General Requirements," ISO, 1997.

[4] ISO 2631-5: 2004, "Mechanical Vibration and Shock-Evaluation of human exposure to whole-body vibration-Part 5: Method for evaluation of vibration containing multiple shocks," ISO, 2004.

[5] Durocher, Robert, Jowz Valley Mine Strike Preliminary Technical Report, Defense research and Development Center, Canada – Valcartier c2003

[6] Coltman, J.W., C. Van Ingen, N.B. Johnson, and R.E. Zimmermann, December 1989. "Aircraft Crash Survival Design Guide Volume II-Aircraft Design Crash Impact Conditions and Human Tolerance.

[7] Aircraft Crash Survival Design Guide Final Report Volume IV, Aircraft Seats, Restraints, Litters, and Cockpit/cabin Delethalization, USAAVSCOM TR 89-D-22D, Simula Inc., c1989.

[8] Moore H., Testerman R., "Effects of Structural and Occupant Provision Improvements to the Static and Dynamic Response of the V-22 Osprey Energy Attenuating Troop Seating System", Proceedings of 61st Annual Forum of the American Helicopter Society, 2005.

[9] Wolf, E. "Development of Seat Shock Isolation Systems," UNLV Dissertation, 2007.

[10] Perry C., Nguyen T., Pint S., "Evaluation of Proposed Seat Cushions to Vertical Impact", Proceedings of Annual Symposium, SAFE Association, 2000, p 50-55.

[11] HFM-090 Task Group 25 , "Test Methodology for Protection of Vehicle Occupants against Anti-Vehicular Landmine Effects," NATO, 2007.

[12] Cheng, Z.Q., Pilkey, W.D., Balandin, D.V., Bolotnik, N.N., Crandall, J.R., and Shaw, C.G., 2001. "Optimal Control of Helicopter Seat Cushions for the Reduction of Spinal Injuries." International Journal of Crashworthiness. Volume 6.3.

[13] BS 6841, "Guide to measurement and evaluation of human exposure to whole-body mechanical vibration and repeated shock," British Standards, 1987.

[14] Hirsch, A.H., January 1964. “Man’s Response to Shock Motions.” Report 1797. David Taylor Model Basin, Structural Mechanics Laboratory, Washington D.C.

[15] Axelsson, H. and Odd S., January 2003. “Mine Clearance Vehicles, Crew Safety Standard.” The Swedish Defense Material Administration, Test Range Karlsborg 8.

[16] Stech, E.L. and Payne, P.R., November 1969. “Dynamic Models of the Human Body.” AMRLTR-66-157, Wright-Patterson AFB, Ohio.

[17] Department of Army, “Occupant Crash Protection Handbook For Tactical Ground Vehicles (Light, Medium, and Heavy Duty).”, November 2000.

[18] Eiband, M.A., “Human Tolerance to Rapidly Applied Accelerations: A Summary of the Literature,” NASA Memo 5-19-59E, 1959.

[19] Alem, N.M., 2004. Personal Correspondence. Aircrew Protection Division, U.S. Army Aeromedical Research Laboratory, Fort Rucker, Alabama.

[20] Payne, P. R.; Stech, E. L. Dynamic Models of the Human Body; AMRL-TR-66-157; Aerospace Medical Research Laboratory: Wright-Patterson Air Force Base, OH, 1969.

[21] Brinkley, J.W.; Shaffer, J.T. Dynamic Simulation Techniques for the Design of Escape Systems; AMRL-TR-71-292; Aerospace Medical Research Laboratory: Wright-Patterson Air Force Base, OH, 1971.

[22] McAndrew, B. “Shock Isolation Parameters Based on a Damped Harmonic Oscillator Model for Mine Blast Protected Seating,” ARL-TR-436, Army Research Lab, 2007.

[23] ISO 10819: 1996, “Mechanical Vibration and Shock- and-arm vibration -- Method for the measurement and evaluation of the vibration transmissibility of gloves at the palm of the hand,” ISO, 1996.

[24] Toward, M, Griffin, M, “HVLab Passive Anthropodynamic Dummy Manual,” Institute of sound and Vibration Research, University of Southhampton, 2004.

VITA

Graduate College
University of Nevada, Las Vegas

George Samaan Ladkany

Degrees:
Bachelor of Science in Engineering, 2006
University of Nevada, Las Vegas

Special Honors and Awards:
Summa Cum Laude

Departmental Honors Scholar

Graebel Mechanical Engineering Student of the Year Award 2005

Publications:
G. Ladkany and M. B. Trabia, "Incorporating Twinkling in Genetic Algorithms for Global Optimization," 34th Design Automation Conference, New York, New York, August 2008.

Theis Title: Design and Characterization of a Shock and Vibration Mitigation Seat System

Thesis Examination Committee:
Chairperson, Dr. Douglas Reynolds, Ph.D.
Committee Member, Dr. Brian. Landsberger, Ph.D.
Committee Member, Dr. William Culbreth, Ph.D.
Graduate Faculty Representative, Dr. Edward Neumann, Ph.D.